Recognition of Neutrophil Extracellular Traps by the Cytosolic DNA Sensor cGAS

Dissertation zur Erlangung des akademischen Grades
Doctor rerum naturalium (Dr. rer. nat.)
im Fach Biologie
eingereicht an der

Lebenswissenschaftlichen Fakultät
der Humboldt-Universität zu Berlin
von

Falko Apel
B.Sc. Biotechnologie
M.Sc. Molecular Medicine

Präsidentin der Humboldt-Universität zu Berlin
Prof. Dr.-Ing. Dr. Sabine Kunst

Dekan der Lebenswissenschaftlichen Fakultät
Prof. Dr. Bernhard Grimm

Gutachter/innen

1. Prof. Arturo Zychlinsky, PhD
2. Prof. Dr. Klaus Osterrieder
3. Dr. Benedikt Beckmann

Tag der mündlichen Prüfung: 24. Januar 2019

für mietze und mäuschen

Zusammenfassung

Eine Entzündung ist eine komplexe und facettenreiche Antwort des Immunsystems gegen Infektionen, welche die Beseitigung des Infektionserregers und die Wiederherstellung der Gewebefunktion zum Ziel hat. Neutrophile Granulozyten sind die erste zelluläre Abwehrlinie des Immunsystems. Sie sind die am häufigsten vorkommende Gruppe weißer Blutzellen und mit ihren antimikrobiellen Mechanismen und ihrer Fähigkeit, weitere Immunzellen zu rekrutieren, nehmen sie eine Schlüsselposition bei der Bekämpfung von Pathogenen ein. Neutrophile produzieren „Neutrophil Extracellular Traps" (NETs), ein mit antimikrobiellen Molekülen bestücktes Netzwerk aus Chromatinfasern, das während eines Zelltodprogramms namens „NETosis" von den sterbenden Neutrophilen ausgestoßen wird. Ihre netzartige Struktur erlaubt es ihnen, eine weitere Verbreitung des Infektionserregers zu verhindern; zudem erzeugen sie eine hohe lokale Konzentration an toxischen Molekülen, die Mikroorganismen töten können. Unter normalen Bedingungen werden NETs von Nukleasen zerkleinert und anschließend von Makrophagen entfernt. Wenn dieser Aufräummechanismus gestört ist, aktivieren NETs das Immunsystem und führen zur Produktion von Autoantikörpern oder entzündungsfördernden Zytokinen. NETs werden mit einer wachsenden Liste von inflammatorischen und Autoimmunerkrankungen in Verbindung gebracht, wie z.B. Sepsis, systemischen Lupus erythematodes oder rheumatoider Arthritis. Wie genau dabei NETs durch das Immunsystem erkannt werden, ist noch nicht bekannt.

In der vorliegenden Arbeit zeige ich, dass NETs durch den zytosolischen DNA Sensor „cyclic GMP-AMP synthase" (cGAS) detektiert werden können und dass dadurch die Expression von Typ I Interferonen (TIIFN) induziert wird. Zu Beginn demonstriere ich, dass NETs durch rekombinantes cGAS erkannt werden und dass mit isolierten NETs stimulierte Immunzellen cGAS-abhängig TIIFN produzieren. Des Weiteren zeige ich, dass Neutrophile, die NETosis begehen, in Nachbarzellen ebenfalls cGAS-anhängig TIIFN induzieren können. Dafür müssen die NETs mittels Phagozytose aufgenommen werden. Abschließend konnte ich diese Ergebnisse in einem *in vivo* Mausmodel für systemische NET-Produktion bestätigen. Wildtyp-Mäuse, die nach Injektion von Concanavalin A systemisch NETs produzieren, regulieren die Transkripte von interferonstimulierten Genen hoch. $cGAS^{-/-}$ Mäuse oder auch $Cybb^{-/-}$ Mäuse, welche nicht zur NET-Bildung fähig sind, zeigten diese Regulierung nicht. Die vorliegende Arbeit zeigt einen Mechanismus, wie NETs durch das Immunsystem erkannt werden und dadurch sowohl zur Entstehung als auch zur Progression von Krankheiten beitragen kann. Sie ermöglicht dementsprechend die Entwicklung neuer Interventionsstrategien, welche zur Heilung oder Linderung einer Vielzahl von Erkrankungen beitragen können.

Summary

Inflammation is a complex multilayered response of the human immune system against infection, aiming to remove the microbial agent and to restore tissue homeostasis. The first line of cellular defense of the immune system are neutrophils. They are the most abundant white blood cell, which exert an array of antimicrobial effector functions and attract other immune cells by releasing “alarmin” signals upon pathogen recognition. The combination of these two characteristics makes them crucial for an effective immune response, because they both contain the infection and activate other immune cells, resulting in effective pathogen clearance. Neutrophils release neutrophil extracellular traps (NETs), a composite of chromatin and antimicrobial molecules, into the extracellular space during a form of regulated cell death called NETosis. NETs are released in response to a variety of microbial stimuli like bacteria, fungi and parasites, but also by host-derived factors. Their net-like structure prevent further dissemination of the invader and establishes a high local concentration of toxic molecules that mediate pathogen killing. Under healthy conditions, NETs are degraded by nucleases in circulation and cleared by macrophages. If this clearance is disturbed, NETs provide a platform for undesired immune activation and contribute to the production of autoantibodies and pro-inflammatory cytokines. NETs are implicated in a growing list of inflammatory and autoimmune diseases, like sepsis, systemic lupus erythematosus (SLE) and rheumatoid arthritis (RA). The exact mechanism how NETs are recognized by the immune system is not fully understood.

In this study, I demonstrate that the cytosolic DNA sensor cyclic GMP-AMP synthase (cGAS) senses NETs and induces the production of type I interferons (TIIFN). I first showed that NETs are recognized by recombinant cGAS and that cells treated with isolated NETs produce TIIFN in a cGAS dependent mechanism. Secondly, I demonstrate that neutrophils undergoing NETosis are taken up by neighboring immune cells and induce cGAS-dependent TIIFN expression. Lastly, I confirmed our *in vitro* results in a mouse model of systemic NET induction. Wildtype mice injected with Concanavalin A significantly upregulate the expression of interferon stimulated genes, while $cGAS^{-/-}$ mice and $Cybb^{-/-}$ mice, which are incapable of producing NETs, fail to induce this response.

Taken together, this study shows a novel mechanism for sensing of neutrophil cell death and demonstrates how NETs contribute to the development and progression of a growing list of diseases. This provides a starting point for drug development, potentially bringing mitigation to affected patients.

Contents

Figures

Abbreviations

ACN	Acetonitrile
AIM2	Absent in melanoma 2
ALT	Alanine-aminotransferase
ANCA	Anti neutrophil cytoplasmic antibodies
APC	Antigen presenting cell
ASC	Apoptosis-associated speck-like protein
AST	Asparatate-aminotransferase
ATP	Adenosintriphosphat
BLAST	Basic local alignment search tool
bp	Base pairs
BPI	Bactericidal/permeability increasing protein
CD	Cluster of differentiation
CG	Cathepsin G
cGAMP	Cyclic guanosine monophosphate–adenosine monophosphate
cGAS	Cyclic GMP-AMP synthase
CGD	Chronic granulomatous disease
CLR	C-type lectin receptor
ConA	Concanavalin A
CRISPR	Clustered regulary interspeaced short palindromic repeats
Ct	Cycle of threshold
DAMP	Danger associated molecular pattern
dH_2O	Distilled water
dsDNA	Double stranded deoxyribonucleic acid
DTT	Dithiothreitol
ER	Endoplasmatic reticulum
EtOH	Ethanol
FcR	Fc-receptor
FCS	Fetal calf serum
gRNA	Guide RNA
GSDMD	Gasdermin D
GTP	Guanosintriphosphat
HCQ	Hydroxychloroquine
HMGB1	High-mobility group box-1
IAA	Iodoacetamide
IFI16	Gamma-interferon-inducible protein 16
IFNAR	Interferon α/β receptor
IL…	Interleukin
IRAK	Interleukin-1 receptor associated kinase
ISG	Interferon stimulated genes
ISRE	Interferon-stimulation response elements
kDa	Kilo Dalton
LDG	Low density granulocyte
LPS	Lipopolysaccharide
MAMP	Microbe associated molecular pattern

MAVS	Mitochondrial antiviral signaling protein
MDA5	Melanoma differentiation antigen 5
MDM	Monocyte derived macrophages
MPO	Myeloperoxidase
NADPH	Nicotinamidadenindinucleotidephosphate
NDG	Normal density granulocyte
NE	Neutrophil Elastase
NETs	Neutrophil extracellular traps
NFκB	Nuclear factor 'kappa-light-chain-enhancer' of activated B-cells
NLR	NOD-like receptor
o.n.	Over night
P/S	Penicillin/Streptomycin
PAD	Protein arginine deaminase
PAM	Protospacer adjacent motif
PBMCs	Peripheral blood mononuclear cells
pdAdT	Poly(deoxyadenylic-deoxythymidylic) acid
pDC	Plasmacytoid dendritic cell
p(I:C)	Polyinosinic:polycytidylic acid
PMA	Phorbol-myristate acetate
PMN	Polymorphonuclear cell
PR3	Proteinase 3
PRR	Pattern recognition receptor
Q	Glutamin
qPCR	Quantitative polymerase chain reaction
RA	Rheumatoid arthritis
RAGE	Receptor for advanced glycation endproducts
RBC	Red blood cell
RIG-I	Retinoic acid inducible gene I
RNA	Ribonucleic acid
ROS	Reactive oxygen species
RT	Room temperature
SAVI	STING-associated vasculitis
SIDT2	SID1 transmembrane family member 2
SLE	Systemic lupus erythematosus / erythematodes
STAT	Signal transducer and activator of transcription protein
STING	Stimulator of interferon genes
TFA	Trifluoroacetic acid
TGF-beta	Transforming growth factor
TIIFN	Type I interferons
TLR	Toll-like receptor
TNF	Tumor necrosis factor

1 Introduction

1.1 Inflammation and the inflammatory cascade

The immune system is a multilayered network of cellular and soluble factors that evolved to recognize and eradicate invading pathogenic microbes, while, at the same time, preserving self-structures. The ongoing development and arms race of pathogens and the immune system is one of the essential driving factors of evolution. The fact that basic immunological concepts like the recognition of invasion followed by a directed response are conserved in evolution from prokaryotes to plants, invertebrates, and mammals, points out their fundamental importance for life as such [1].

The mammalian immune response consists of an innate and an adaptive arm. The innate system is based on a definite set of germ-line encoded receptors that allow fast recognition of a large variety of different pathogens. The adaptive immune system, on the other, hand evolves highly specific receptors to each new challenge that are codified as immunological memory and can be activated during repeated infections. Both arms are required for the recognition and effective resolution of an infection during a process called inflammation.

Inflammation encompasses a complex response of the host to a disturbed tissue homeostasis that needs tight regulation, both temporally and spatially [2]. Controlled inflammation is beneficial for the host, because it eradicates the invader, clears the damage and reestablishes tissue homeostasis. Uncontrolled inflammation on the other hand can become chronic and results in tissue damage and consequently in disease [3].

Four key components define the process of inflammation: inducer, sensor, mediator and effector. Inflammation can be induced by the recognition of endogenous and exogenous stimuli that signalize infection or tissue damage. Exogenous signals of microbial origin are summarized as microbial associated molecular patterns (MAMPs) that represent conserved structures that microbes require for their survival. Examples are lipopolysaccharide (LPS) of gram-negative bacteria and flagellin, a protein of the mobility apparatus of bacteria. Endogenous stimuli of inflammation are host-derived molecules that are not “visible” for the immune system under homeostatic conditions. Their presence indicates uncontrolled cell death in response to infection or injury, which is why they are called danger associated molecular patterns (DAMPs). Examples of DAMPs are uric acid crystals, high-mobility group box 1 (HMGB1), as well as RNA and DNA. In living cells, DNA is concealed in the nucleus and hidden from immune recognition, but it becomes highly immunogenic if it is released into the extracellular space by necrotic cell death [4,5]. The importance for the recognition of nucleic acids by the immune

system is supported by the fact that DNA recognition is conserved during evolution from plants to mammals [6].

The immune system has a plethora of germ-line encoded sensors to recognize infection or tissue damage. Receptors of the innate system are summarized as pattern recognition receptors (PRR) and divided into four subfamilies: (1) Toll-like receptors (TLRs) are membrane bound receptors that recognize a large variety of MAMPs and DAMPs, increasing their spectrum of recognition by forming homo- and heterodimers. (2) C-type lectin receptor (CLRs) recognize carbohydrates presented on the surface of microbes, such as zymosan, and play a crucial role in the recognition of pathogenic fungi. (3) NOD-like receptors (NLRs) are cytosolic sensors that detect a broad variety of ligands, including crystals and MAMPs of intracellular pathogens. Lastly, (4) nucleic acid sensors like retinoic acid inducible gene I (RIG-I), melanoma differentiation antigen 5 (MDA5), absent in melanoma 2 (AIM2) and cGAS detect cytoplasmic DNA or RNA of viral or bacterial origin [7–10].

Activation of these receptors by ligand binding induces different intracellular signaling cascades like the NFκB pathway or interferon regulatory factors. This results in the production of inflammatory mediators, most importantly pro-inflammatory cytokines and chemokines. Their expression marks the locus of infection and induces recruitment of the effectors of inflammation, which are innate and adaptive immune cells. Innate immune cells involve granulocytes, monocytes, macrophages and dendritic cells. They are the first line of defense that quickly responds and prevents dissemination of the invader. The adaptive immune response consists mostly of B- and T-cells and requires more time to allow the production of high affinity receptors for the pathogen, namely antibodies and T-cell receptors. It also establishes a long-term memory that allows a quicker and stronger response if the same invader infects the host again. The cells of innate and adaptive immunity work in a cooperative way and together orchestrate an effective immune response to eradicate invading microbes [2,11].

Once the infection is cleared the resolution of inflammation starts. Neutrophils undergo apoptosis and macrophages clear them by phagocytosis. This induces a switch in macrophages towards an anti-inflammatory phenotype. They release anti-inflammatory cytokines like transforming growth factor β (TGF-β) and IL10 that signalize the return to tissue homeostasis [12].

1.2 Neutrophils – the foot soldiers of innate immunity

Neutrophilic granulocytes, short neutrophils, are the most frequent type of innate immune cells and arrive as a first line of defense at the side of infection. They exert a plethora of antimicrobial functions, which makes them a key player in the rapid recognition and clearance of invading pathogens. The human immune system is dependent on functional neutrophils. Patients carrying a mutation in the Neutrophil Elastase gene (*ELANE*) develop severe congenital neutropenia, also known as Kostmann's syndrome, and show that neutrophil insufficiencies predispose to a variety of different infectious diseases, such as mouth ulcers, otitis, pharyngitis and pneumonia [13].

1.2.1 Activation of neutrophils

Neutrophils represent up to 70 % of the white blood cell compartment. They are characterized by a high number of granules in their cytoplasm and a multi-segmented nucleus, which is why they are also referred to as polymorphonuclear cells (PMN) [14]. Neutrophils are relatively short lived and dying neutrophils are cleared in the spleen, the liver and the bone marrow [15]. To replenish the pool, the bone marrow produces approx. $1{,}5 \times 10^{11}$ neutrophils per day from a myoblast precursor population and releases them as fully differentiated cells into the blood stream where they patrol for signs of infections [16]. In order to do so, neutrophils are equipped with an array of innate PRRs, like TLRs, CLRs and NLRs. Furthermore, they express Fc-receptors (FcR) and Complement receptors to recognize opsonized microbes [17]. With the help of chemokine and cytokine receptors, neutrophils can follow a chemotactic gradient towards the site of infection, where tissue-resident antigen-presenting cells (APCs) or endothelial cells recognized MAMPs and secreted chemo- and cytokines. In parallel to chemokine secretion, endothelial cells upregulate P- and L-selectin on their surface that faces the blood vessel lumen. The neutrophil approaches the activated endothelial cells and binds the selectins with their respective ligands, resulting in a rolling and finally a firm adhesion to the endothelium at the infection site. The neutrophil transmigrates through the endothelial layer in the infected tissue where it releases further chemokines to attract additional neutrophils, monocytes and macrophages. More importantly, they can employ a battery of antimicrobial effector functions in order to kill microbes and contain the infection (Fig. 1.1) [14].

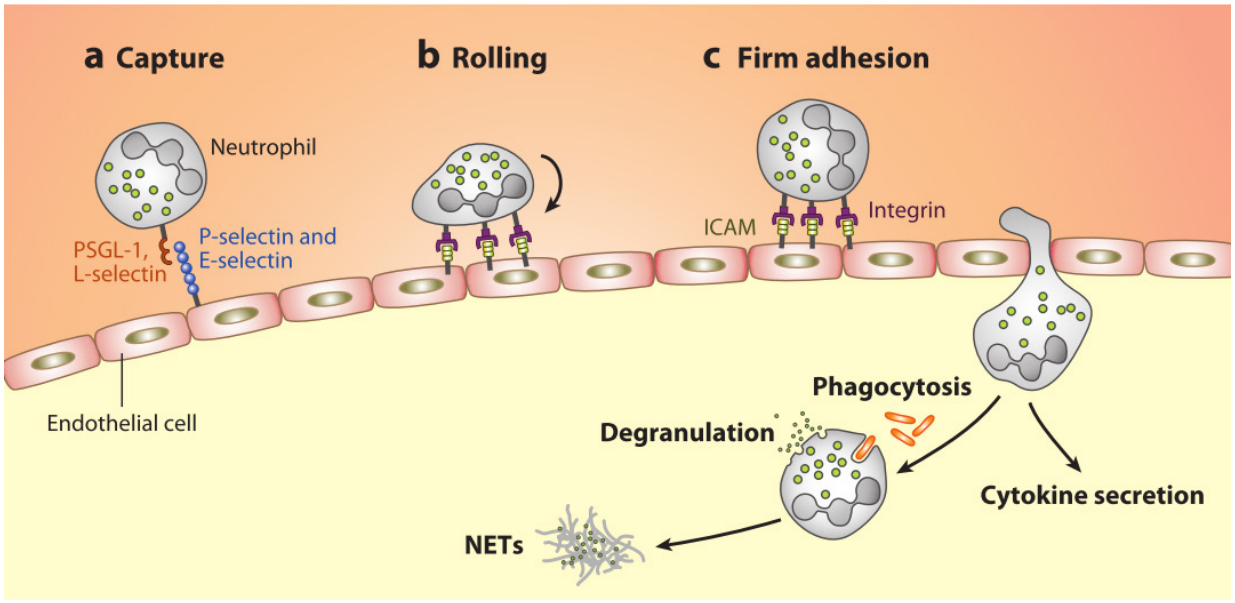

Figure 1.1 Activation of neutrophils during infections
Activated endothelial cells upregulate selectins that are recognized by neutrophils patrolling the blood stream. Upon selectin binding (a), neutrophils roll over the endothelium (b) and tightly adhere close to the side of infection (c). After extravasation through the endothelial layer, neutrophils secrete cytokines to recruit further immune cells and exert different effector functions to eliminate the infection. (Figure taken from Amulic et al., 2012)

1.2.2 Neutrophil effector functions

Communication with other immune cells by cytokines and chemokines

Neutrophils are important producers of chemokines and cytokines that are required to coordinate an efficient antimicrobial response during infections. Although neutrophils are not the most potent cytokine producers, their high abundance and early arrival at the inflammatory site assigns them an important position in the inflammatory cascade. The major chemokine they produce is IL-8 (CXCL8) [18]. Interestingly neutrophils themselves respond to IL8 by upregulation of adhesive molecules and chemotaxis, resulting in an increased neutrophil recruitment. Furthermore IL8 primes neutrophils to undergo a stronger reactive oxygen species (ROS) burst and enhanced phagocytosis [19]. Another chemokine that they produce is MIP1α, a chemokine that recruits monocytes and macrophages to the inflammatory site.

Neutrophils also produce pro-inflammatory cytokines like IL1β, IL6 and TNF [20]. These factors regulate the innate immune response during the acute phase of inflammation on both a local and a systemic level. They induce the attraction of further immune cells or license immune cell functions e.g. by inducing phagocytosis in macrophages. Systemically, these cytokines induce fever, trigger the release

of antimicrobial acute phase proteins from the liver and upregulate the expression of endothelial surface receptors, enabling immune cells to extravasate to the inflammatory site [21].

Production of ROS

During a process called the oxidative burst, neutrophils produce high amount of short-lived oxygen-based molecules summarized as ROS, using an enzyme complex called NADPH-oxidase [22]. This complex catalyzes molecular oxygen to superoxide, a highly reactive molecule that myeloperoxidase (MPO) further processes to hypochlorous acid or hydrogen peroxide [23]. Different ROS species are potent antimicrobials that kill microbes by oxidizing and thereby damaging DNA, lipids and proteins [24]. Due to missing specificity, ROS released by neutrophils also affect host structures and lead to tissue damage[25].

Patients suffering from Chronic Granulomatous Disease (CGD) demonstrate the importance of ROS for the innate immune defense. Due to a mutation in NADPH-oxidase the cells of these patients cannot produce sufficient amounts of ROS, resulting in an increased susceptibility to bacterial and fungal infections [26].

Release of antimicrobial molecules by degranulation

Neutrophils are equipped with a large array of pre-synthetized antimicrobial molecules with different bactericidal mechanisms. Cationic peptides comprising α-defensins, LL37 and bactericidal/ permeability increasing protein (BPI) interfere with the bacterial membrane integrity, a mechanism they have in common with the neutrophil proteases lysozyme, Proteinase3 (PR3), Neutrophil Elastase (NE), Cathepsin G (CG) and Azurocidin. Another class of antimicrobials present in neutrophils are metal chelator proteins like Lactoferrin and Calprotectin that inhibit bacterial growth by complexing essential ions like iron, manganese or zinc [27].

To prevent self-damage the antimicrobials are packed into specific organelles called granules that are stored in the cytoplasm. There are three major types of granules, characterized by their protein content and their mobilization potential. Primary granules (also known as azurophilic) are the first type of granule produced during neutrophil development. They contain MPO, defensins, BPI and the proteases NE, CG and PR3 and are thereby the most important carriers of the antimicrobial activity. The secondary or specific granules are formed after the primary granules and contain Lactoferrin, LL37 and lysozyme. The third class, the tertiary granules are deposits for the metalloproteases Gelatinase and Leukolysin [28]. During activation, the neutrophil mobilizes the granules consecutively, starting with the azurophilic granules, followed by specific and tertiary granules. They either fuse with the phagosome (discussed below) or with the plasma membrane, releasing their cargo into the

extracellular space. This process, called degranulation, establishes an antimicrobial environment in the surrounding of the neutrophil, resulting in bacterial killing and containment of the infection [29].

Uptake and killing of microbes by phagocytosis

Neutrophils clear microbes by engulfing and digesting them by a mechanism called phagocytosis. Phagocytosis is a receptor-mediated process, during which the neutrophil forms a membrane invagination that surrounds the microbe, forming a separated compartment known as the phagosome. Neutrophils induce phagocytosis upon recognition of microbes either directly by sensing their PAMPs by PRRs or indirectly by binding antibody-opsonized microbes with their FcR. Different than in macrophages, neutrophil phagosomes establish their bactericidal environment by fusion with granules and the assembly of the NADPH oxidase on the phagosomal membrane, resulting in a cocktail of antimicrobial molecules and ROS that together eradicate enclosed microbes [30–32].

1.2.3 Neutrophil extracellular traps

An additional effector mechanism is the release of NETs into the extracellular space [33]. NETs are defined by a chromatin backbone that is decorated with histones and a variety of antimicrobial molecules, such as NE, PR3, CG, MPO, LL37 and defensins [34]. They originate from a programmed form of necrotic cell death named NETosis [35], which is evolutionary conserved from plants to mammals [36].

Inducers of NET formation

The production of NETs is reported for a variety of microbial stimuli, such as bacterial components and entire bacteria, fungi, viruses and protozoa [33,37–43]. It is reported that neutrophils are capable of recognizing the size of microbes and either phagocytose them if possible or selectively release NETs in response to large opponents [44]. In addition to microbial inducers, a variety of self-molecules cause NET formation. Neutrophils treated with complement factors, autoantibodies, ureate crystal or activated platelets undergo NETosis [45–48]. To reduce the complexity during experimental procedures, standardized inducers like the mitogens Phorbol-Myristate-Acetate (PMA), Concanavalin A (ConA) and phytohaemagglutinin as well as the calcium ionophore A23187 or the fungal toxin Nigericin are used [38]. Interestingly, NET formation results from an aborted reentry into the cell cycle, since it shares similarities with the onset of mitosis, like the activation of CDK6, upregulation of Ki-67 or breakdown of the nuclear envelope [49].

Mechanisms of NET formation

The mechanism leading to NETosis is dependent on the stimulus. Whereas stimuli like PMA, ConA and *Candida albicans* require ROS production for NET formation, other stimuli like A21387 and Nigericin activate NETs by a ROS independent pathway. Interestingly, CGD patients, which are not able to produce ROS due to mutations in NAPDH oxidase, are also not able to produce NETs in response to ROS-dependent stimuli. This is reflected by an increased rate of fungal infections by *C. albicans* or *Aspergillus nidulans* [26], that can be cured by a gene therapy approach that restores ROS-dependent NET production [50].

The ROS-dependent pathway leading to NET formation is the most accurately described mechanism. PMA activates protein kinase C, resulting in an intracellular Ca^{2+} release and the activation of the Raf-MEK-ERK pathway, finally triggering NADPH oxidase that produces ROS at granular membranes [35,51]. Subsequently, ROS activate a multi-protein complex called the azurosome that, among other proteins, contains MPO. MPO converts ROS to halic acid that permeabilizes the granular membrane and allows the liberation of NE and other proteases [52]. NE processes Gasdermin D (GSDMD) into its active form, which induces additional NE release from the granules by a feed-forward mechanism [53]. NE transmigrates into the nucleus via the GSDMD pores where it processes histones and induces chromatin decondensation, nuclear delobulation and expansion [39]. During this process, the rising Ca^{2+} levels activate protein arginine deaminases (PAD) that citrullinate histones inducing further chromatin decondensation [38]. Finally, the nuclear envelope disintegrates, the exposed chromatin is decorated with liberated granular content and expelled into the extracellular space. In contrast to this suicidal NETosis, it is described that neutrophils can survive the ejection of NET material in response to *Staphylococcus aureus*, a process named vital NETosis [54].

NETs trap and kill microbes

NETs indirectly limit infections by trapping bacteria [33,55] or fungi [42] and prevent further dissemination in the host. More importantly, NETs provide a highly inhospitable environment by establishing high local concentrations of bactericidal agents like histones or antimicrobial peptides, and even the DNA is reported to be antimicrobial [56]. NETs kill bacteria like *Escherichia coli* and *Salmonella flexneri* [33,35,38] and fungi like *C. albicans* [42]. Also *Leishmania amazonensis,* the parasite causing Leishmaniasis, is killed by NETs *in vitro* [57]. Interestingly, there are different adaptation strategies of microbes to NETs. Different pathogens have developed virulence factors that allow the escape from NET-mediated killing, e.g. *Streptococcus pneumoniae* which expresses an endonuclease that degrades NETs [55]. Other

pathogens like *Haemophilus influenzae* and *S. aureus* deliberately induce NETs, to shield them from immune cell recognition [58,59].

Neutrophil extracellular traps in disease

The formation of NETs has not only beneficial outcomes for the host. Although the liberation of high concentrations of antimicrobial molecules like histones and ROS is an effective way to fight infections, these molecules are unspecific and can be cytotoxic to host tissues. Especially in circulation, NETs induce endothelial damage and provide a framework for thrombotic events. Thus, it is not surprising that NETs are implicated as negative contributors in a growing list of diseases. So far, NETs have a proposed role in cancer [60], diabetes [61], sepsis [62], thrombosis [63], arteriosclerosis [64] and an array of autoimmune diseases.

1.3 Neutrophil extracellular traps in autoimmunity

Autoimmune diseases are characterized by a dysfunction of the immune system that results in a loss of tolerance towards self-structures, leading to an uncontrolled formation of autoantibodies or auto-reactive cytotoxic T-cells. Effects of autoimmune diseases can be local or systemic, depending on the target that the immune system erroneously recognizes. Since innate and adaptive immune system are tightly connected, false regulation of innate effector functions can severely influence adaptive immunity and vice versa. NETs are implicated in a number of autoimmune diseases, like SLE, vasculitis, gout, RA and psoriasis [65]. Although these diseases differ in symptoms and pathogenesis, they share some remarkable characteristics when it comes to NETs. The pathogenesis of these diseases produces specific molecules that prime neutrophils or directly induce NETosis, like MSU crystals in gout or immune complexes in SLE. Increased appearance of spontaneous NET formation is described for some of the diseases, whereas others show increased levels of NET-associated proteins like NE or MPO in plasma or synovial fluids [66,67]. These observations show that NETs play a role in autoimmune diseases although it is not entirely understood if they are a symptom or a driver of pathogenesis.

1.3.1 SLE as an example of a NET–associated diseases

SLE is a multifactorial autoimmune disease that is characterized by systemic inflammation of connective tissue, the formation of autoantibodies and a type I interferon (TIIFN) signature. The average incidence of SLE is approx. 0,1 %, depending very much on sex and ethnicity. Women of child bearing age display the highest incidence of SLE development and people of Hispanic and African ethnicity show a higher incidence than Caucasians [68]. Genetic risk factors for the development of SLE are e.g. mutations in the nucleases DNAse-1 and DNase1-like 3 [69,70]. SLE progresses in flairs and patients

go through phases of exacerbation and remission. SLE patients present with a large variety of symptoms that advance over time [71]. During the early phase of disease, patients suffer from fatigue, fever and loss of appetite. Patients also often develop a characteristic skin rash in the face, known as butterfly rash. As the disease progresses patients experience joint and muscle pain and a variety of organs get affected [72]. Most prominently, patients develop lupus nephritis, resulting in an impairment and finally destruction of the kidneys. Other organs affected are the lung, the heart and skin [71,73].

Autoantibodies and their contribution to SLE pathology

In SLE these auto-antibodies recognize a large variety of antigens [74] like dsDNA [75] and chromatin [76]. Interestingly, patients also develop antibodies targeting NET-related proteins like histones, MPO, PR3 and NE [77–81]. By binding their respective antigen, they form immune complexes that cause vascular damage leading to glomerulonephritis [82,83]. Additionally, they can indirectly exacerbate the disease by further activating innate immune cells. SLE neutrophils stimulated with immune complexes produce NETs [84,85] and plasmacytoid dendritic cells (pDCs) respond by producing TIIFN [81,84,86,87], thus contributing to the second hallmark of SLE: the TIIFN signature.

The TIIFN signature in autoinflammatory diseases

TIIFN are a group of pro-inflammatory cytokines that bind the IFN α/β-receptor (IFNAR) and are expressed as mediators of an antiviral response. They are induced upon activation of viral nucleic acid sensors like RIG-I or cGAS. The most prominent subclass of TIIFN is IFNα, representing 13 subtypes, and IFNβ. Binding of IFNAR by TIIFN induces signaling via different STAT proteins, finally inducing a plethora of interferon stimulated genes (ISGs) that establish an antiviral defense state [88]. TIIFN play a crucial role in the development of SLE [89,90]. Transcriptome analysis of pediatric and adult SLE patients revealed a global upregulation of TIIFN and ISGs, when compared to healthy donors or patients with RA [91,92]. By expressing this signature, SLE is part of a group of diseases that all show TIIFN overexpression, the type I interferonopathies. The receptors leading to TIIFN production in SLE are not clearly identified yet.

1.3.2 Neutrophil extracellular traps in SLE

NET components like DNA, nucleosomes, MPO and NE are found in the circulation of SLE patients [93–95]. The fact that 40-60 % of SLE patients are neutropenic, suggests that these circulating molecules can be attributed to increased neutrophil cell death [96]. Normal SLE neutrophils are prone to undergo apoptosis [84,97], but are not predisposed to spontaneous NET formation [98]. However, when stimulated, they form more NETs, most likely due to TIIFN priming [84]. Furthermore, autoantibodies against LL37 [81]

and ribonuclear particles [84] can induce NETs. Interestingly, SLE patients present with a subtype of neutrophil-like cells termed low density granulocytes (LDGs). They migrate together with the peripheral blood mononuclear cells (PBMCs) on a density gradient, instead of with the normal density neutrophils (NDGs) [91,99]. They serve as a marker for juvenile SLE and their occurrence correlates with vasculitis and skin involvement in SLE patients [67,100]. Compared to NDGs, LDGs have a more pro-inflammatory phenotype. They spontaneously undergo NETosis, produce elevated levels of pro-inflammatory cytokines (IL6, IL8, TNF and TIIFN) and contribute to disease pathogenesis by causing endothelial damage [67,98]. Neutrophils undergoing NETosis were detected in skin and the nephritis associated glomeruli of SLE patients [98,101,102].

Inefficient NET clearance due to DNAse1 and macrophage insufficiencies

In healthy individuals, NETs are cleared by a combination of soluble factors and phagocytes. In a first step, DNases degrade NETs into smaller fragments [101] and subsequently, NET remnants are removed by macrophages in an immunologically silent way [103]. In SLE, the clearance of dead cells by macrophages is impaired [97,104]. Additionally, there are different mechanisms impairing the functionality of DNAse1, an endonuclease that is secreted from the liver and the main degrading enzymes of NETs [101]. Mutations in DNAse1 and DNAse1L3 cause familial forms of SLE with high autoantibody titers against nuclear antigens and high prevalence of lupus nephritis [69,70], a phenotype that is recapitulated in mice [105,106]. Insufficiencies in DNAse1 activity correlate with diseases severity and contribute to the occurrence of lupus nephritis [98,101,107]. Interestingly, also the mutation of an intracellular cytoplasmic DNAse known as TREX1 results in interferon-driven autoimmunity and SLE [108,109].

1.3.3 NETs as inflammatory stimulus in SLE

The prolonged half-life of NETs in circulation caused by insufficient degradation by DNAse1 and clearance by macrophages provides a platform for undesired autoimmune activation. NETs activate different immune sensors of the innate immune system and induce the production of pro-inflammatory cytokines that drive disease progression. NET proteins activate the NLRP3 inflammasome and induce IL1β and IL18. IL18 induces NETosis, potentially resulting in an inflammatory feed forward loop [110–112]. Furthermore, NETs induce expression of IL6 and IL8 in human epithelial cells[113].

NETs also serve as a stimulus for the induction of TIIFN. Most studies describe pDCs as the main producers of NET-induced TIIFN production, but also monocytes can fulfil this function [114]. NETs need to be phagocytosed to stimulate intracellular DNA sensors. Their uptake is supported by NET bound

proteins such as LL37 and HMGB1 [81,87]. Notably, different groups report that oxidized mitochondrial DNA serves as stimulus TIIFN production, not only the genomic DNA component of NETs [81,84,85,115].

Although different papers suggest TLR9 as a potential NET receptor that induces TIIFN expression, its role is not completely clear. Surprisingly, TLR9 seems to be protective in SLE, since $TLR9^{-/-}$ mice present with a exacerbated renal phenotype and increased autoantibody production [116,117]. Notably, oxidized DNA and DNA-LL37 complexes induce TIIFN induction in a stimulator of interferon genes (STING) dependent manner, both in isolated human monocytes, pDCs and in an *in vivo* mouse model, indicating that the cGAS-STING pathway might be involved in NET recognition [85,114].

1.4 The cGAS STING pathway

DNA is not only a carrier of the genetic information, but also a potent stimulator of innate immune system. It can originate from viruses, bacteria or from dying cells that release DNA as a DAMP into the extracellular space. A battery of nucleic acid sensing receptor facilitates the recognition of DNA, which upon activation induce the production of TIIFN. Only recently, the cytosolic DNA sensor cGAS was discovered [118].

1.4.1 The cytosolic DNA sensor cGAS

cGAS is a cytoplasmic receptor that recognizes DNA of different origin. It senses the genomes of viruses like cytomegalovirus, herpes simplex viruse-1, vaccinia virus, adenovirus, hepatitis B virus and Kaposi-Sarcoma-Herpesvirus [119–125]. cGAS also recognizes reversely transcribed cDNA of HIV-1 and HIV-2, when the capsid membrane of the viruses is damaged by host factors [118,126]. It is important to note that many of these viruses developed mechanisms to escape cGAS recognition to prevent immune recognition. cGAS is also capable of recognizing bacterial DNA of *Mycobacterium tuberculosis* and *Francisella tularensis* [127,128]. Apart from external pathogen-derived DNA, cGAS also senses self-DNA like mitochondrial DNA, DNA damage side products or chromatin fragments [129–131]. In principal, cGAS recognizes dsDNA larger than 40 base pairs (bp) in a sequence independent manner [132,133].

The cGAS-STING signaling cascade

cGAS is a protein of approx. 59 kDa and contains two DNA binding domains and a nucleotidyltransferase domain [134]. Ligand binding induces the formation of a 2:2 complex of cGAS and DNA, resulting in a conformational change activating the nucleotidyltransferase domain, that is autoinhibited in the inactivated state [135,136]. This conformational change enables the catalysis of guanosintriphosphate (GTP) and adenosintriphosphate (ATP) to cyclic guanosine monophosphate–

adenosine monophosphate (cGAMP), a cyclic dinucleotide connected by two phosphodiester bonds that serves as a second messenger [137]. The ER-bound immune adapter molecule STING recognizes cGAMP and translocates to the Golgi-apparatus [138,139]. Upon translocation, STING recruits the kinase TANK binding protein 1 (TBK1) that phosphorylates the transcription factor Interferon regulatory factor 3 (IRF3), resulting in its dimerization and translocation into the nucleus [140]. There IRF3 binds to Interferon-stimulation response elements (ISRE) and induces the expression of TIIFN to upregulate the antiviral response [141].

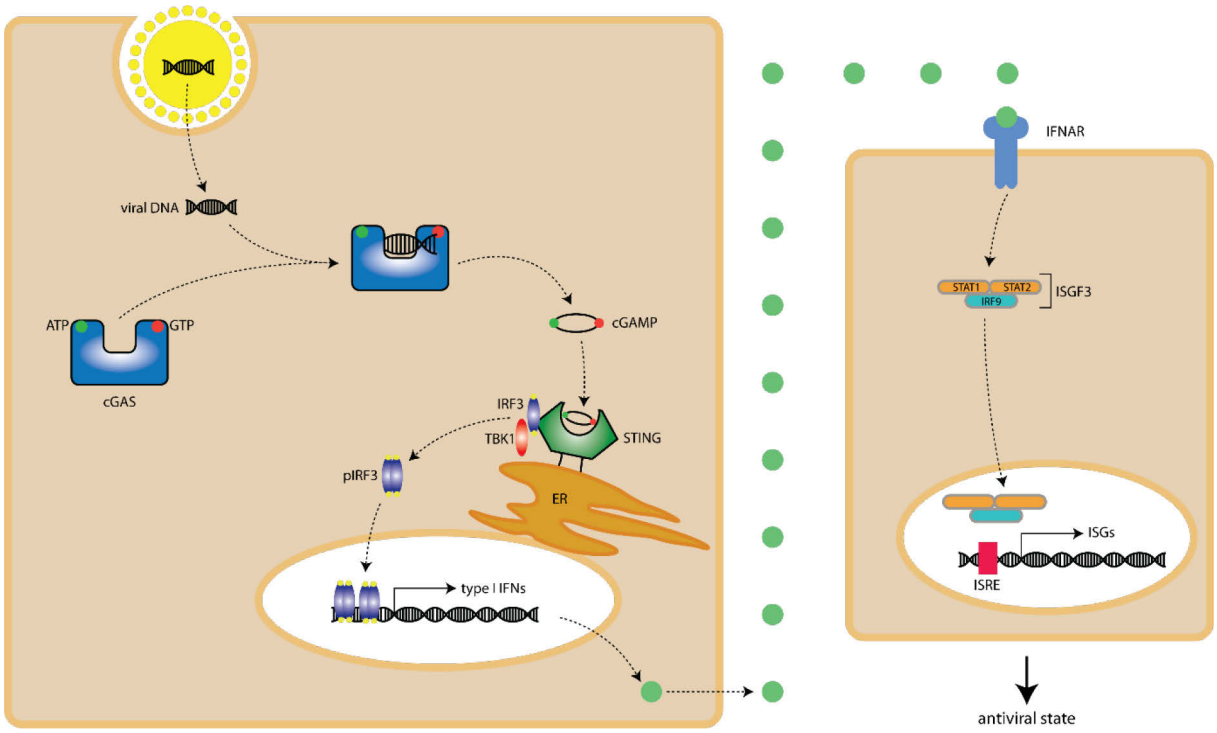

Figure 1.2 The cGAS-STING pathway
After viral entry, the viral DNA is recognized in the cytoplasm by a dimer of cGAS molecules, resulting in the production of the cyclic dinucleotide cGAMP. cGAMP activates the ER-bound signaling adapter STING, leading to the phosphorylation and translocation of the transcription factor IRF3. TIIFN are secreted and activate the IFNAR receptor of neighboring cells, inducing an antiviral state by upregulation of an array of ISGs.

1.4.2 The cGAS-STING pathway in autoinflammation

cGAS is not only able to recognize foreign DNA introduced by viruses and bacteria, but also self-DNA. It recognizes mitochondrial DNA [142] and transcripts of endogenous retroelements [143] and was shown to induce STING dependent immune activation [85]. Furthermore it was demonstrated that DNA damage induces cGAS activation [129].

Under steady conditions, excess DNA is cleared by nucleases. As described above, DNAse1 degrades DNA in the circulation. DNAse2 is located in lysosomes and degrades DNA of particles that are taken

up by endocytotic pathways. Another intracellular DNAse is TREX1, also known as DNAse3. It is localized in the cytoplasm and shuttles to the nucleus upon oxidative stress. TREX1 clears excess DNA originating from endogenous retroelements or DNA damage repair- and replication intermediates [144]. In cases where this DNA homeostasis is impaired, the cGAS-STING pathway induces severe autoinflammatory syndromes. Mice depleted of TREX1 suffer from a systemic organ inflammation and die untimely. A knockout of cGAS rescues this phenotype by reducing tissue inflammation and protects from premature lethality [145]. A similar phenotype can be observed for DNAse2$^{-/-}$ mice. The knockout is embryonic lethal and liver-resident macrophages produce high amounts of TIIFN in a STING dependent manner due to an accumulation of undigested DNA. This phenotype is rescued by cGAS [145] and IFNAR deletion [146,147]. Also in human patients, impairment of intracellular DNAses leads to the induction of autoinflammatory diseases. TREX1 insufficiency is associated with the Aircardi Goutière syndrome [148] and SLE [108], while mutations in DNAse2 are connected to an arthritis-like syndrome [149,150]. The close similarity to the murine phenotypes suggests an involvement of the cGAS-STING pathway in these diseases, although this has not been directly shown yet. Interestingly, gain-of-function mutations in STING lead to autoinflammatory diseases that share similarities with SLE [151].

1.5 Aim of the study

NETs can be beneficial to the host because they prevent spreading and kill pathogens. NET production is accompanied by the release of cytotoxic and immune-stimulatory molecules and therefore requires a tight regulation and efficient clearing system once the infection clears. Auto-inflammatory diseases, like SLE, not only show an overproduction of NETs, but also insufficient NET clearing due to limited uptake by phagocytes or non-functional DNAses. Especially the lack of functional intra- and extracellular DNAses, either caused by mutation or by blocking of accessibility, causes NET accumulation and prolonged exposure to the immune system.

cGAS, a innate sensor of microbial DNA, recognizes DNA independently of its sequence and senses self-DNA. The aim of this study was to investigate whether NETs induce expression of TIIFN by activating cGAS, to understand the role of NETs as an inflammatory stimulus. To reach this aim I took three consecutive steps. First, I investigated if isolated NETs activate cGAS in human and murine cells *in vitro*. Second, I tested if neutrophils undergoing NETosis induce cGAS in neighboring cells to produce TIIFN *in vitro*. Thirdly, I confirmed my findings in a mouse model of systemic NET induction.

Taken together, the aim of this thesis was to investigate a new mechanism of NET induced immune activation and thereby explore new intervention strategies for NET-associated diseases.

2 Results

2.1 NETs activate recombinant cGAS

NETs were initially described as a new antimicrobial defense mechanism against invading pathogens. There is an increasing body of literature suggesting that an insufficient clearance of NETs provides the basis for autoimmune activation in a plethora of diseases. The exact mechanism how NETs drive autoimmune activation is not well characterized. Here, I investigate the role of the cytosolic DNA sensor cGAS as a potential receptor of NETs.

2.1.1 Isolation of NETs

To generate NETs, I isolated human neutrophils from peripheral blood of healthy donors [35]. I determined the purity of the preparation by FACS and identified neutrophils as $CD15^{+}CD66b^{+}$ (Fig. 2.1A). The average purity was 97 %. After inducing NETosis by stimulation with 100 nM PMA for 3 h [33], I verified NET formation by immune fluorescence where NETs stained positive for DNA, NE and a histone/DNA complex (Fig. 2.1B).

To isolate NETs, I stimulated neutrophils for 4 h with PMA (100 nM), washed them with PBS and detached them from the plate by scraping. Since the harvested NETs formed large aggregates, I sonicated or digested them with DNAse1 to generate smaller fragments for further experiments (see paragraph 2.1.2, Fig. 2.2B). I analyzed the protein content by mass spectrometry. As expected, I detected NET-associated proteins that were identified before like NE, MPO, Cathepsin G and different histone variants (Fig. 2.1C) [34]. The full proteome is listed in appendix A.

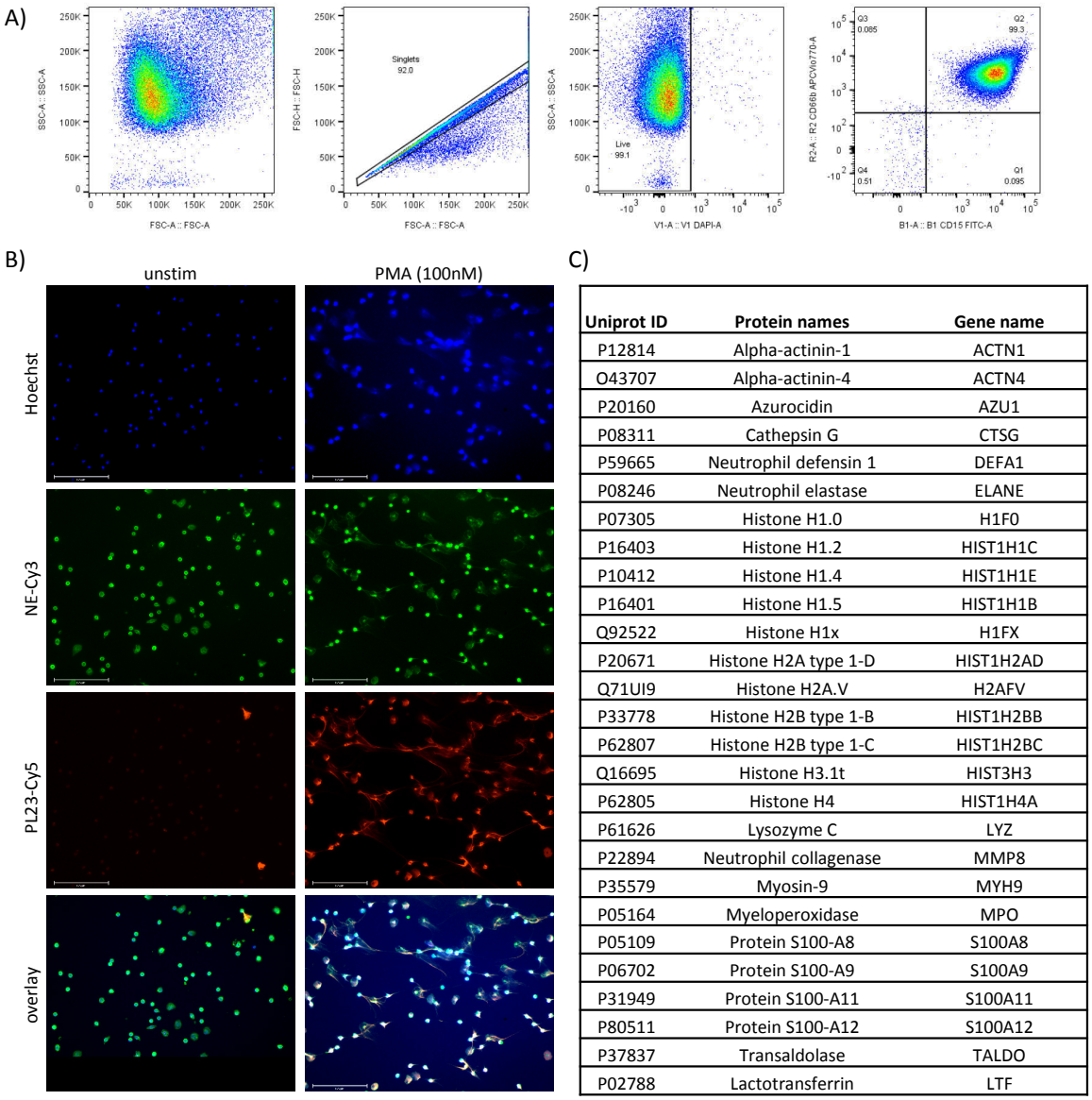

C)

Uniprot ID	Protein names	Gene name
P12814	Alpha-actinin-1	ACTN1
O43707	Alpha-actinin-4	ACTN4
P20160	Azurocidin	AZU1
P08311	Cathepsin G	CTSG
P59665	Neutrophil defensin 1	DEFA1
P08246	Neutrophil elastase	ELANE
P07305	Histone H1.0	H1F0
P16403	Histone H1.2	HIST1H1C
P10412	Histone H1.4	HIST1H1E
P16401	Histone H1.5	HIST1H1B
Q92522	Histone H1x	H1FX
P20671	Histone H2A type 1-D	HIST1H2AD
Q71UI9	Histone H2A.V	H2AFV
P33778	Histone H2B type 1-B	HIST1H2BB
P62807	Histone H2B type 1-C	HIST1H2BC
Q16695	Histone H3.1t	HIST3H3
P62805	Histone H4	HIST1H4A
P61626	Lysozyme C	LYZ
P22894	Neutrophil collagenase	MMP8
P35579	Myosin-9	MYH9
P05164	Myeloperoxidase	MPO
P05109	Protein S100-A8	S100A8
P06702	Protein S100-A9	S100A9
P31949	Protein S100-A11	S100A11
P80511	Protein S100-A12	S100A12
P37837	Transaldolase	TALDO
P02788	Lactotransferrin	LTF

Figure 2.1 Characterization of Neutrophil extracellular traps
A) Gating strategy to determine the purity and viability of isolated human neutrophils that were identified as $DAPI^-$ $CD15^+CD66b^+$ by FACS. B) NET formation of unstimulated or PMA (100 nM) treated neutrophils was analyzed by immunofluorescence staining with DAPI (blue), anti-NE- (green) and anti-DNA-histone-complex staining (red). C) Excerpt of NET associated proteins identified by mass spectrometry.

2.1.2 Isolated NETs activated recombinant human and murine cGAS

Upon activation with DNA, cGAS produces the second messenger cGAMP that activates the downstream signaling adaptor STING [152,153]. To show that NETs are a substrate for cGAS, I sonicated them and incubated them with recombinant cGAS in the presence of radioactively labeled ATP. Plasmid DNA served as a positive control. This resulted in the production of the second messenger cGAMP which I detected by thin-layer chromatography, showing that NETs are recognized by cGAS (Fig. 2.2A).

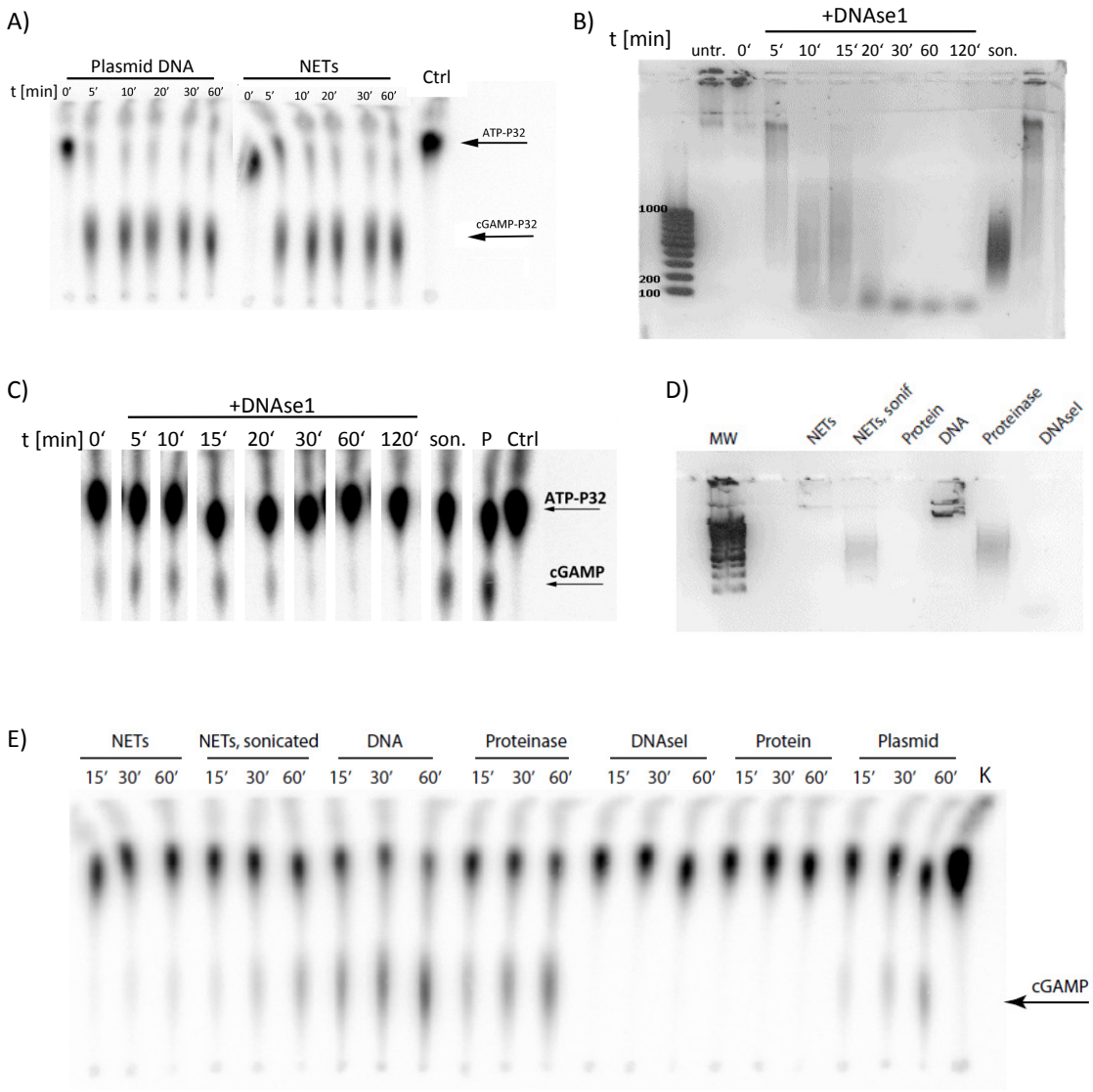

Figure 2.2 Recombinant cGAS recognizes isolated human NETs
A) Stimulation of murine recombinant cGAS with plasmid DNA or sonicated NETs in the presence of radioactively labeled ATP for the indicate time. cGAMP production was visualized by thin-layer chromatography. B) DNAse1 digested NETs were separated by agarose gel electrophoresis and C) used for stimulation of human recombinant cGAS. The indicated time reflects the time of digestion with DNAse1, only the 10 min time point of incubation of NETs with cGAS and ATP is shown. D) NETs were separated into DNA and proteins or digested with DNAse1 or Proteinase K. Resulting fractions were analyzed using agarose-gel electrophoresis and subsequently used to stimulate recombinant cGAS for the indicated time (E).

I digested NETs with DNAse1 for different times and analyzed the resulting fragment sizes by agarose gel electrophoresis (Fig. 2.2B). Due to their high charge, undigested NETs form large aggregates that barely migrate into the gel. NET digestion with DNAse 1 results in smaller fragments of heterogeneous sizes. After 20 min, NET fragments reached nucleosome size of approx. 150 bp (Fig. 2.2B). I stimulated recombinant cGAS with the resulting fragments (Fig. 2.2C). Undigested NETs are poor stimulators of cGAS, probably due to their high charge-dependent aggregation status, leaving only few available cGAS

binding sites. NETs digested with DNAse1 for up to 20min activated cGAS, whereas NET fragments of nucleosome size (150 bp) did not activate cGAS anymore. This is consistent with previous publications suggesting that cGAS requires a minimum length of 36 bp of free DNA for activation [137], which is not present in nucleosomes because the remaining DNA is wrapped around the histone core and thereby inaccessible for cGAS. To proof that the DNA of NETs activates cGAS, I extracted the nucleic acid from NETs by phenol chloroform extraction as well as digested them for 1h with either DNAse1 or Proteinase K. In parallel, I isolated NET-bound proteins. DNA was absent in the protein extract and in NETs extensively treated with DNAse1-treated samples, whereas DNA was detectable in NETs treated with Proteinase K (Fig. 2.2D). As expected, the isolated DNA or proteinase-digested NETs induced cGAMP production by recombinant cGAS, whereas NET proteins and DNAse1-digested NETs failed to activate a response (Fig. 2.2E). In summary, these results demonstrate that the DNA of NETs is a potent activator of recombinant cGAS.

2.2 Isolated NETs activate human and murine immune cells *in vitro*

After showing that NETs are a substrate for cGAS I investigated if they are recognized by cGAS in living cells *in vitro*.

2.2.1 Generation and characterization targeted CRISPR knockouts in human THP1 cells and murine immortalized Balb/c macrophages

To test the activation of cGAS by NETs *in vitro*, I generated an number of gene specific knockout mutants (summarized in 4.1.4) using the clustered regulary interspeaced short palindromic repeats (CRISPR)/Cas9 technology [154,155]. As target cells I chose the human monocytic cell line THP1 or murine immortalized Balb/c macrophages. In total, I targeted seven human and eight murine genes with two independent guide RNAs (gRNAs) each. For each gRNA I generated single cell clones by limited dilution cloning, sequenced 32 clones per construct by next generation sequencing and analyzed the mutations using the Outknocker tool [156]. Outknocker compares the retrieved sequences to the genomic reference locus and creates a pie chart containing a piece for every uniquely identified indel detected, while the pie chart size corresponds to the number of reads for that locus. Examples of the graphical output are shown for human and murine cGAS and STING (gene name hTMEM173) in Fig. 2.3. Using Outknocker I verified out of frame mutations in all targeted genes, resulting in a total of 168 modified single clones.

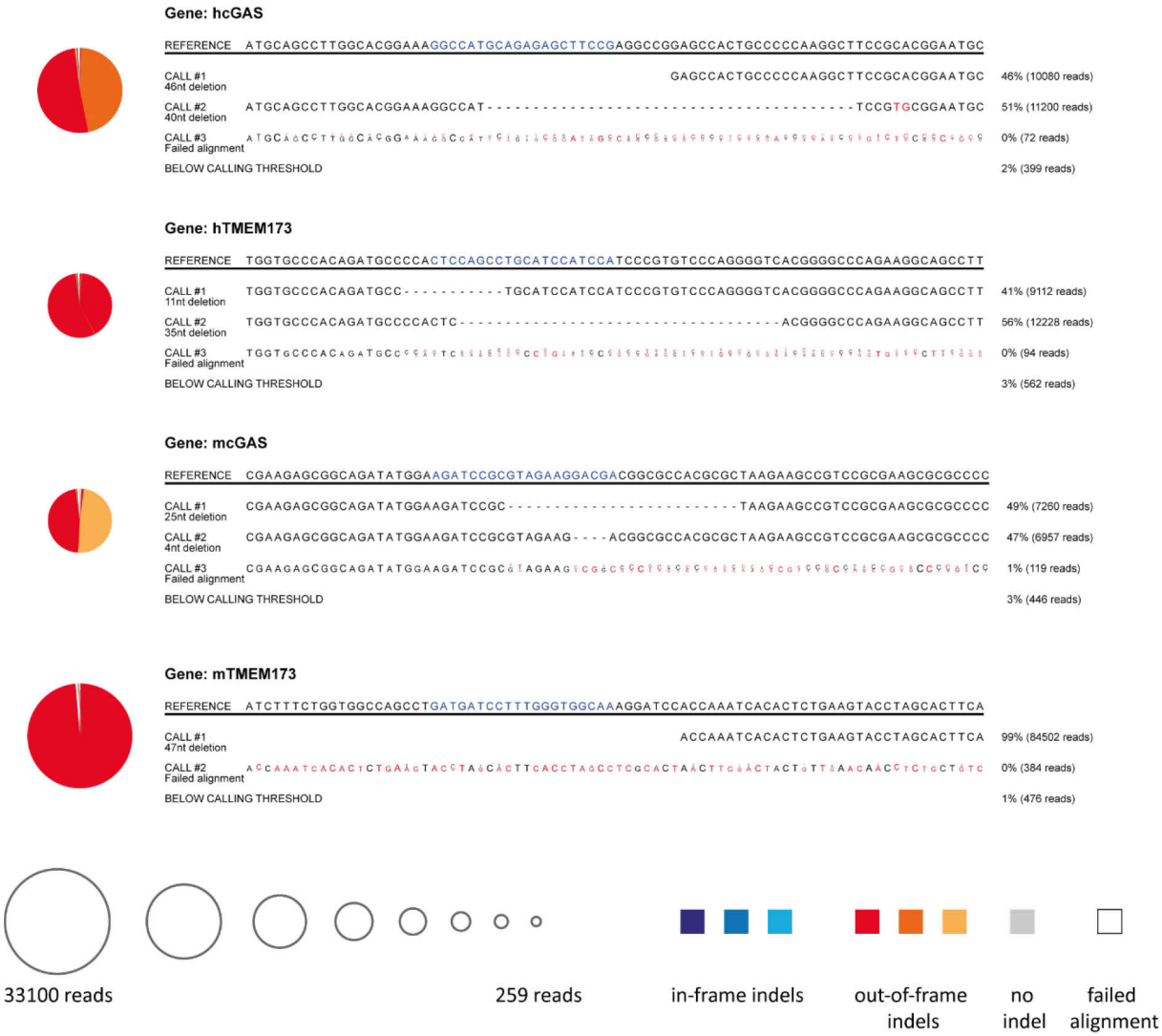

Figure 2.3 Generation of genetic knockouts in the human THP-1 cell line and immortalized Balb/c macrophages using CRISPR
Representative Outknocker analysis for knockouts generated by CRISPR/Cas9 in human THP1 or murine immortalized Balb/C macrophages targeting cGAS or STING (TMEM173). The pie chart represents a clone, its size representing the numbers of processed reads and its fractions uniquely detected indels in comparison to the reference sequence.

2.2.2 Detection of TIIFN expression in human and murine cells

The activation of cGAS by DNA ligands ultimately results in the production of TIIFN [134]. To use TIIFN production as a functional readout for NET recognition by cGAS, I established systems to measure TIIFN in both human and murine primary cells.

Human PBMCs expressed both hIFNA1 and hIFNB in response to stimulation with the TLR4 agonist LPS, the TLR3 agonist polyinosinic:polycytidylic acid (p(I:C), the TLR9 agonist ODN2216 and lipofectamine transfection with synthetic dsDNA-sequence poly(deoxyadenylic-deoxythymidylic) acid (pdAdT) (Fig. 2.4A). Interestingly, p(I:C) and pdAdT induced stronger hIFNB expression than hIFNA1. To confirm

protein production, I used a reporter cell line that specifically produces a secreted phosphatase upon stimulation with human TIIFN, but not with IFNγ (Fig. 2.4B), that can be quantified by color-shift of the phosphatase substrate.

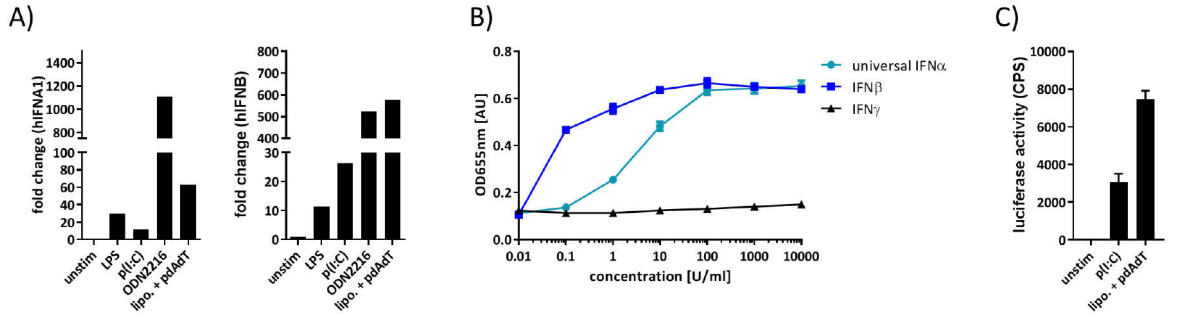

Figure 2.4 Measurement of TIIFN expression in the human and murine system
A) Expression of IFNA1 and IFNB by PBMCs stimulated with LPS (500 ng/ml), p(I:C) (1 µg/ml), ODN2216 (5 µM) or transfected with pdAdT (2 µg/ml) was analyzed by qPCR. B) HEK Blue IFNα/β reporter cells were stimulated with serial dilution of human recombinant universal IFNα, IFNβ or IFNγ. Reporter cell activity was quantified by Quanti-Blue assay (OD655 nm). C) Murine Wildtype BMM were stimulated with p(I:C) (1 µg/ml) or transfected with pdAdT (2 µg/ml). TIIFN in the supernatant were assessed using reporter cells expressing luciferase under the control of IFNAR. All results are presented as mean±SD (n=3).

To validate the murine system, I stimulated primary Wildtype BMM with p(I:C) or transfected them with pdAdT. I detected TIIFN production using a reporter cell line expressing luciferase upon TIIFN recognition (Fig. 2.4C) [157].

Taken together these results show that I are able to measure TIIFN production in both murine and human cells.

2.2.3 Isolated NETs induce TIIFN production in human immune cells *in vitro*

I analyzed the TIIFN response of different cell types towards isolated NETs. Shortly after neutrophils arrive at the side of inflammation, monocytes migrate into the inflammatory side and differentiate into macrophages [158]. Due to their high phagocytic potential and their role in the resolution of inflammation, macrophages are promising candidates for the uptake of NETs. Interestingly, an earlier publication described the induction of TIIFN by macrophages transfected with NETs, showing that they are able to respond to NET material [103].

I stimulated human PBMCs, monocyte-derived macrophages (MDM), as well as the monocytic cell line THP1 before and after differentiation into macrophage-like cells and measured their TIIFN response. Of note, NETs that were frozen and stored did not induce TIIFN production in any of the cell types

when added on cells. However, when I transfected those NETs as described by Ferrera & Fadeel (2013), TIIFN production is initiated. Freshly isolated NETs on the other hand induced a response in MDM (Fig. 2.5A), but not in the other primary cells or the THP1 cells. The inhibition of NE by two different inhibitors resulted in a reduced TIIFN production of macrophages, indicating that NE is required in that process (Fig. 2.5B). Importantly, the NE inhibitors did not reduce activation of macrophages by transfected pdAdT, suggesting that the NE effect is NET specific (Fig. 2.5C). Utilization of a pan-Cathepsin (K777) or a pan-caspase (zVAD-FMK) inhibitor had no influence on macrophage activation (Fig. 2.5B and C).

It is described that mitochondrial DNA (mtDNA) in NETs is interferogenic [85,115]. To assess the contribution of mtDNA during NET induced macrophage activation I isolated mtDNA from HEK cells and stimulated macrophages in comparison to fresh NETs. mtDNA did not induce TIIFN production in my hands. (Fig. 2.5D).

In the next step, I aimed to verify that the NET induced TIIFN production is cGAS dependent. Since genetic manipulation of primary MDM is not feasible and THP1 cells do not respond to NETs alone (Fig. 2.5A), I transfected THP1 CRISPR clones with NETs and analyzed TIIFN induction. Wildtype, scrambled (scr) and two clones targeting Neutrophil Elastase (NE), which served as control, produced TIIFN upon stimulation, whereas clones carrying mutations for cGAS, STING or IRF3 failed to do so. Furthermore, I tested knockouts of other DNA sensors. Clones carrying mutations deficient for the DNA sensors DAI [159], Gamma-interferon-inducible protein 16 (IFI16) [133] or TLR9 [160] produced TIIFN levels comparable to the control clones (Fig. 2.5E), indicating that NETs are specifically recognized by cGAS.

NET stimulation induces other signs of cGAS activation. cGAS activation results in phosphorylation of the transcription factor IRF3 [134,138], that regulates the expression of TIIFN. I showed IRF3 phosphorylation after transfection of human primary monocytes with NETs (Fig. 2.5F), indicating cGAS activation.

Complement factors, autoantibodies or DNA binding proteins [84,161,162] in the serum of SLE patients facilitate the uptake of NETs in immune cells. To test if these factors convey NETs into target cells and induce cGAS activation I stimulated human PBMCs with NETs in the presence of serum from eight SLE patients or healthy controls. The sera alone were not able to induce PBMC activation, whereas all SLE sera were able to induce TIIFN induction in the presence of NETs, while only a subgroup of the control sera was able to do so (responders) and the other was not (non-responders) (Fig. 2.5G).

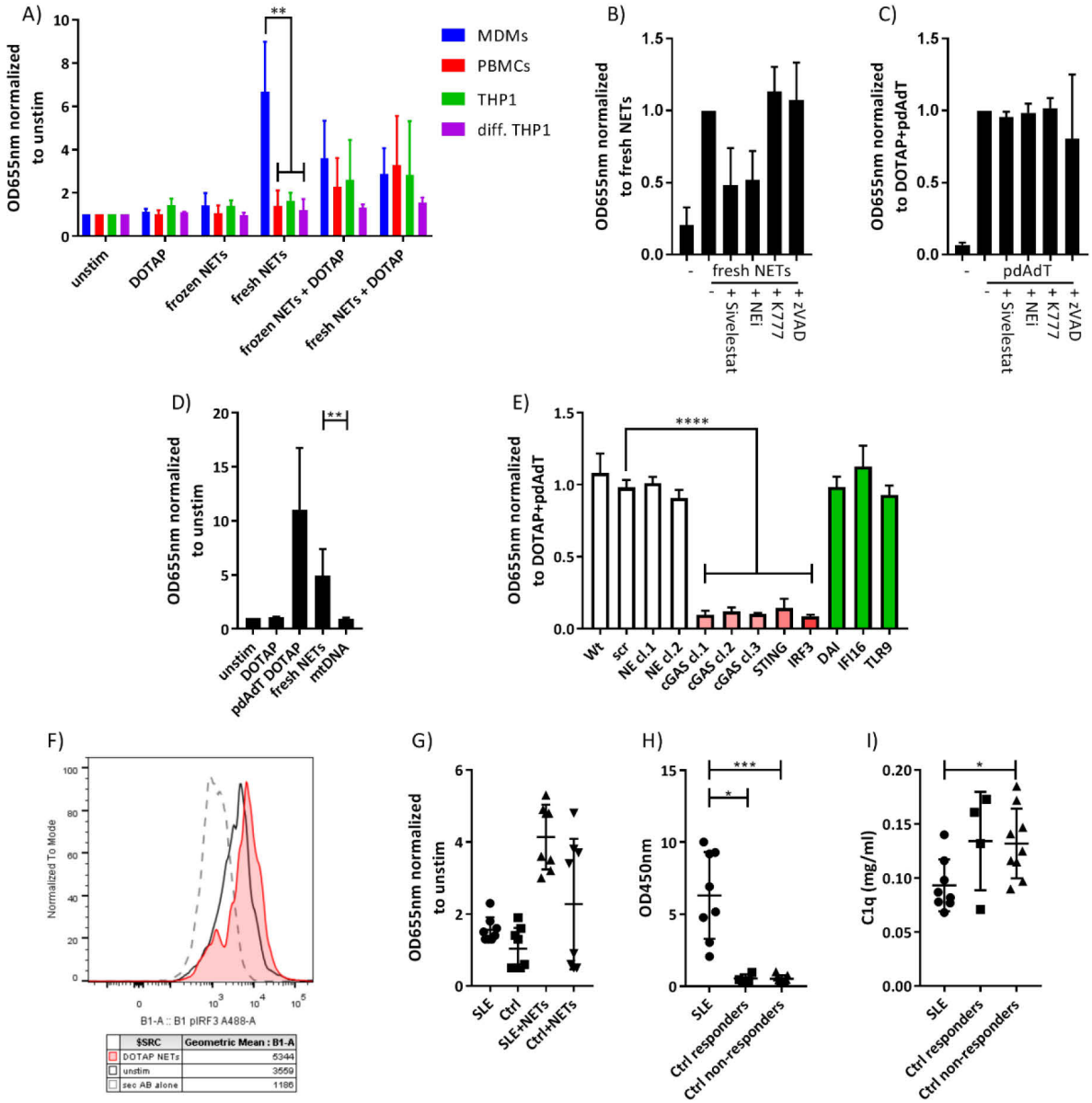

Figure 2.5 Isolated NETs induce TIIFN production in human cells by activating cGAS in vitro
A) TIIFN production of MDMs, PBMC, THP1 cells and PMA-differentiated THP1 cells after stimulation with NETs (n=3). B/C) TIIFN production of MDM treated with either with fresh NETs (B) or pdAdT (C) in the presence of NE inhibitors. D) TIIFN production of MDMs treated with mtDNA. (n=3) E) THP1 CRISPR clones transfected with NETs. TIIFN production was normalized to pdAdT transfection (n=3). F) Representative FACS analysis of IRF3 phosphorylation in human monocytes after stimulation with NETs. G) Summary of stimulation of PBMCs with NETs and sera of different donors normalized to unstimulated cells. (n=3) H) ELISA for ANA-antibodies and I) complement factor C1q in the sera of SLE patients and healthy control donors. A, B, C, D, E, G) TIIFN production was quantified by Interferon-reporter cell assay, values represent mean±SD. Data were analyzed by Kruskal-Wallis test α=0,05 followed by Dunn's multiple comparison test α=0,05. *p<0,05, ***p<0,001,****p<0,0001.

To determine the factor that separates the responder and the non-responder healthy control sera in their ability to induce TIIFN production together with NETs, I measured the presence of anti neutrophil

cytoplasmic antibodies and complement factor C1q. I did not detect a difference in the two analyzed factors between the two groups (Fig. 2.5H and I).

Taken together these results show that isolated NETs induce TIIFN production in human cells *in vitro* by activating the cGAS-STING pathway. Notably, NETs do not need transfection to activate the cytosolic DNA sensor.

2.2.4 Isolated NETs induce TIIFN expression in murine immune cells *in vitro*

To verify the finding made with human cells I analyzed if NETs also induce TIIFN production in murine cells. I stimulated murine BMM with increasing concentrations of sonicated NETs with DOTAP or NETs that had been treated with DNAse1 for different time periods. I measured a dose-dependent production of TIIFN after stimulation, as well as a decreasing response the longer the NETs were digested with DNAse1 (Fig. 2.6A).

Next, I tested the hypothesis that the NET-induced TIIFN production is cGAS-dependent. I treated immortalized Balb/c BMM carrying knockouts in different target genes with isolated NETs and DOTAP. Scrambled control cells or cells with a knockout of NE that I used as a negative control produced TIIFN as expected. Also, a clone carrying a mutation in TLR9 produced comparable amounts of TIIFN. Importantly, clones with a knockout of cGAS or STING produced significantly less cytokines upon stimulation with NETs (Fig. 2.6B). Finally, I tested knockouts of two isoforms of DNAse2. The DNAse2 knockout is embryonic lethal in mice due to an accumulation of endogenous nuclear DNA, a phenotype that can be rescued by STING depletion [147,163]. The link between DNAse2 deficiency and STING activation led us to investigate the role of DNAse2 in NET recognition. Clones deficient for DNAse2 did not produce significantly different amounts of TIIFN than control cells (Fig. 2.6B).

To further consolidate the role of cGAS in NET recognition I compared primary BMM of Wildtype and cGAS$^{-/-}$ mice. Upon stimulation, I detected TIIFN production by Wildtype BMM, while cGAS$^{-/-}$ failed to induce a TIIFN response to NETs (Fig. 2.6C). Interestingly, cGAS$^{-/-}$ BMM did not respond to pdAdT stimulation either, although pdAdT is thought to be recognized by a variety of DNA sensors and also indirectly by the RNA sensor RIG-I.

To analyze general functionality of cGAS$^{-/-}$ BMM, I tested NLRP3 and AIM2 inflammasome activation. Interestingly, other groups reported that cGAS has a role in DNA inflammasome activation [164,165]. I primed Wildtype, cGAS$^{-/-}$, AIM2$^{-/-}$, MYD88$^{-/-}$ and CASP1/11$^{-/-}$ BMM with LPS and further stimulated them with Nigericin (activator of NLRP3), pdAdT (activator of AIM2) or NETs. All cells of different genotypes except cGAS$^{-/-}$ produced TIIFN upon NET stimulation (Fig. 2.6D). Notably, AIM2$^{-/-}$, MYD88$^{-/-}$ and

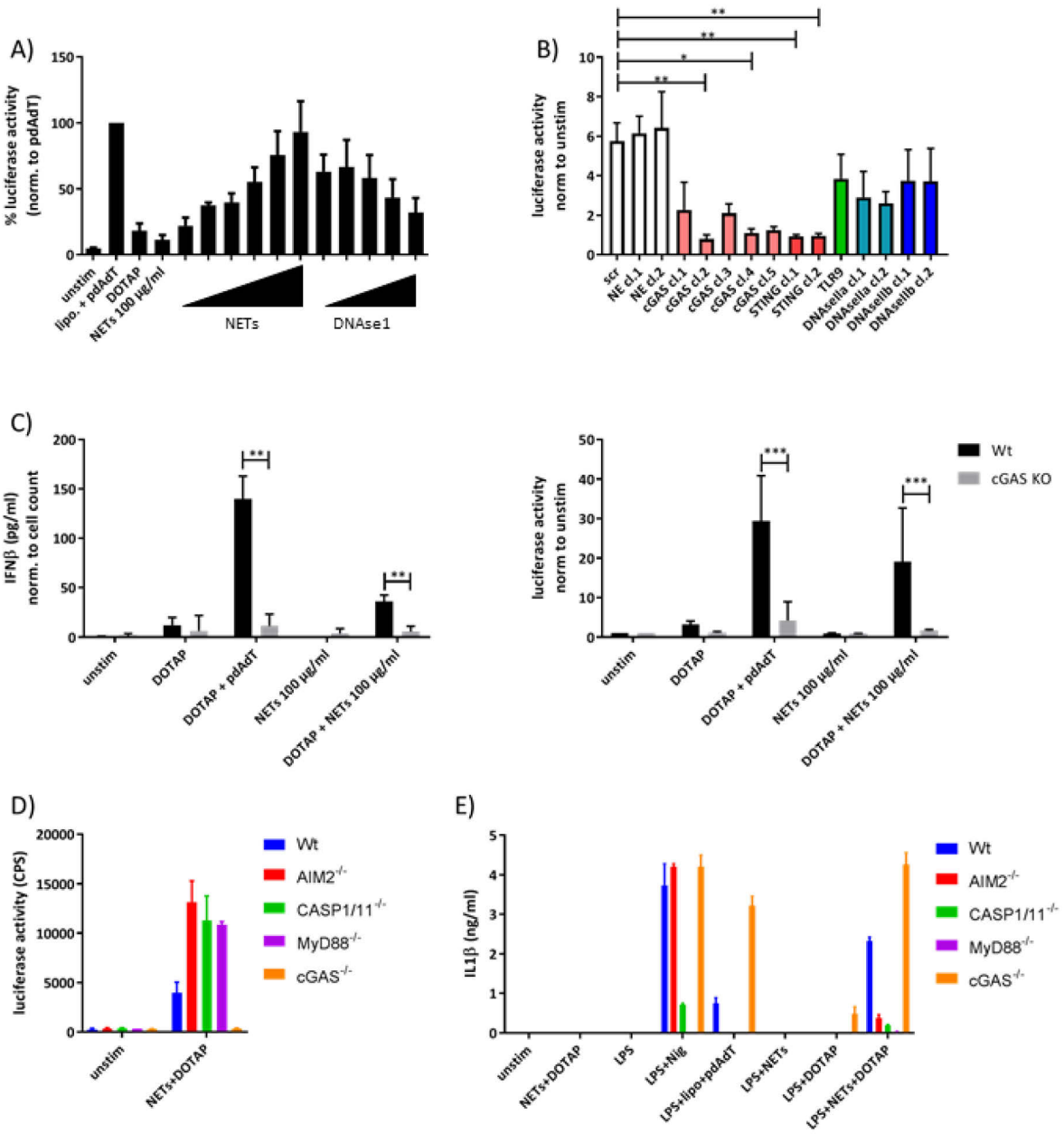

Figure 2.6 Isolated NETs induce TIIFN expression in murine primary cells
A) TIIFN production by primary BMM stimulated with increasing amounts of NETs (100 µg/ml -1 µg/ml) with DOTAP or NETs digested with DNAse1 for different periods (1-20 min) and DOTAP (n=3). B) Stimulation of immortalized Balb/c BMM CRISPR clones with NETs and DOTAP, interferon production values are normalized to the cell count. The data were analyzed by Kruskal-Wallis test (α=0,05) followed by Dunn's multiple comparison test (α=0,05), *p<0,05, **p<0,01. (n=4) C) Comparison of interferon production of primary BMM from Wildtype and cGAS$^{-/-}$ mice stimulated with NETs. The data were analyzed by Mann-Whitney test (α=0,05), **p<0,01, ***p<0,001, (n=4). D) Primary BMM of different genotypes were primed with LPS (500 ng/ml) or left unprimed and subsequently stimulated with NETs, Nigericin (15 µM) or pdAdT (2 µg/ml). TIIFN andIL1β production was measured. (n=3) A-D) TIIFN production was measured by luciferase reporter cell assay, IL1β and IFNβ were quantified by ELISA. Values are presented as mean±SD.

CASP1/11$^{-/-}$ BMM produced higher amounts of TIIFN than Wildtype BMM. As expected, Wildtype, cGAS$^{-/-}$ and AIM2$^{-/-}$ BMM produced IL1β after NLRP3 activation with LPS and Nigericin, while MyD88$^{-/-}$ and CASP1/11$^{-/-}$ did not respond. Upon LPS priming and stimulation with the DNA stimuli pdAdT and NETs, only Wildtype and cGAS$^{-/-}$ cells produced IL1β, while AIM2$^{-/-}$, MyD88$^{-/-}$ and CASP1/11$^{-/-}$ cells were

not activated (Fig. 2.6E). Here, cGAS$^{-/-}$ produced more IL1β than Wildtype. These data show that cGAS depletion does not affect inflammasome activation and that cGAS$^{-/-}$ BMM are functional in responding to inflammasome stimuli.

2.3 Neutrophil undergoing NETosis activate human immune cells *in vitro*

I demonstrated that recombinant cGAS recognizes isolated NETs and that these are able to induce TIIFN in human and murine primary cells by activating the cGAS-STING axis. In the next section, I analyze the ability of neutrophils undergoing NETosis to induce TIIFN expression in human primary target cells directly.

2.3.1 Co-cultivation of NET-forming neutrophils with human immune cells induces TIIFN

I co-cultivated human PBMCs and neutrophils in the presence of NET-inducing stimuli and analyzed TIIFN expression. PBMCs co-cultivated with PMA-stimulated neutrophils (Fig. 2.7A) upregulate the expression of the TIIFN IFNα and IFNβ, when compared to unstimulated PBMCs. I observed the same result when I coincubated PBMCs with ConA activated neutrophils (Fig. 2.7B). Since IFNα and IFNβ expression significantly correlate with each other (Fig. 2.7C), I further on only present IFNα expression.

PBMCs consist of T-, B-, NK-cells, monocytes and dendritic cells [166], hence I investigated which cell type is responsible for TIIFN production upon NET recognition. Experimental evidence shows that monocytes [114] and plasmacytoid dendritic cells (pDCs) [81,87] are promising candidates for NET recognition. To test this, I isolated monocytes and pDCs and co-cultivated them with neutrophils undergoing NETosis. Both monocytes and pDCs expressed TIIFN when stimulated with PMA stimulated neutrophils (Fig. 2.7D and E).

I analyzed the supernatants of co-cultures to show that neutrophils undergoing NETosis do not only induce TIIFN expression but also secretion. I detected significant release of bioactive TIIFN by a reporter cell assay. Furthermore I were able to detect IFNα and the interferon surrogate marker CXCL10 [167] by ELISA (Fig. 2.7F-H).

Taken together, these results show that neutrophils undergoing NETosis induce TIIFN production in neighboring target cells.

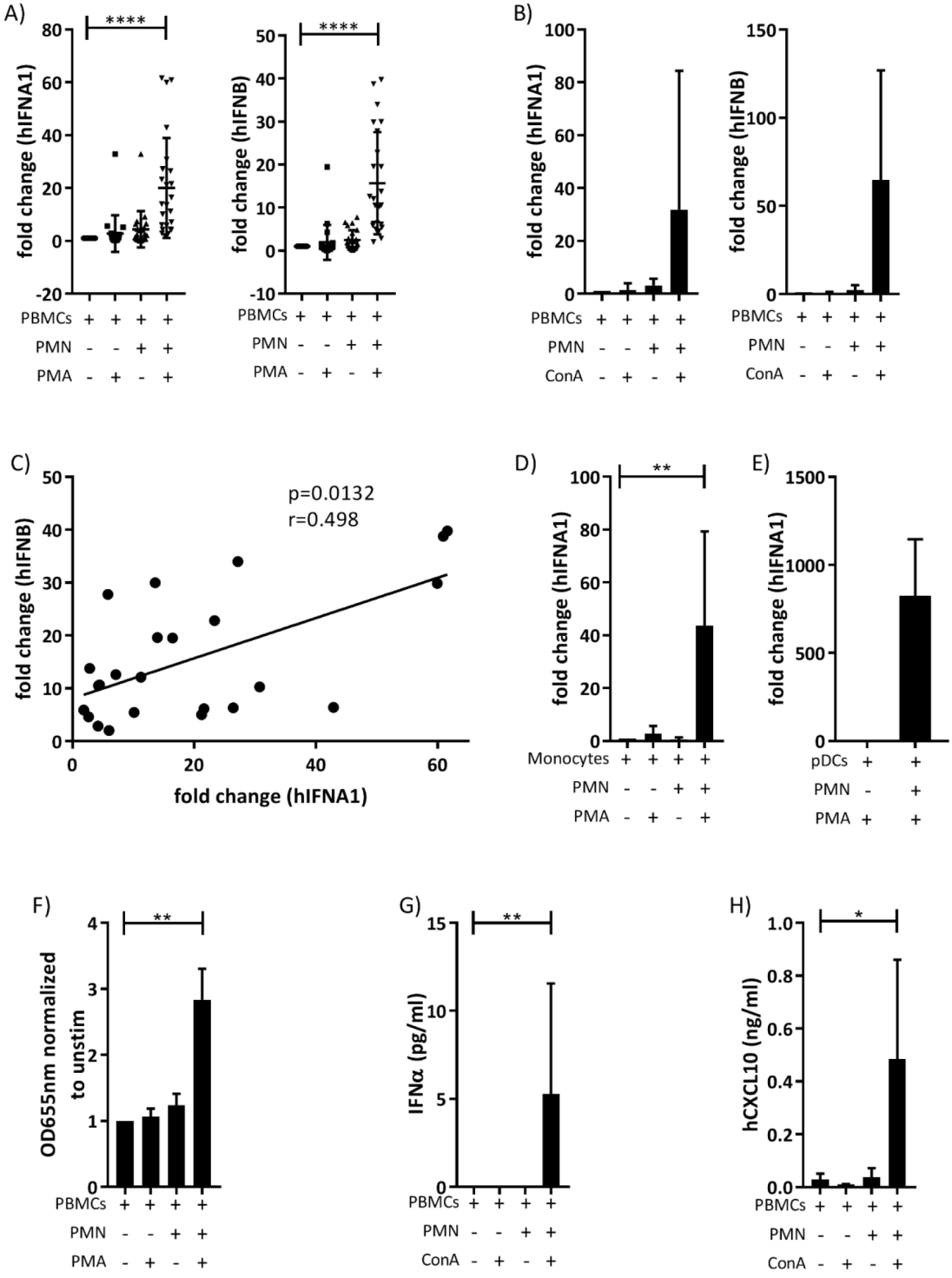

Figure 2.7 Induction of TIIFN in PBMCs by neutrophils undergoing NETosis in vitro

Co-cultivation of human PBMCs with neutrophils in the presence of A) PMA (n=24) or B) ConA (n=5). Data were analyzed by Kruskal-Wallis test (α=0,05) followed by Dunn's multiple comparison test (α=0,05), ****p<0,0001. C) Correlation of IFNA1 and IFNB expression, analyzed using Spearman r test (α=0,05), *p<0,05. D) TIIFN expression after co-cultivation of PMA-stimulated neutrophils with D) monocytes (n=5) or E) pDCs (n=3). F-H) Measurement of cytokine production in co-cultivation supernatants using F) a interferon reporter cell assay (n=5) or G) ELISA for human IFNα (n=11) and H) human CXCL10 (n=4). Data were analyzed by Mann-Whitney test (α=0,05), *p<0,05, **p<0,01. Values represent the mean±SD. A-E) TIIFN expression was measured by qPCR.

2.3.2 The induction of TIIFN by neutrophils is cGAS-dependent

To show that TIIFN expression in human PBMCs activated by neutrophils undergoing NETosis is dependent on cGAS, I repeated the co-cultivation in the presence of pharmacological inhibitors. The inhibition of cGAS by RU.521 [168] resulted in a significantly decreased TIIFN expression when PBMCs were co-cultivated with neutrophils and PMA. This result was supported by the observation that the inhibition of the downstream signaling molecules STING by CCCP and TBK1 by Amlexanox show the same effect (Fig. 2.8A). To prove that the observed effect is not due to reduced NET formation I stimulated neutrophils with PMA in the presence of the above mentioned inhibitors. The inhibitors did not influence NET formation (Fig. 2.8B), indicating that they reduce TIIFN expression by inhibiting their corresponding target molecule. Furthermore, I co-cultivated PMA-differentiated THP1 CRISPR clones with primary neutrophils undergoing NETosis. Clones with knockouts in cGAS and STING expressed significantly less TIIFN when compared to scrambled. A clone carrying a mutation IRF3 showed a markedly, but not significant, reduction (Fig. 2.8C). NETs and complexes of self-DNA and antimicrobial peptides were shown to induce TIIFN by a TLR9-dependent mechanism before [81,84,87]. To investigate if TLR9 is involved in my model I co-cultivated PBMCs with neutrophils undergoing NETosis in the presence of Bafilomycin A1, a potent inhibitor of lysosomal TLRs [169,170]. I did not detect a difference in TIIFN expression between co-cultivations with or without Bafilomycin A1 (Fig. 2.8C), indicating that TLR9 is not involved in NET recognition in my experimental setting.

These results show that PBMCs recognize NETs by the cGAS-STING-pathways.

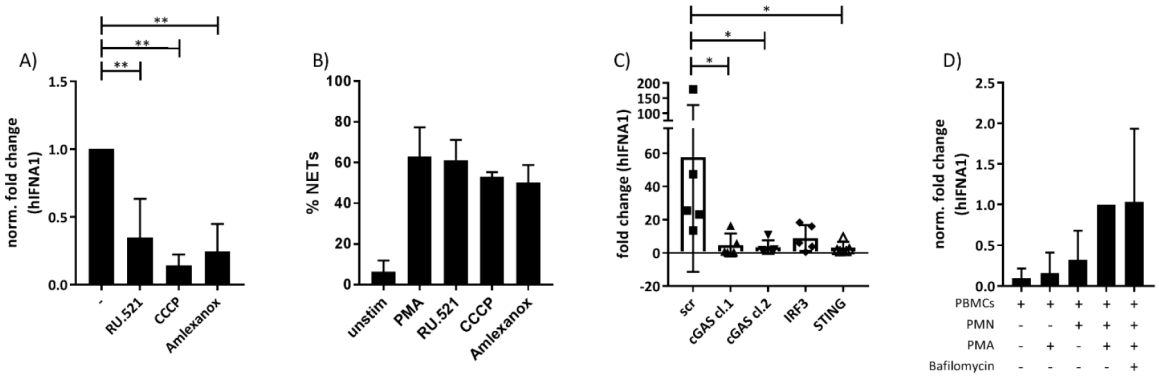

Figure 2.8 TIIFN induction by neutrophils is cGAS-dependent
A) Co-cultivation of human PBMCs with neutrophils and PMA in the presence of RU.521 (10 µM) (n=7), CCCP (10 µM) (n=4) or Amlexanox (10 µg/ml) (n=4). hIFNA1 expression was quantified by qPCR, values were normalized to co-cultivation without inhibitors B) Human neutrophils stimulated with 100 nM PMA in the presence of indicated inhibitors. NET formation was assessed by immunofluorescence staining. C) Co-cultivation of PMA-differentiated THP1 CRISPR clones with neutrophils and 100 nM PMA. (n=5) D) Co-cultivation of human PBMCs and neutrophils in the presence of 100 nM PMA and Bafilomycin (1 µM) (n=4). Induction of TIIFN was quantified by qPCR. Results are presented as mean±SD. The results were analyzed using Kruskal-Wallis test (α=0,05) followed by Dunn's multiple comparison test (α=0,05), *p<0,05, **p<0,01.

2.3.3 DNAse1 enhances the TIIFN expression in PBMCs co-cultivated with NET-forming neutrophils

In the circulation of the human body NETs are degraded by the exonuclease DNAse1 [101,171]. To determine the effect of DNAse1 on TIIFN induction by neutrophils undergoing NETosis, I co-cultivated PBMCs with neutrophils and PMA in the presence of the enzyme. DNAse1 treatment increased the production of TIIFN by PBMCs after co-cultivation with neutrophils undergoing NETosis (Fig. 2.9).

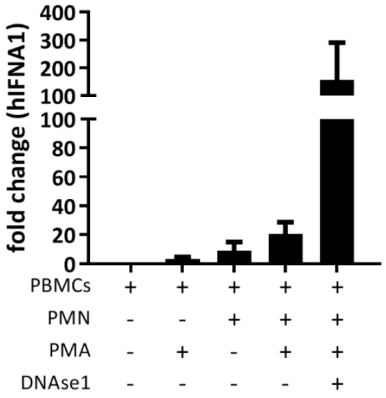

Figure 2.9 Presence of DNAse1 increases TIIFN expression in co-cultivation system
Co-cultivation of PBMCs and PMA stimulated PMN in the presence of DNAse1 (5U/ml). hIFNA1 expression was quantified by qPCR. Data represent mean ± SD. (n=4)

2.3.4 Neutrophil mediated TIIFN expression in PBMCs is dependent on NET-formation

So far, I showed that neutrophils undergoing NETosis are able to induce TIIFN production in PBMCs. During the process of NETosis the cell undergoes necrosis-like disintegration, membrane rupture and releases a large variety of molecules into the extracellular space [35]. To ensure that NETs themselves induce the observed TIIFN expression, I co-cultivated PBMCs with neutrophils in the presence of fMLP to induce degranulation. The release of granular content did not induce TIIFN expression (Fig. 2.10A). Furthermore, I did not detect TIIFN induction when I stimulated PBMCs with the supernatant of cultured neutrophils in combination with PMA (Fig. 2.10A).

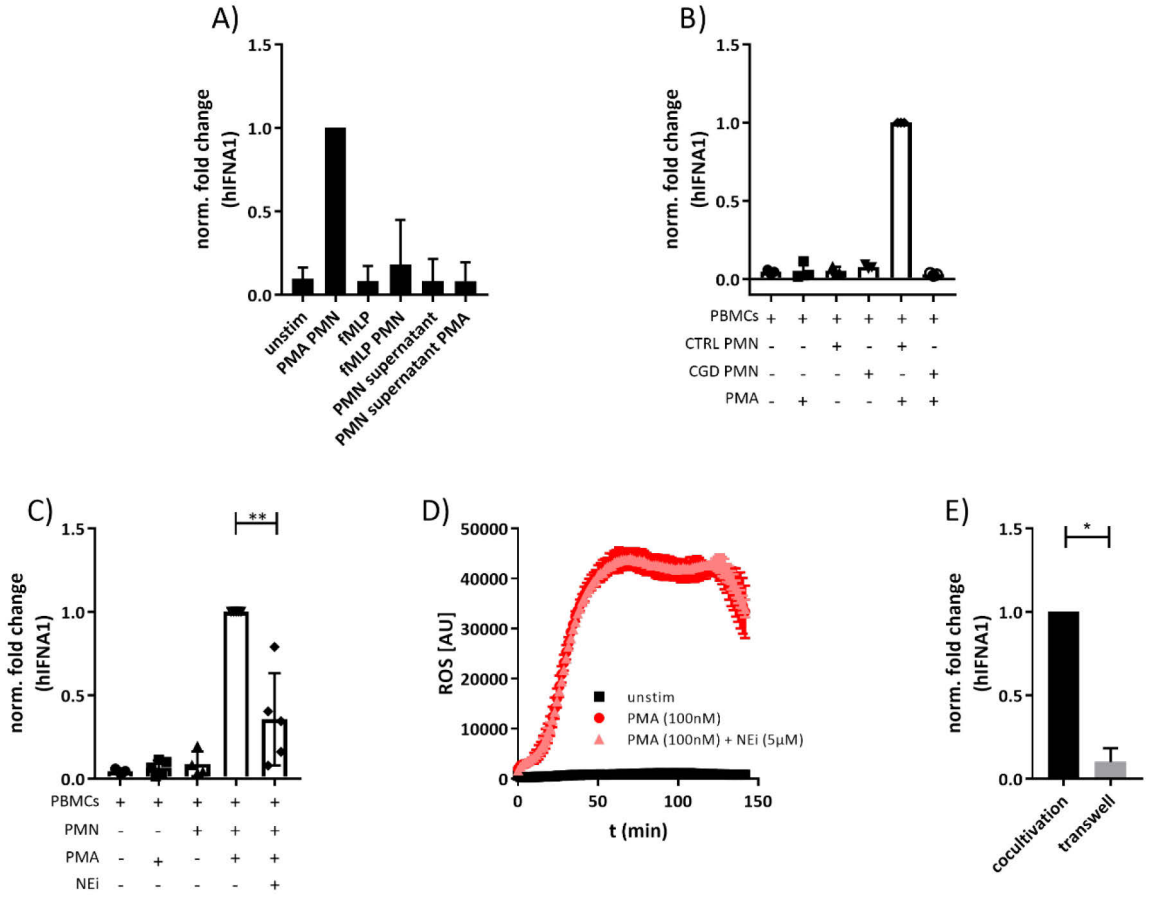

Figure 2.10 Neutrophils induce cGAS-dependent TIIFN expression by releasing NETs
A) PBMCs stimulated with different control stimuli (n=4). Data were normalized to PBMCs coincubated with PMN and PMA (100 nM). B) PBMCs were coincubated with PMN from either CGD patient or PMN from a healthy donor in the presence of PMA (100 nM). Data were normalized to the co-cultivation of healthy donor PBMCs and healthy neutrophils (n=3). C) Co-cultivation of PBMCs and PMN in the presence of PMA and an NE-inhibitor (20 µM). Data were normalized to the co-cultivation without inhibitor and analyzed by Mann-Whitney test (α=0,05), **p<0,01. D) ROS production of PMN stimulated with PMA (100 nM) in the presence of NE-inhibitor (20 µM) was measured by luminol assay (representative result of n=3). E) During co-cultivation PBMCs and PMA stimulated PMN were separated by 0,4 µm pore-sized membrane in a transwell system (n=4). Expression of hIFNA1 was analyzed by qPCR in all experiments. All results represent the mean±SD.

During activation with PMA, neutrophils undergo a potent ROS burst. ROS function not only as antimicrobial agent, but also as signaling molecules [172]. Patients suffering from CGD present with mutations in NADPH oxidase. Their neutrophils fail to induce a ROS burst and are not capable of producing ROS-dependent NETs. Neutrophils of these patients were not able to induce TIIFN expression in PBMCs of healthy donors when stimulated with PMA (Fig. 2.10B), indicating that a ROS-dependent process is required for TIIFN induction, which is likely NET formation. To further address the question whether TIIFN induction occurred due to the oxidative burst or due to NET release, Ialso inhibited NET formation using a pharmacological inhibitor of neutrophil elastase (NEi). Although NEi-treated neutrophils are still able to produce ROS (Fig. 2.10C), they induced significantly reduced levels of TIIFN in PBMCs (Fig. 2.10D). Lastly, I performed the co-cultivation in a transwell system, separating

the PBMCs and the neutrophil by a 0,4 µm membrane. When the cells were separated, PMA-stimulated neutrophils were not able to induce TIIFN expression in PBMCs (Fig. 2.10E).

Taken together these results demonstrate not only that the induction of TIIFN is dependent on NETs, but also that the cells require direct contact for the activation and that the observed TIIFN induction is not mediated by soluble factors.

2.3.5 TIIFN induction requires phagocytosis of NETs by PBMCs

To induce cGAS activation, NETs most likely need to get into the cell and reach the cytoplasm. Since macrophages phagocytose isolated NETs [147], I investigated if this is also observed under my co-cultivation conditions.

With a live cell imaging approach, I observed macrophages that encountered PMA-activated neutrophils and ingested a fraction of them as soon as they disintegrated and released their DNA into the extracellular space (Fig. 2.11A). To validate that NETs were taken up, I stained the macrophages for NET markers and observed colocalisation of DNA, DNA-histone complexes and NE in the macrophage cytoplasm, indicating that they had internalized NETs (Fig. 2.11B, upper panel). When I added the phagocytosis inhibitor Cytochalasin B (CytoB) to the co-cultivation, I could not observe uptake of NET material (Fig. 2.11B, lower panel). The cells were treated with 20 U DNAse1 during the last 15 min of the incubation to ensure that NETs do not stick to the cell surface and detected NET signal is intracellular.

Next I investigated the necessity of phagocytosis for TIIFN induction. Cells treated with the phagocytosis inhibitors CytoB or Nystatin expressed significantly less TIIFN when challenged with PMA stimulated neutrophils (Fig. 2.11C). The ability of neutrophils to undergo NETosis was not affected by the inhibitors (Fig. 2.11D), demonstrating that the observed effect is due to phagocytosis inhibition.

Taken together these results demonstrate that NETs need to be taken up by phagocytosis in order to induce a TIIFN response.

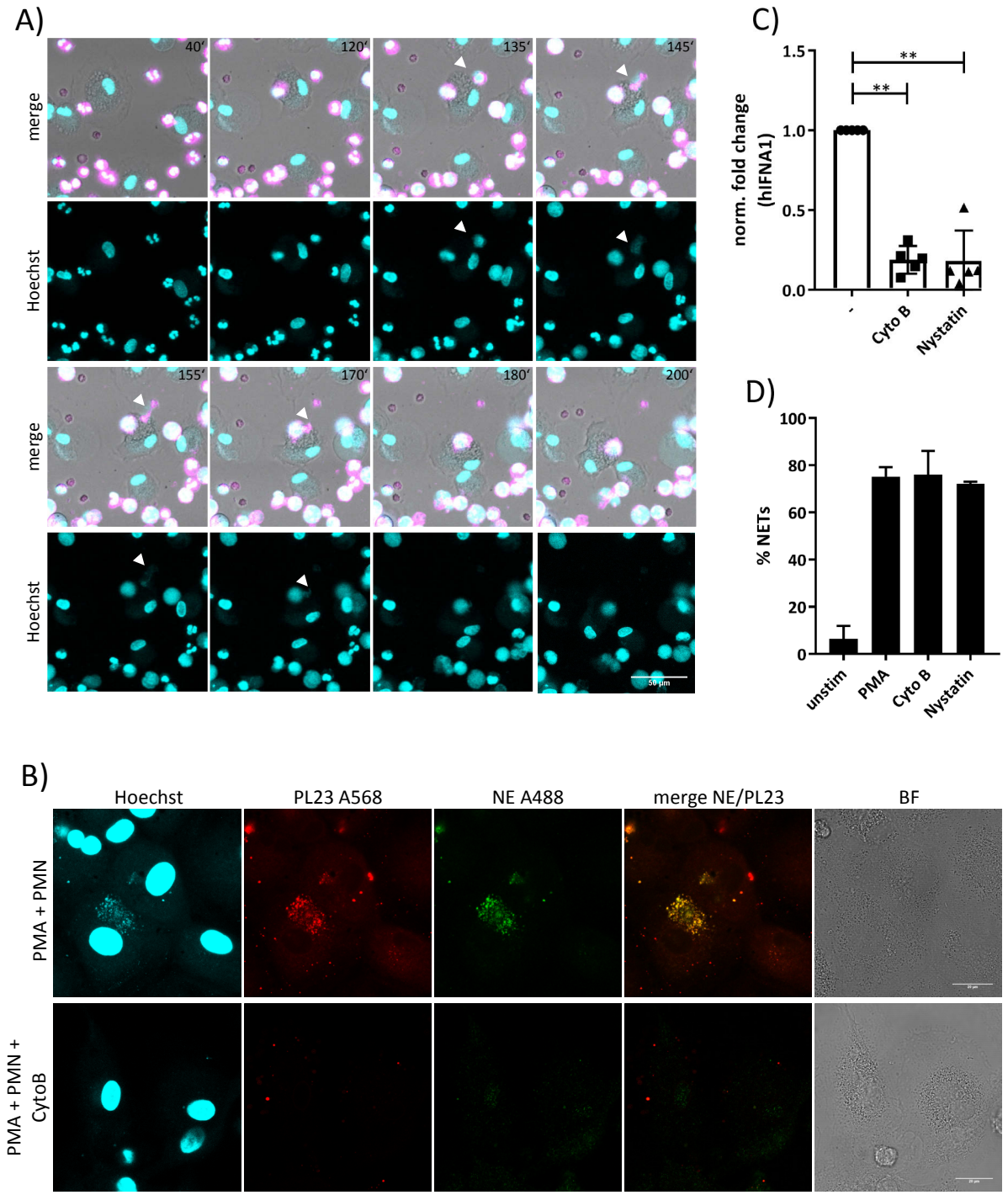

Figure 2.11 TIIFN induction requires NET internalization by phagocytosis

A) Fixed images of a video of a human MDM phagocytosing a PMN stimulated in the presence of 100 nM PMA. All cells are labeled with Hoechst (cyan), PMN are marked with cell tracker (pink). Scale bars represent 50 µm. B) Co-cultivation of MDM with PMN and PMA (100 nM) in the presence of Cytochalasin B. Cell were stained with Hoechst (blue), PL23 (red) and NE (green). Scale bars represent 20 µm. C) Co-cultivation of PBMCs with PMN and PMA in the presence of the phagocytosis inhibitors Nystatin (10 µg/ml) and Cytochalasin B (5 µg/ml). The expression of hIFNA1 was quantified by qPCR and normalized to the co-cultivation without inhibitors. The data were analyzed with the Kruskal-Wallis test (α=0,05) followed by Dunn's multiple comparison test (α=0,05) **p<0,01 (n=5). D) NET formation of PMA stimulated PMN (100 nM) after 4 h, quantified by immunofluorescence staining (n=3). Data are presented as mean±SD.

2.3.6 Phagocytosed NETs escape from the phagosome into the cytoplasm

I demonstrated that NETs are internalized by phagocytosis. To activate cGAS they need to escape from the phagosome to get into the cytoplasm. I co-cultivated PMA stimulated neutrophils and macrophages in the presence of lysotracker, a dye staining acidified phagosomes. After fixation, cells were stained with Hoechst and for NE to visualize NETs. In PMA-treated macrophages no NE or cytosolic DNA signal was observed, while the lysotracker signal was faint (Fig. 2.12, upper panel). NE was detected in neutrophils in the control condition, but not in macrophages (Fig. 2.12, middle panel). When macrophages were co-cultivated with neutrophils in the presence of PMA, I observed NE and DNA positive NETs in the cytoplasm that mostly colocalized with a strong lysotracker signal (Fig. 2.12, lower panels). These data show that NETs mostly end up in phagosomes. However, there are also NE and DNA positive areas that are negative for lysotracker indicating that NETs escaped from the phagosome into the cytoplasm where they would be able to activate cGAS.

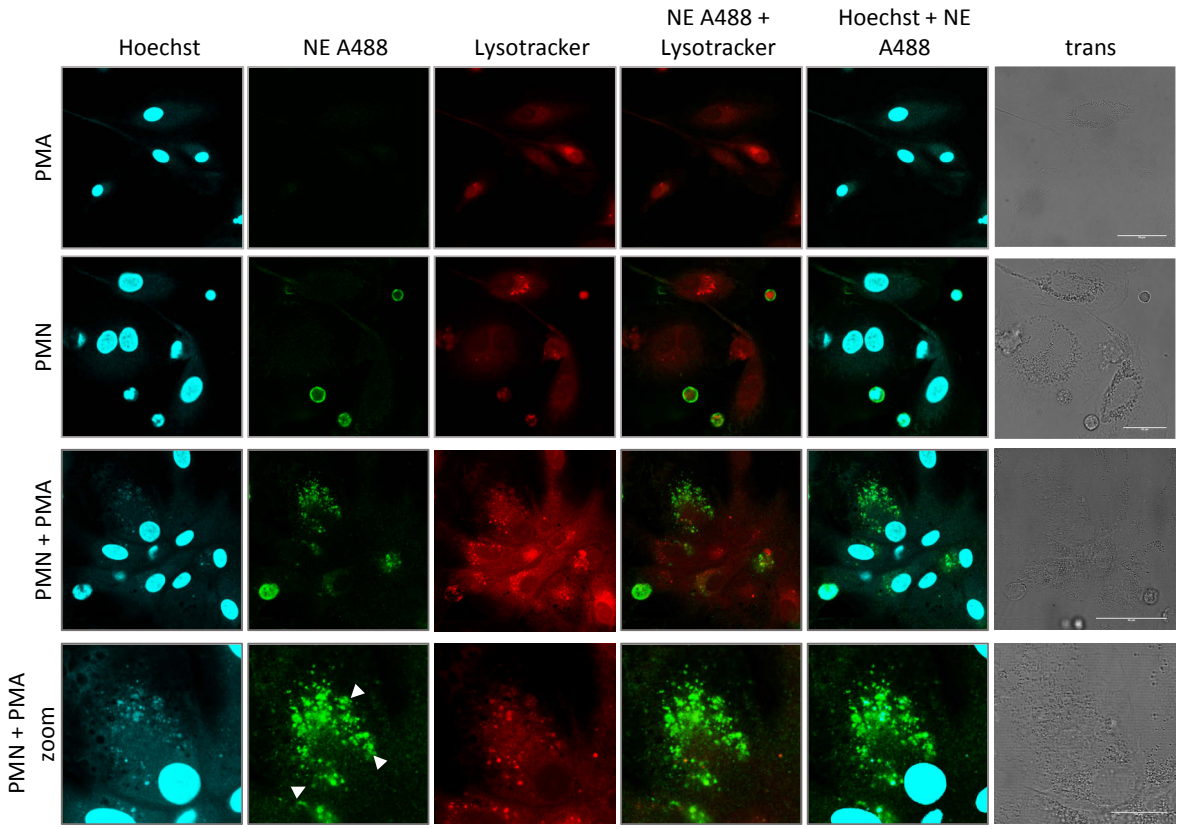

Figure 2.12 NETs escape from the phagosome into the cytoplasm
MDM were coincubated with PMN and 100 nM PMA for 4 h. Samples were stained with Hoechst (blue), NE (green) and lysotracker (red). White arrows mark NE-positive lysotracker-negative areas. Scale bars represent 50 µm, for the zoom in 20 µm.

2.4 Neutrophil extracellular traps induce TIIFN *in vivo* by a cGAS-dependent mechanism

In the previous sections I demonstrated that NETs are taken up by phagocytosis into target cells and induce a TIIFN response by activating the cGAS-STING-pathway. In the next section, I will show that cGAS-dependent recognition of NETs also plays a role *in vivo*.

2.4.1 Characterization of cGAS$^{-/-}$ neutrophils

Phenotypes of cGAS$^{-/-}$ mice are so far only described in the context of viral and bacterial infections, but not in the context of neutrophil biology. First, I analyzed neutrophils of cGAS$^{-/-}$ mice to ensure their functionality and exclude that observed phenotypes are due to neutrophil insufficiencies.

cGAS$^{-/-}$ mice present similar amounts of circulating neutrophils as Wildtype mice (Fig. 2.13A). For functional characterization, I included Cybb$^{-/-}$ mice as a control. Like CGD-patients, Cybb$^{-/-}$ mice carry a mutation in a subunit of NADPH-oxidase. Due to a resulting inability to mount a ROS burst, they cannot produce NETs in response to ROS-dependent stimuli. When I isolated neutrophils from the peritoneal cavity of animals after casein injection, I found that the recruitment of neutrophils was the same in Wildtype, Cybb-and cGAS-deficient mice. Peritoneal neutrophils of Wildtype and cGAS$^{-/-}$ animals produced a similar ROS burst after PMA stimulation (Fig. 2.13B) and made comparable amounts of NETs upon stimulation with PMA and ConA (Fig. 2.13C). As expected, Cybb$^{-/-}$ neutrophils produce neither ROS nor NETs after PMA stimulation.

I therefore conclude that the response of cGAS$^{-/-}$ neutrophils to both PMA and ConA is comparable to that of Wildtype neutrophils.

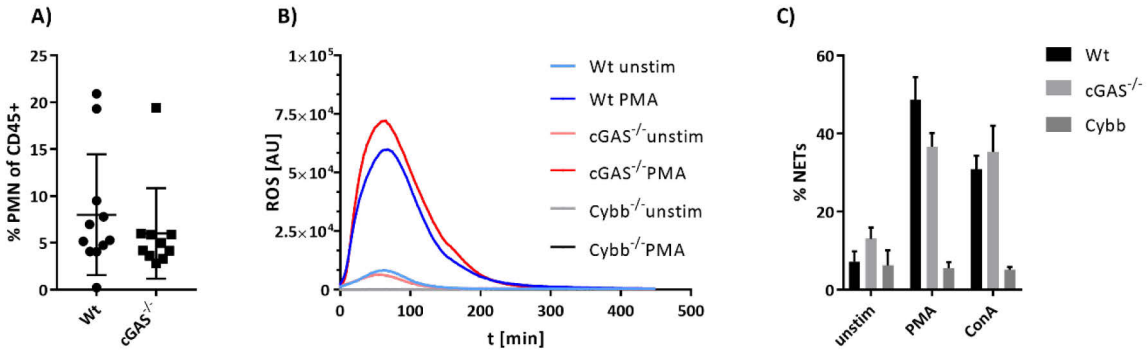

Figure 2.13 cGAS$^{-/-}$ mice have normal neutrophil functions
A) Quantification of whole blood neutrophils by FACS. Neutrophils were defined as CD3^{-}, CD45^{+}, Ly6G/C ^{high} (Gr1) and CD115^{-}. B) ROS production of neutrophils after stimulation with 100 nM PMA measured by chemiluminescence assay (representative of n=3). C) NET formation of Wildtype and cGAS$^{-/-}$ neutrophils stimulated with 100 nM PMA for 16 h (n=3). Results are represented mean±SD, B) shows mean values, error bars are not included for visibility.

2.4.2 Systemic NET induction *in vivo*

There are only limited models available to investigate NETosis *in vivo*. One option is the i.p. injection with LPS [173]. Since LPS administration can induce TIIFN production in itself, this system was not applicable for us. A recent report described the induction of NETs by the plant lectin ConA [174]. I.v. administration of ConA is an established model for acute immune-mediated hepatitis that leads to liver destruction [175], and I consider it a promising model to investigate NET formation *in vivo*. I injected mice with 15 mg/kg ConA i.v. and measured markers of liver damage in the serum to ensure that the system works in my hands. Both alanine-aminotransferase (ALT) and asparatate-aminotransferase (AST) are elevated in mice after 12 h ConA administration and I did not observe a difference between Wildtype, cGAS$^{-/-}$ and Cybb$^{-/-}$ mice (Fig. 2.14A and B). Although the variation between the animals was very high, all ConA injected mice present AST/ALT levels that are above diagnostic threshold. In parallel, I assessed NET production by sandwich ELISA for NE and DNA. Wildtype and cGAS$^{-/-}$ produce comparable amounts of NETs. Cybb$^{-/-}$ mice, which I used as a negative control, did not produce NETs after ConA challenge (Fig. 2.14C). As a further readout for ConA induced cell death I quantified nucleosome in the sera of ConA injected mice by ELISA. No difference between Wildtype, cGAS$^{-/-}$ and Cybb$^{-/-}$ mice was observed.

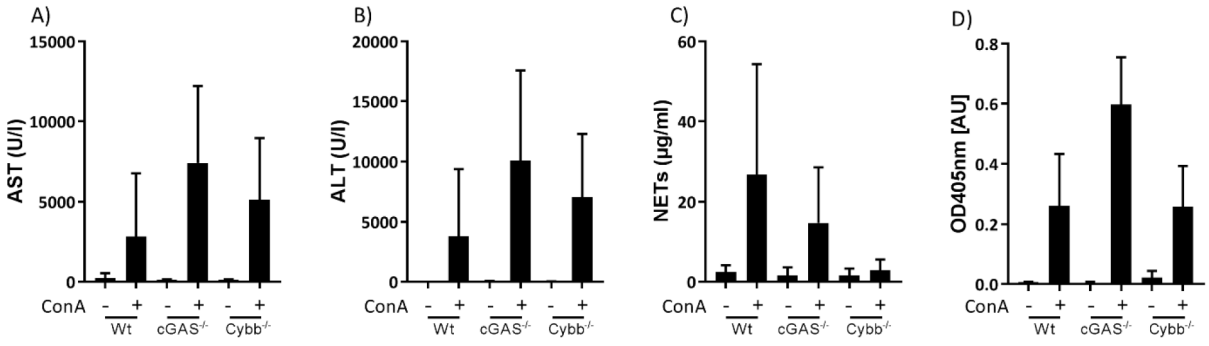

Figure 2.14 Systemic NET induction by i.v. ConA administration
The liver damage markers AST (A) and ALT (B) were measured in serum of mice 12 h after injection with 15 mg/kg ConA (n=5) C) Quantification of NET induction by sandwich ELISA for NE and DNA in sera of ConA injected mice (n=10). D) Quantification of nucleosomes in the sera of ConA injected mice by ELISA (n=5).

2.4.3 Injection of ConA induce cGAS-dependent ISG expression *in vivo*

To test the effect of systemic NET induction *in vivo* I injected mice with the NET inducer ConA. The TIIFN IFNA2 and IFNB were not detectable by qPCR in white blood cells, so I measured ISGs that I used as surrogate markers for TIIFN expression and signaling. Wildtype mice significantly upregulated the expression of the ISGs CXCL10, MX1, IFIT1, IFIT2, IFIH1 and OAS1A 12 h after ConA challenge. In comparison to Wildtype mice, cGAS$^{-/-}$ animals expressed significantly lower amounts of all of the above-mentioned ISGs after ConA stimulation (Fig. 2.15), indicating that the cGAS-STING pathway is involved in ISG upregulation in response to ConA.

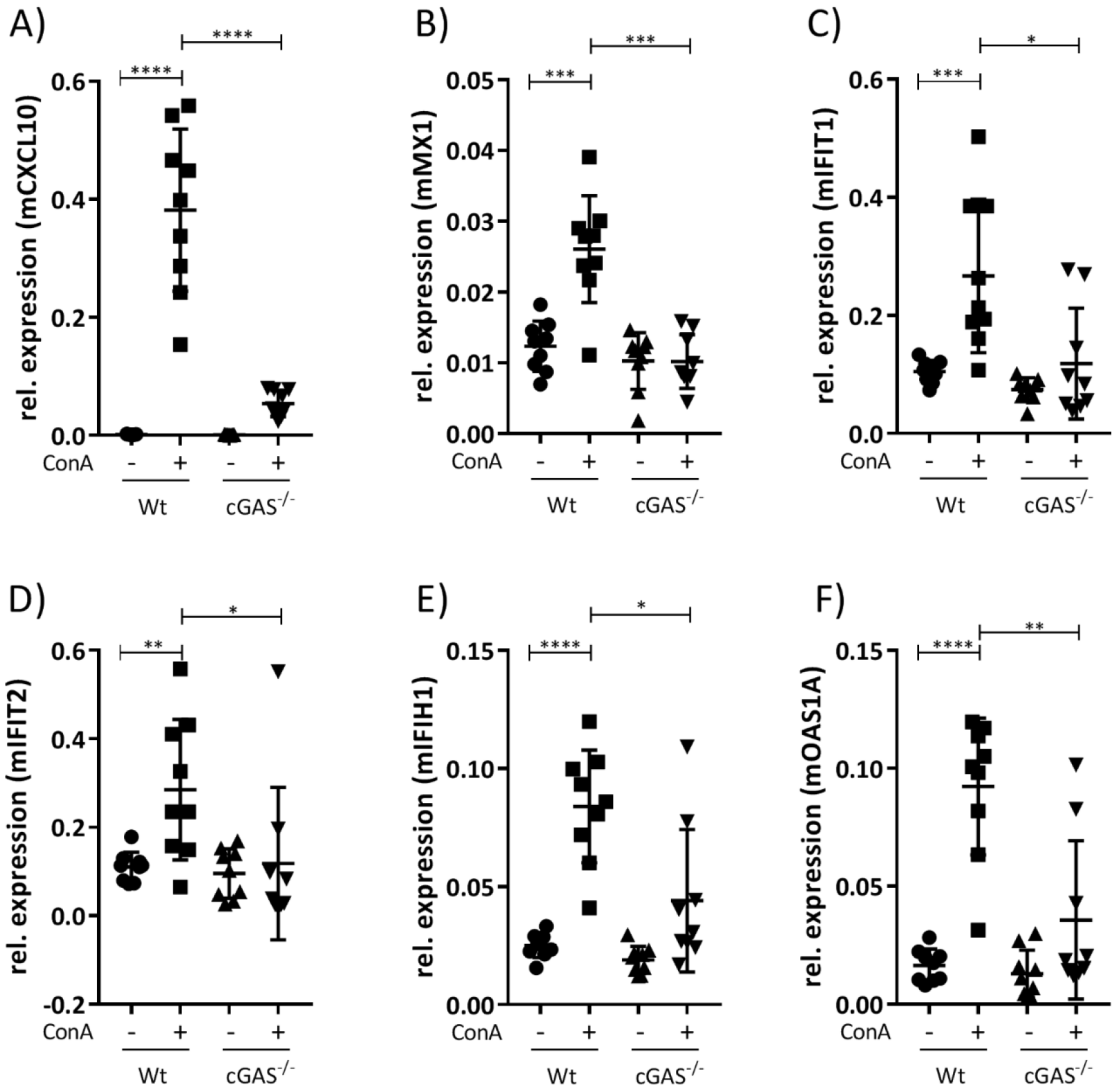

Figure 2.15 ConA injection results in cGAS-dependent upregulation of ISGs
Expression of ISGs in Wildtype and cGAS$^{-/-}$ mice 12 h after i.v. injection of ConA (15 mg/kg). Expression levels were quantified by qPCR, data represent mean±SD (n=9). Data were analyzed by Mann-Whitney test, α=0,05, *p<0,05, **p<0,01, ****p<0,0001.

2.4.4 Reduced ISG upregulation in cGAS$^{-/-}$ mice is a global phenomenon after ConA stimulation

In the previous experiment, I compared the expression of six well-described ISGs after ConA stimulation between Wildtype and cGAS$^{-/-}$ mice. To further analyze the response to ConA in a broader and unbiased way, I subjected the same samples to a microarray analysis to assess global differences

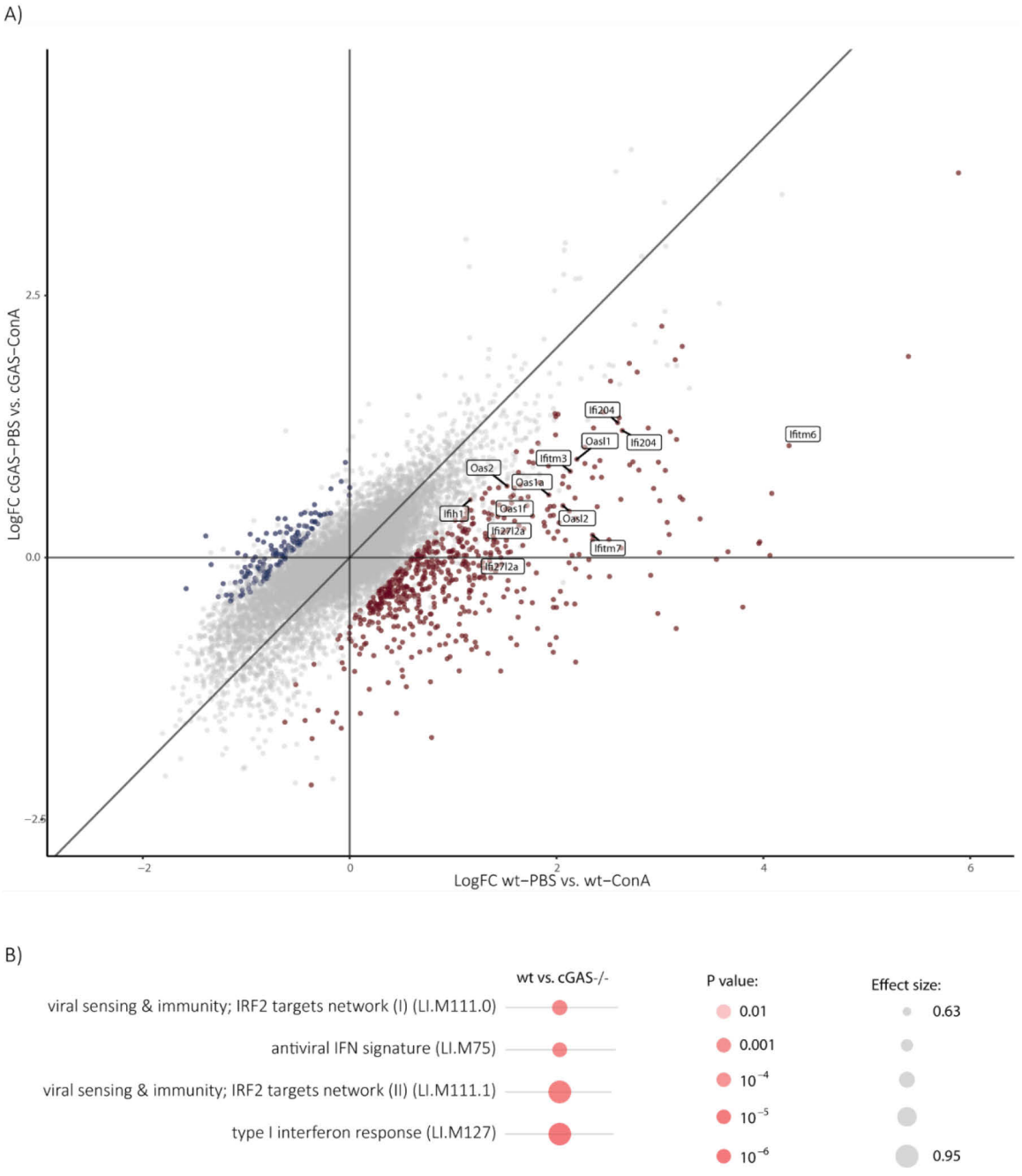

Figure 2.16 Increased global upregulation of ISGs in Wildtype mice when compared to cGAS$^{-/-}$ mice after ConA injection
A) Scatterplot comparing log fold change PBS vs. ConA (15 mg/kg, 12 h) between Wildtype and cGAS$^{-/-}$ mice. Annotated genes are examples of ISGs. B) GO-term analysis of genes significantly upregulated in Wildtype over cGAS$^{-/-}$.

between the two mouse strains. By comparing the fold changes of significantly regulated genes between PBS- and ConA injected mice between genotypes, I detected a number of genes that were stronger upregulated in Wildtype mice than in cGAS$^{-/-}$ animals (Fig. 2.15A). A gene-ontology analysis of these significantly stronger regulated genes revealed an significant enrichment for the terms “viral sensing & immunity” (LI.M111.0), “antiviral IFN signature” (LI.M75) and “type I interferon response” (LI.M127) (Fig. 2.15B). These results show that not only the six previously selected ISGs are effected by cGAS depletion, but that TIIFN regulated genes show a weaker induction in cGAS$^{-/-}$ mice than in Wildtype mice on a global scale.

2.4.5 Neutrophil depletion has a limited effect on ISG expression in Wildtype mice after ConA injection

To test if ConA-induced upregulation of ISGs is dependent on NETs I depleted neutrophils by treating mice with a Ly6G-specific depletion antibody (1A8) or the corresponding isotype control (2A3) [176]. I verified neutrophil depletion 24 h after antibody injection before ConA injection using whole blood FACS analysis and identified neutrophils as CD3^{-}, CD45^{+}, Ly6G/C^{high}(Gr1) and CD115^{-} (Fig. 2.17A). The neutrophil counts in depleted animals were reduced but not completely abolished (Fig. 2.17B). I measured NETs and nucleosomes in the sera of the antibody-depleted mice by ELISA and did not observe a difference between mice treated with the depleting antibody or the isotype control (Fig. 2.17C and D). This results can be explained by an emergency release of neutrophils from the bone marrow induced by ConA administration. The effect on the ISG response after ConA injection was variable between the different ISGs. The expression of IFIT2 was significantly reduced (Fig. 2.17H) in Ly6G-depleted animals in comparison to isotype treated animals and CXCL10 and IFIH1 were at least partially reduced (Fig. 2.17E and I). No effect could be observed for the ISGs MX1, IFIT1 and OAS1A (Fig. 2.17F, G and J).

These results indicate that neutrophils only partially contribute to ISG induction, although the data need to be interpreted carefully with regard to the incomplete neutrophil deletion.

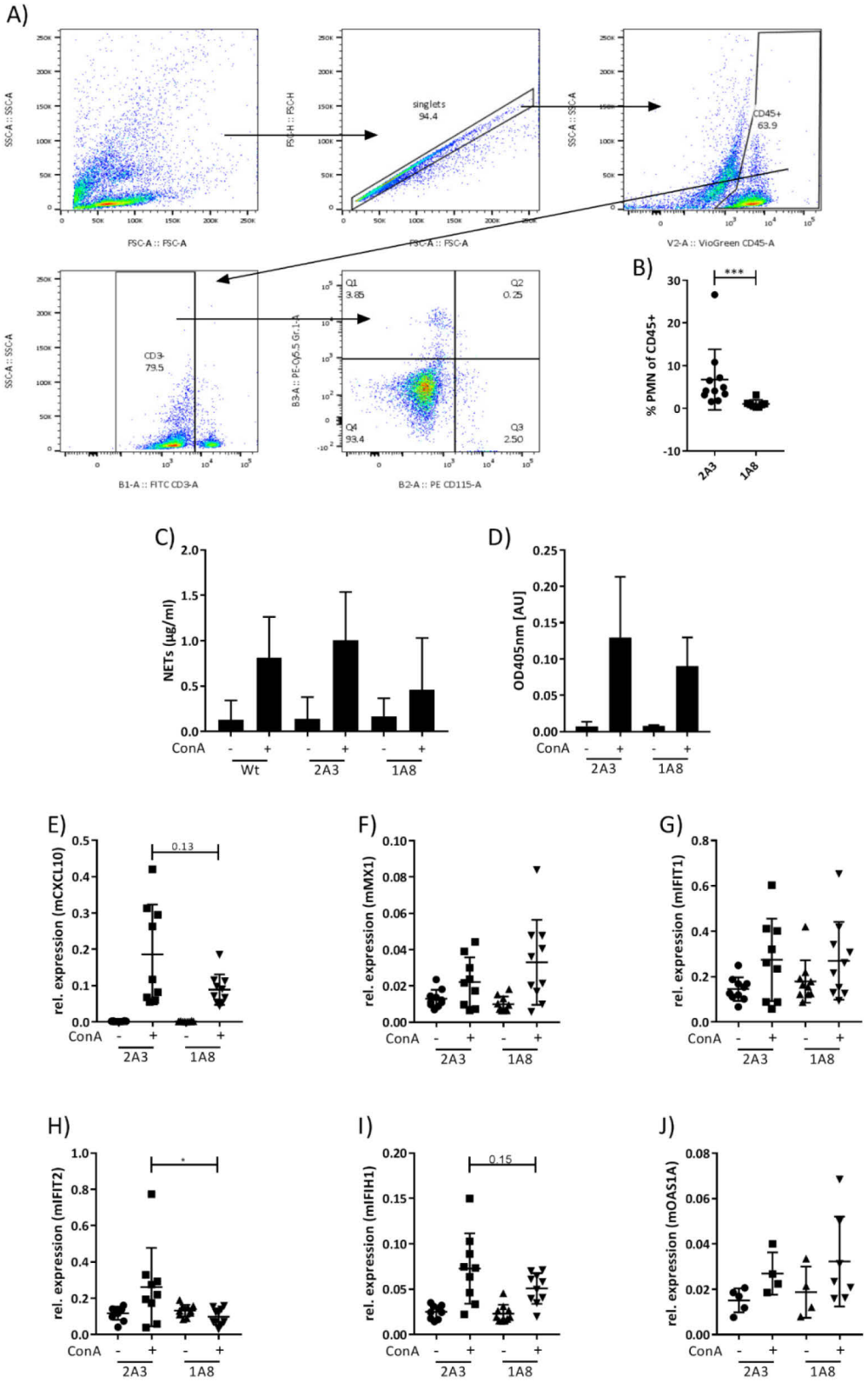

Figure 2.17 Neutrophils contribute to cGAS-dependent ISG upregulation after ConA injection
A) Gating strategy for identification of neutrophils in full blood as $CD3^-$, $CD45^+$, Ly6G/C ^{high}(Gr1) and $CD115^-$.B) Quantification of neutrophils 24h after antibody administration by FACS. C) ISG expression in Ly6G-depleted (1A8) or isotype-treated (2A3) Wildtype mice injected with PBS or ConA (15 mg/kg) for 12 h. ISGs were quantified in white blood cells by qPCR (n=10). Data were analyzed by Mann-Whitney test, α=0,05, *p<0,05, values represent the p-value. Data are presented as mean±SD.

3.4.6 NET formation induces ISG expression *in vivo*

Since neutrophil depletion was incomplete, I tested the contribution of NET formation to the induction of ISGs genetically. As shown before, Cybb$^{-/-}$ mice are not capable of producing NETs in response to ROS-inducing stimuli such as PMA or ConA. Upon ConA injection Cybb$^{-/-}$ mice expressed significantly lower amounts of transcripts for the ISGs IFIT2, IFIH1 and OAS1A as Wildtype animals and two other ISGS, MX1 and IFIT1, showed the same trend (Fig. 2.18).

These data strongly suggest that NET formation also plays a role in ISG induction *in vivo*.

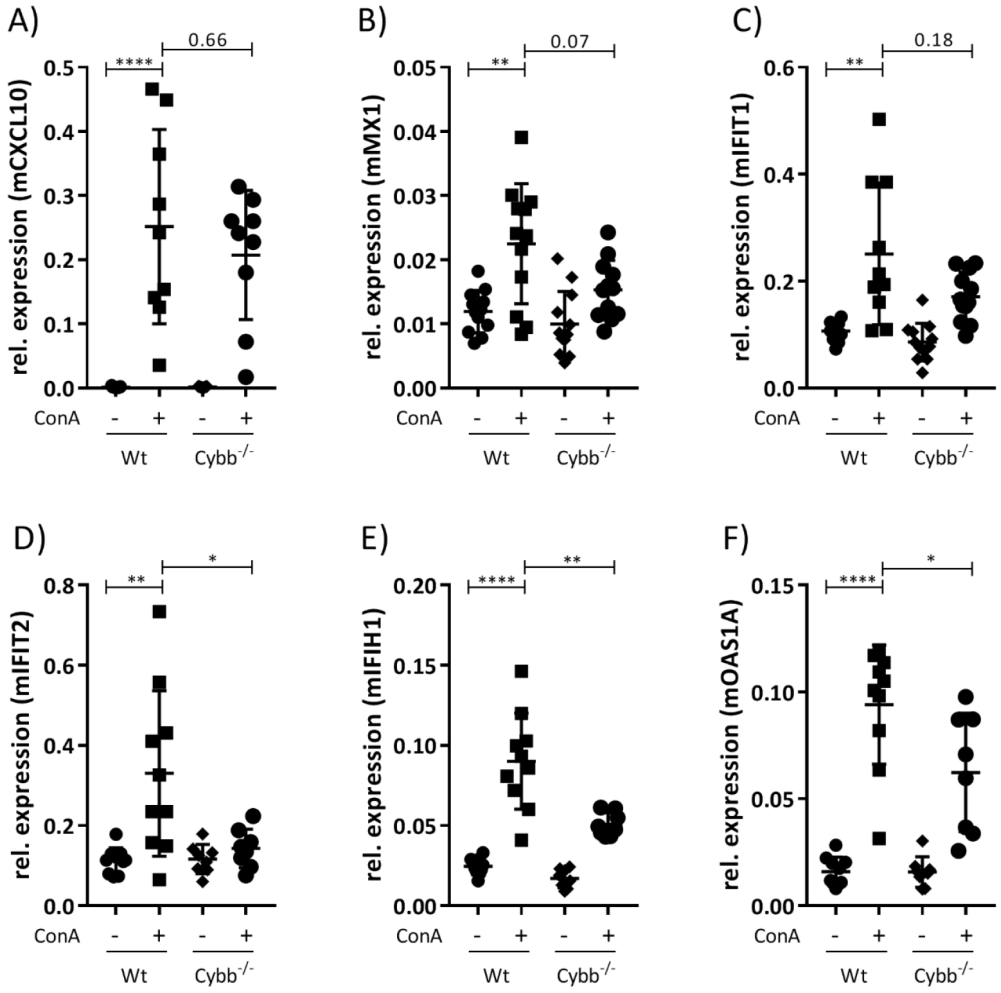

Figure 2.18 NETs induce ISG upregulation in ConA injected mice
Expression levels of ISGs in white blood cells of Wildtype and Cybb$^{-/-}$ mice 12 h after injection with either PBS or ConA (15 mg/kg) (n=10). Data are plotted as mean±SD and analyzed by Mann-Whitney test, α=0,05, *p<0,05 **p<0,01 ***p<0,001 ****p<0,0001, values represent the p-value.

2.5 NET induced TIIFN expression is dependent on Cathepsins *in vitro* but not *in vivo*

In the previous sections I demonstrated that NETs can escape the phagosome and enter the cytoplasm where they activate cGAS and induce TIIFN, both *in vitro* and *in vivo*. In this section, I want to investigate the molecular mechanism for this phagosome escape. A study from 2015 shows that silica particles are liberated from the phagosome by a combination of Cathepsins [177]. Cathepsins are a family of endoproteases that consists of 15 different enzymes with different catalytical mechanisms. Azurophilic granules of neutrophils contain Cathepsin G, a serine protease that digests phagocytosed pathogens [178]. Other neutrophil-expressed Cathepsins, Cathepsin B, C and S, are cysteine proteases and fulfill a variety of functions in the cell.

To test the role of Cathepsins in NET-induced TIIFN expression I co-cultivated human PBMCs with PMA-stimulated neutrophils in the presence of the pan-Cathepsin inhibitor K777 [179] and observed a significantly reduced expression of TIIFN in cells treated with the inhibitor (Fig. 2.19A). I performed a NET formation assay in the presence of K777 and observed no difference in comparison to the untreated control (Fig. 2.19B). This result indicates that the measured effect on TIIFN expression is due to Cathepsin inhibition and not due to inhibited NET formation.

To show that Cathepsins also play a role *in vivo*, I tested mice carrying a triple knockout for the Cathepsins B, C and S (BCS TKO mice). BCS TKO mice presented comparable amounts of neutrophils in blood when compared to Wildtype mice (Fig. 2.19C). BCS TKO mice injected with ConA showed a increased levels of liver damage compared to Wildtype mice, which I assessed by measurement of the liver enzymes ALT and AST in serum (Fig. 2.19D and E). Furthermore, sera of ConA injected BCS mice contained equal amounts of NETs and nucleosomes (Fig. 2.19F and G). I subsequently assessed ISG expression in white blood cells of ConA injected mice. None of the measured ISGs showed as significant difference when comparing Wildtype and BCS TKO mice (Fig. 2.19H-M).

The observation that Cathepsins are required for the NET-induced TIIFN expression *in vitro* could not be validated *in vivo*. To finally determine their role in NET release from the phagosome, further experiments are required.

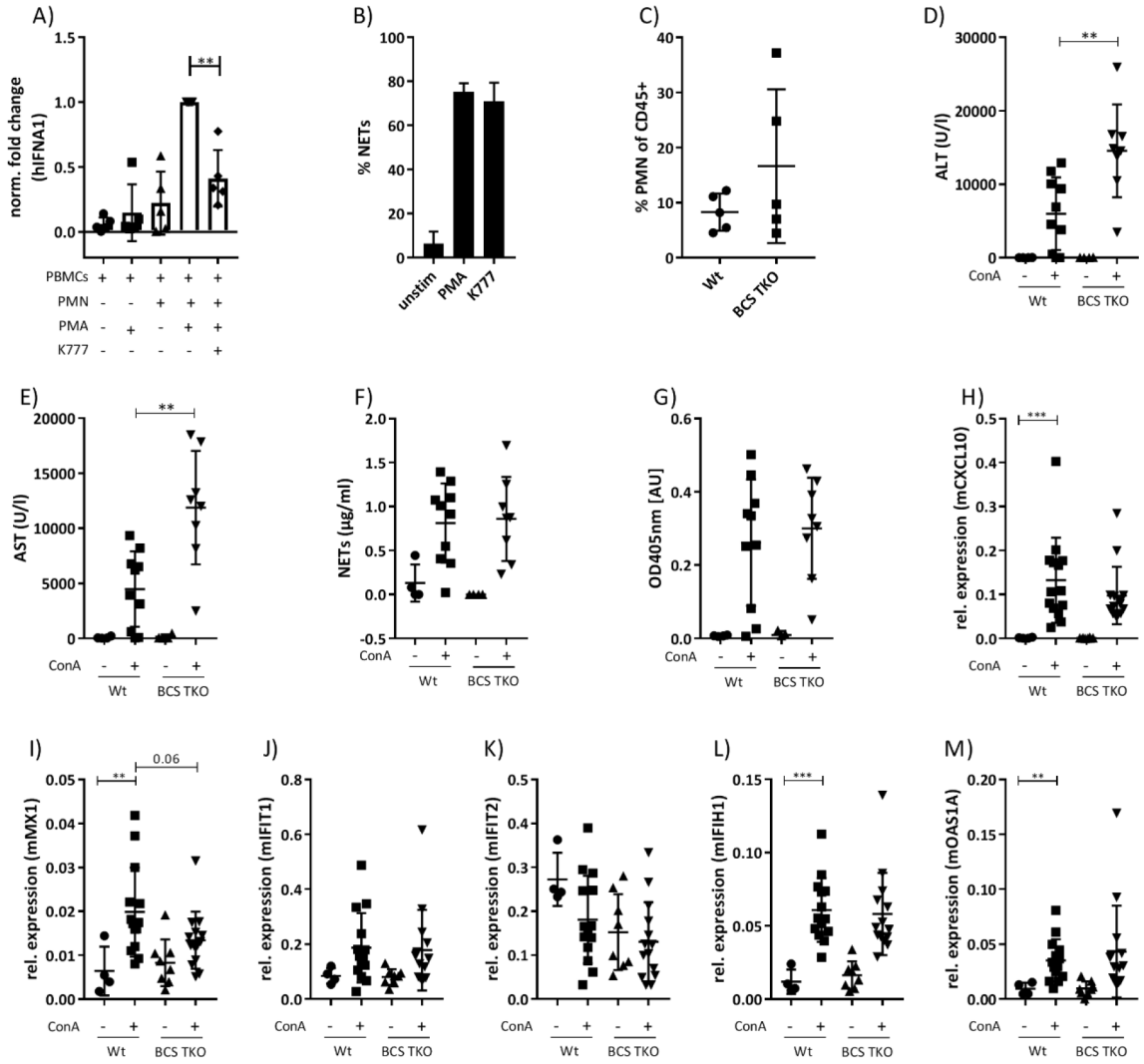

Figure 2.19 BCS TKO mice produce reduced ISGs after stimulation with ConA

A) Co-cultivation of PBMCs with PMA-stimulated neutrophils in the presence of the pan-Cathepsin-Inhibitor K777 (10 µM). IFNA1 expression was quantified by qPCR, results are normalized to the co-cultivation without inhibitor (n=5). B) NET formation of PMN stimulated with 100 nM PMA in the presence of K777 was quantified by immunofluorescence staining (n=3). C) Quantification of whole blood neutrophils by FACS. Neutrophils were defined as $CD3^-$, $CD45^+$, $Ly6G/C^{high}$ (Gr1) and $CD115^-$. D/E) Quantification of liver damage after 12 h of ConA measured by ALT/AST concentrations in serum. F/G) Concentration of NETs and nucleosomes in sera of ConA injected mice after 12 h. H-M) ISG expression levels in Wildtype and BCS TKO mice injected with either PBS or ConA (12 h, 15 mg/kg) were quantified by qPCR (n=12). Data are plotted as mean±SD and analyzed by Mann-Whitney test, α=0,05, *p<0,05 **p<0,01 ***p<0,001 ****p<0,0001, numerical values depict actual p-values.

3 Discussion

Neutrophils play a central role in the defense against invading pathogens, both by exerting a variety of antimicrobial effector functions and by recruiting additional immune cells to the locus of infection. One of the most important neutrophil effector functions is the release of NETs into the extracellular space, a composite of chromatin and antimicrobial molecules that can trap and kill invading microbes. Under healthy conditions, nucleases cleave NETs and macrophages dispose remnants by phagocytosis. If this clearance system is impaired, NETs remain in the circulation and induce the production of pro-inflammatory cytokines by activating immune cells. These cytokines can promote disease progression and deteriorate the outcome of the affected patients. How exactly NETs induce cytokine expression is not completely understood. In this thesis, I show that NETs induce TIIFN expression in human and murine immune cells *in vitro* by activating the cytosolic DNA sensor cGAS. I recapitulated this finding in an *in vivo* mouse model of systemic NET induction, showing its physiological relevance. This finding does not only represent an interesting insight into a self-activating mechanism of the immune system under pathological conditions, but also provides a possibility for new intervention strategies for a growing list of NET-associated diseases.

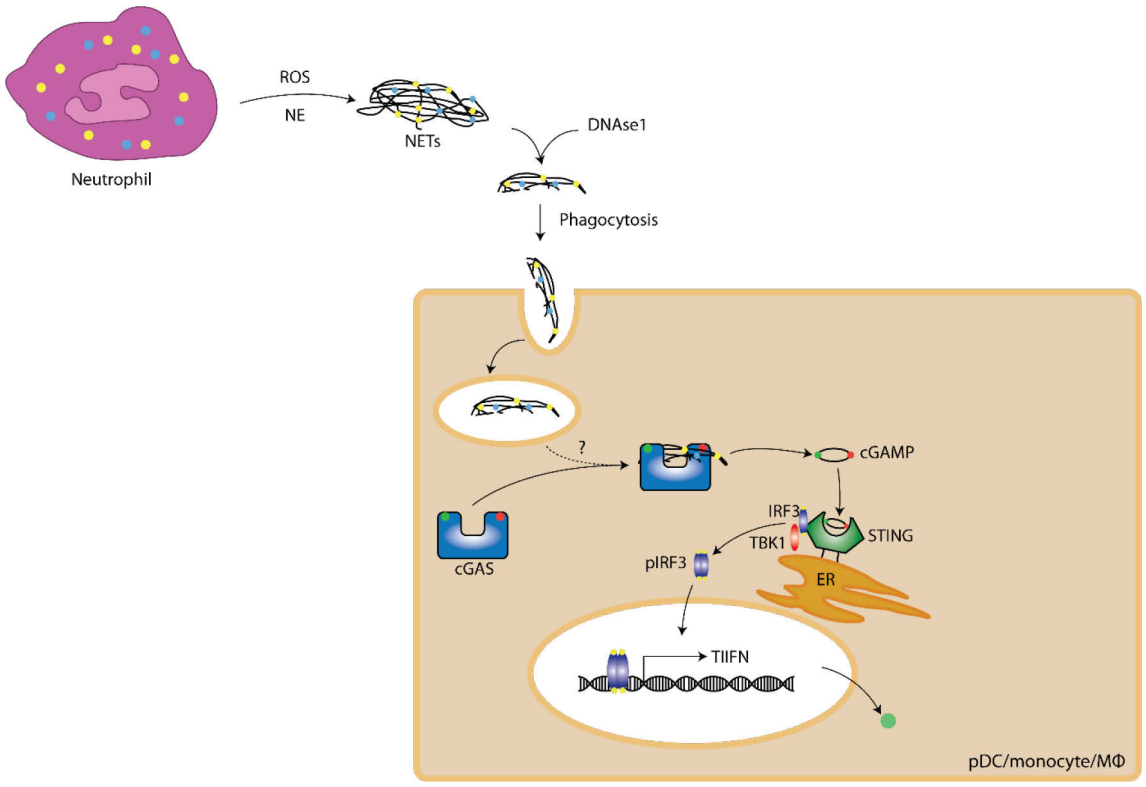

Figure 3.1 Recognition of NETs by the cGAS STING pathway
Neutrophils produce NETs that are digested by DNAse1 and phagocytosed by target cells. After liberation from the phagosome, NETs are recognized by cGAS, resulting in the production of the second messenger cGAMP and the activation of the signaling adaptor STING. STING and TBK1 induce the phosphorylation of the transcription factor IRF3 that translocates to the nucleus and induces TIIFN expression.

3.1 Recognition of NETs by cGAS – a new perspective in understanding disease development

3.1.1 cGAS as a receptor of NETs

cGAS is a cytosolic DNA sensor that evolved to recognize viral genomes and bacterial DNA. Due to its sequence-independent sensing mechanism, cGAS also recognizes self-DNA. In fact, cGAS senses mitochondrial DNA, DNA damage side products, endogenously amplified retroelements and chromatin fragments *in vivo* [130,180,181]. Notably, these self-ligands originate from cell intrinsic events and accumulate due to defects in the clearance system. In this thesis, I present NETs as a naturally occurring substrate of cGAS. To my knowledge, NETs are the first endogenous extracellular DNA-containing stimulus that activates cGAS in immune cells.

For *in vitro* experiments, most publications fall back to plasmid or artificially generated DNA species [182,183]. Although these experimental systems are required to further elucidate the function and mechanism of cGAS, they are artificial in the sense that the DNA is not protein-bound as it occurs in nature. Furthermore, entry into the cell requires transfection. NETs, on the other hand, have a distinguished position among self-molecules as an extracellular source of protein-DNA complexes that activate the immune system. NETs represent naturally occurring DNA bound to different molecules like histones, nucleosomes, HMGB1 and others, individually described as DAMPs. Interestingly these molecules are intrinsically immunostimulatory and can activate different PRRs [184]. Furthermore, NETs carry different antimicrobials like NE and LL37, which might facilitate the release of NET material from the phagosome into the cytoplasm. By combining these two characteristics, NETs specifically provide all requirements to be a potent activator of cGAS, by combining the substrate of the enzyme and accessory molecules facilitating the release from the phagosome into the cytoplasm.

3.1.2 DNAse insufficiencies – the crossroads where NETs and cGAS meet

Malfunctions in DNAses are associated with diseases like the Aicardi-Goutière syndrome, SLE or familial chilblain lupus [108,109,148,185]. These examples point out the importance of DNA clearance to avoid immunopathology. During the interplay between NETs and cGAS, both partners require functional nucleases to avoid unwanted immune cell activation. The recognition of self-DNA by cGAS is mostly described in the context of impaired DNA clearance due to missing intracellular nuclease activity in the lysosome or the cytoplasm. The two most important intracellular nucleases are the lysosomal DNAse2 and the cytoplasmic TREX1. TREX1$^{-/-}$ mice suffer from a systemic inflammation, while DNAse2$^{-/-}$ mice die *in utero*. Both phenotypes are caused by accumulation of self-DNA leading to uncontrolled TIIFN production and can be rescued by depletion of cGAS or IFNAR [144,147]. These reports show that cGAS can

be activated by self-DNA in the context of nuclease insufficiency. The clearance of genetic material by DNAse1 in blood on the other hand is described to be important to avoid undesired immune activation [101,186]. This genetic material can originate from NET formation, but there are also other potential sources, like damaged necrotic endothelium [98]. In SLE, insufficient DNAse1 activity is caused by a variety of factors, e.g. mutations, binding of autoantibodies or inhibition by other molecules. Interestingly, also mutations of TREX1 and DNAse2 are associated with SLE development. To summarize, the insufficient clearance of NETs by extracellular DNAse1 can result in prolonged exposure that might lead to uptake of NETs and the activation of cGAS.

The experimental conditions chosen for the cocultivation experiment (Fig 2.7) resemble the situation in patients with SLE. While the intracellular DNAses are functional, DNAse1 does not degrade NETs in the extracellular space. Notably, NETs induce cGAS dependent TIIFN expression with the intracellular DNAses are functional. Hakkim et al. show that NETs are stable for up to 90 h *in vitro* in the absence of DNAse1 [101], resulting in prolonged exposure of NETs to the target cells. The half-life of NETs in circulation or tissues is not known. I repeated the cocultivation in the presence of DNAse1, expecting an abrogation of TIIFN expression due to NET degradation. Surprisingly, I observed the opposite effect (Fig. 2.9). One possible explanation is that a certain size of NETs favors their uptake by target cells. Alternatively, cGAS could recognize NET fragments of a certain size or accessibility better than large compact structures. My data support the second explanation, because I observed that recombinant cGAS poorly responds to large NET structures, but shows strong activation when NETs are processed by DNAse1(Fig. 2.2). This observation does not rule out the first explanation, both mechanisms might apply in parallel.

3.1.3 TIIFN in NET-associated diseases

An extending list of diseases is either indirectly or directly associated with NETs. These “NETopathies” do not only include autoimmune and auto-inflammatory diseases like gout, RA , vasculitis, psoriasis and SLE, but also metabolic disorders like diabetes, lung diseases like cystic fibrosis and COPD, and cancer [187]. However, care must be taken when evaluating the impact of NETs on a disease, because some publication infer NET-involvement simply from measuring NET components in circulation. Since the detection of NETs in serum and tissue samples remains difficult, further research might add more diseases to that list. To complicate matters further, NET-bound proteins have a high intrinsic affinity to bind DNA. Antimicrobial molecules like LL37 could be released by neutrophils during degranulation and bind DNA from another source, resulting in NET-like structures that are not neutrophil derived.

A majority of the listed diseases are not only associated with NETs, but also with TIIFN. SLE, as the most prominent example, shows a global upregulation of ISGs, resulting in a characteristic TIIFN signature [91,92]. This signature can also be found in in a subset of patients suffering from RA, which show a particularly poor outcome [188]. In skin lesions of psoriasis patients ISGs like IFI27, IFI56 and MX1 are upregulated and form a psoriasis TIIFN signature [189,190].

TIIFN are not only inhibitors of viral amplification. As activators of the immune system they can actively drive disease progression of autoimmune and autoinflammatory diseases. They influence the immune system on three levels. i) They directly induce the secretion of pro-inflammatory cytokines from other immune cells. ii) They intensify the immune functions of other immune cells, like antigen presentation by professional APCs, the release of pro-inflammatory cytokines by macrophages or autoantibody formation by plasma cells. Interestingly, up to 19 % of cancer patients treated with TIIFN produce autoantibodies [191,192]. iii) They shape the microenvironment by inducing chemokine release resulting in increased immune cell recruitment or influence the differentiation of immune cells, e.g. by driving monocytes towards a DC-phenotype [193,194].

Taken together, TIIFN are not only a marker of pathologic immune activation in autoimmune diseases, but actively contribute to development and the progression of these diseases.

3.1.4 NETs as a stimulus for TIIFN production

The fact that NETs serve as a stimulus for TIIFN production has far-reaching consequences. It substantiates the notion that NET formation is not only a symptom of a generally activated immune status in patients, but also becomes a driving factor in the pathogenesis and the progression of diseases. In a non-autoimmune setting on the other hand, NET induced TIIFN production might also have a positive effect, because it induces the upregulation of innate and adaptive defense mechanism, which could help the fight invading pathogens and prevent further dissemination in the host. Although it was reported before that NETs induce TIIFN production in other immune cells [84,85], a deeper understanding of how NETs are recognized by the immune system is needed.

Since NET formation is a process that is specific to neutrophils, I was able to induce NETs with PMA, while the target cells like PBMCs and macrophages remained unaffected. This makes it intrinsically difficult to compare NET formation to other forms of cell death, because the target cells would also respond e.g. to inducers of apoptosis like cis-platin or ultraviolet light. This is an experimental drawback of this work that could not be circumvented.

Two different publications from 2016 show that the mtDNA that is present in NETs is the main inducer of TIIFN production and that the genomic DNA in NETs is less interferogenic [85,115]. In my experiments, isolated mtDNA alone does not induce TIIFN production in human primary cells (Fig. 2.5). This discrepancy might occur because the mtDNA used in the publications was artificially oxidized subsequent to the isolation and transfected into the target cells to induce TIIFN production. Whether mtDNA expelled during NET formation plays a role in TIIFN induction cannot be concluded from the experiments performed in this thesis, but merits further investigation.

A proposed candidate for NET recognition is TLR9. Although TLR9 was not required for NET recognition in my experimental setting (Fig. 2.5; Fig. 2.8), different groups report TLR9-dependent TIIFN production by pDCs that were stimulated with NETs or complexes of DNA and the antimicrobial peptide LL37 *in vitro* [81,84,87]. The results of a $TLR9^{-/-}$ in different mouse models of SLE are controversial. A TLR9 knockout in the lupus-prone $MRL.FAS^{lpr}$ background results in a exacerbated lupus phenotype [116,117], an observation that was recapitulated in a model of pristine-induced lupus [195]. On the other hand, reports show that a blocking of TLR9 by chemical antagonists leads to an ameliorated phenotype in $MRL.FAS^{lpr}$ mice and that TLR9 knockout is beneficial in pristine induced lupus [196,197]. The conflicting data could indicate the involvement of an alternative receptor that recognizes NETs.

In this thesis, I show that cGAS is a NET receptor and thereby it could contribute to disease. In fact, changes in cGAS expression is associated with the prime example of a NET-associated diseases, which is SLE. PBMCs of SLE express higher levels of cGAS when compared to healthy donors, positively correlating with the expression of the ISGs MX1, CXCL10 and protein kinase R. cGAMP, the second messenger produced by cGAS, was detected in the PBMCs of a subset of SLE patients by mass spectrometry, whereas healthy controls and PBMCs of RA patients remained negative [198]. The finding that oxidized DNA, as it is also present in NETs, can induce TIIFN production in a STING-dependent manner, supports the observation that cGAS is a receptor of NETs [85]. Furthermore, stimulation of monocytes with DNA-LL37 complexes results in STING-dependent TIIFN production, supporting the observations made in this thesis [114]. Interestingly, Chamilos et al. (2012) report that pDCs are sensitive for TLR9 inhibition by Bafilomycin A1 when stimulated with DNA-LL37 complexes, whereas monocytes are not affected. This finding suggests that different cell types might utilize different receptors for NET recognition.

By inducing TIIFN, NETs do not only contribute to general activation of the immune system, but they also induce further stimulation of other neutrophils. Human neutrophils primed with TIIFN are reported to produce NETs upon stimulation with autoantibodies [84]. This could result in an ongoing

inflammatory circuit that could be accountable for the disease flares observed in SLE (Fig.3.2). Moreover, NET formation could link the two molecular hallmarks of SLE, which are the production of autoantibodies and the TIIFN signature. In this model, neutrophils would undergo NETosis, either spontaneously as reported for SLE LDGs or after stimulation with immune complexes [67,84]. The resulting NETs, which are not degraded due to DNAse1 insufficiency, remain in circulation and activate the two arms of the immune system in parallel. Innate APCs recognize NETs by cGAS and produce TIIFN that further activate the immune system and prime neutrophils to undergo NETosis. In parallel, the adaptive immune system produces autoantibodies recognizing NET proteins, further stimulated by TIIFN. By binding their antigen, they form immune complexes that in turn activate neutrophils to undergo NETosis, so that the cycle starts again.

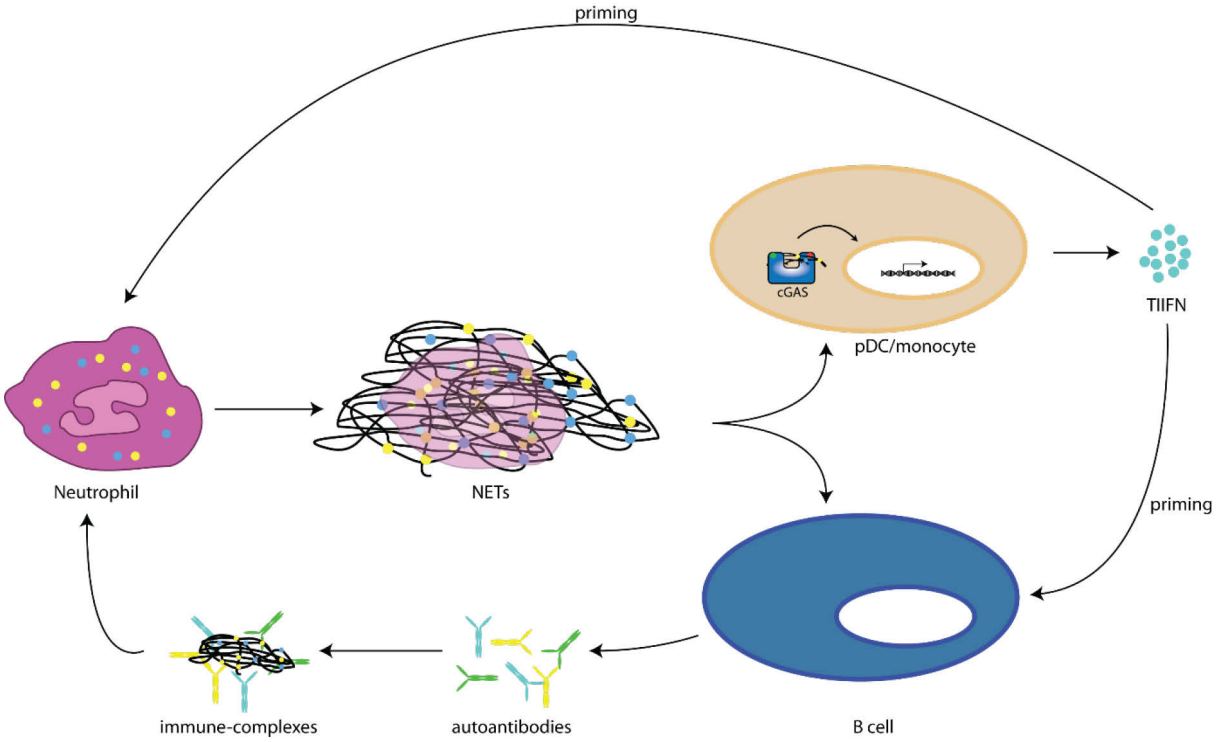

Figure 3.2 NET formation as the driving force in inflammatory diseases
Primed neutrophil undergo spontaneous NET formation in autoinflammatory diseases. Due to defective clearance mechanisms, NETs are taken up by APCs and activate cGAS-mediated TIIFN production. TIIFN simultaneously prime neutrophils for further NET formation, as well as B cells to produce increased amount of autoantibodies. Autoantibodies form immune complexes by binding their antigen, which cause both endothelial tissue damage and neutrophil activation.

3.1.4 cGAS as a therapeutic target in NET-associated diseases

Due to their involvement in a multitude of diseases, NETs and NET-mediated effects are a promising therapeutic target. In NET-associated autoimmune diseases TIIFN are the target in a variety of clinical studies applying monoclonal antibodies. Sifalimumab and Rontalizumab, both IFNα-depleting

antibodies, were tested in a phase 2 clinical trials and significantly reduced the TIIFN signature in 40-50 % of the SLE patients [199,200]. Furthermore, blocking of the IFNAR receptor using the monoclonal antibody Anifrolumab significantly reduced disease activity in a clinical phase 2 trial [201,202]. The usefulness of this clinical TIIFN reduction is further consolidated by the observation that a subgroup of SLE patients spontaneously develop anti-IFNα-antibodies. Their appearance correlates with reduced ISG expression and an diminished disease activity, resulting in an improved outcome [203].

Even more useful than a retroactive targeting of inflammatory mediators would be the development of treatment approaches aiming to avoid the formation of these. I show that cGAS is a promising candidate for this kind of intervention, because it is the initial receptor of a potentially self-amplifying system of TIIFN and NET formation. Different inhibitors are under development [204] and targeting of cGAS by a small molecule inhibitor resulted in reduced TIIFN expression in macrophages of a interferonopathy mouse model of Aicardi-Goutières syndrome [168].

Interestingly, another treatment option frequently applied in the NET-associated diseases SLE are antimalarials, especially hydroxychloroquine (HCQ) [205]. HCQ administration reduces flares, organ damage and thrombotic events. Furthermore, the overall survival of SLE patients is increased by HCQ treatment [206]. Additionally, it allows a reduced steroid administration [207]. Initially discovered as an antimalarial drug that prevents the blood stage progression of *Plasmodium falciparum*, its mode of action in autoimmune diseases is not completely understood. Potential mechanism are the inhibition of autophagy that results in a reduced production of pro-inflammatory cytokines like IL1β, IL6 and TNF [208] or the inhibition of TLR9 signaling [209]. Importantly, antimalarials like quinacrine, HCQ and 9-amino-6-chloro-2-methoxyacridine were recently shown to inhibit cGAS activation by blocking its interaction with DNA [210,211]. Also patients suffering from RA, a disease associated with both NETs and cGAS contributing to disease progression, are treated with antimalarials [212,213]. Although cGAS inhibition by antimalarials might not be an exclusive mechanism, the fact that NET-associated diseases are already treated with cGAS inhibitors supports the importance of the findings reported in this thesis.

The concept of interfering with NET recognition to reduce TIIFN might also be applicable in Malaria itself. Malaria is a disease caused by infection with the parasite *P. falciparum*. During its life cycle malaria parasites infect red blood cells and lyse them simultaneously resulting in periodically reoccurring fever. Disease progression is driven by an array of pro-inflammatory cytokines that are induced by the parasite itself or the release of bioactive molecules like hemozoin. Among these cytokines are TNF, IL1α, IL1β and TIIFN [214]. TIIFN play an important role in Malaria pathogenesis. Different studies indicate that TIIFN are required to contain the parasite but also in contributing to

vascular damage, indicating that a tight regulation of TIIFN is required [215]. *Plasmodium*-induced TIIFN production can be induced by a variety of different PRRs, such as TLR9 and TLR4. Also cGAS is reported to sense parasite derived DNA in Malaria infection [216]. In the light of the discovery made in this thesis, cGAS could also contribute by another mechanism to TIIFN-driven Malaria pathogenesis. There are different indications that NETs might play a role in Malaria pathogenesis. Indeed, an accumulation of NET-associated proteins is described for pediatric patients suffering from cerebral Malaria, a severe variant of Malaria affecting the brain. Another report directly shows NETs in blood smears of pediatric Malaria patients [217,218]. According to my results, these NETs could also be recognized by cGAS and induce increased production of TIIFN, thereby contributing to an inflammatory feed-forward loop as described above for SLE. Notably, TIIFN primed neutrophils are shown to contribute to vascular damage in Malaria, one of the major risk factors in Malaria pathogenesis [219].

3.2 Escape of NETs from the phagosome into the cytoplasm

cGAS and NETs have to get in contact to induce TIIFN production. One possibility is that cGAS migrates to the phagosome and recognizes NETs there. cGAS is only known as a cytoplasmic protein and to date, no translocation of cGAS to the phagosome is described. Alternatively, NETs could escape from the phagosome to activate cGAS in the cytosol. There are different potential mechanisms how NETs could pass the membrane.

Inflammasomes are multi-protein complexes that recognize a variety of ligands. The NLRP3 inflammasome senses large crystalline structures, like silica or mono-sodium ureate crystals. These structures are internalized by macrophages by phagocytosis and also need to escape into the cytoplasm to activate the cytosolic receptor NLRP3. In 2015 Orlowski et al. demonstrated that Cathepsins, intracellular serine proteases, facilitate the liberation of crystals from the phagosome and mediate NLRP3 activation. Since NETs are also large structures, I reasoned that a similar mechanism might apply during their release. Initially, *in vitro* cocultivation of PMA-stimulated neutrophils and PBMCs in the presence of the pan-Cathepsin inhibitor K777 substantiated this assumption, because only reduced amounts of TIIFN were expressed (Fig. 2.19A). This phenotype was not reproduced in my *in vivo* mouse model when I tested mice carrying a triple knockout for the Cathepsins B, C and S (Fig. 2.19). This discrepancy could be caused by missing specificity of K777. Alternatively, K777 could inhibit a Cathepsin other than B, C or S. To finally solve this questions, an *in vitro* system for the activity of different Cathepsins in the presence of K777 would need to be established.

As described above, NETs are a very potent immune-stimulators, because they combine different DAMPs in one complex. Some of these molecules have the ability to alter membrane characteristics

and thereby allow escape of NETs from the phagosomes. NETs contain histones that are bound to the DNA as nucleosomes. Histones can be liberated from DNA when the surrounding milieu is acidic, like in the phagosomes of macrophages. This results in free highly charged histones that can bind the phosphodiester bonds of membrane phospholipids, inducing changes in membrane permeability. This could lead to the disruption of membranes and liberation of contained material, as shown for the lysis of endothelial cells by histones [220,221].

An antimicrobial protein that has similar characteristics to histones and is present in NETs is LL37. Similar to histones it has a high positive charge and could be released from NETs in an acidic environment like the phagosome. LL37 was shown to destabilize membranes by formation of membrane pores [222]. In complex with DNA, as it would occur in NETs, LL37 was described to induce TIIFN expression in pDCs [81], suggesting that it might support NET uptake.

Another NET-bound protein that is of interest in this context is high-mobility group box-1 (HMGB1). HMGB1 is a chromatin remodeling enzyme that has two DNA binding motifs. Apart from that, it is a potent alarmin that is actively released by monocytes and macrophages, but also passively during lytic cell death [223]. HMGB1 was shown to be present on NETs and is involved in NET-mediated TIIFN induction in pDCs [84]. HMGB1 can bind to the receptor of advanced glycation end-products (RAGE) and induce dynamin-dependent endocytosis. In this context, HMGB1 was shown to damage lysosomal membranes and confer liberation of intra-lysosomal content [224]. Although DNA import by RAGE alone is possible, HMGB1-RAGE interaction was shown to be required for lysosomal damage and the establishment of a potent TIIFN response towards DNA and RNA [225,226]. Only recently HMGB1 was reported to enhance cGAS activation by forming DNA-protein ladders that allow enhanced binding of cGAS [227].

The potential mechanisms suggested above have in common that NET-bound factors interfere with membranes and thereby could facilitate the release of NETs from phagosomes. Alternatively, cytosolic factors of the target cells that have taken up the NETs might contribute to the transport of NETs into the cytoplasm.

SID1 transmembrane family member 2 (SIDT2) is a transmembrane protein localized at the membrane of lysosomes. It shuttles dsRNA from the lysosome to the cytoplasm, where it is recognized by PRRs like mitochondrial antiviral signaling protein (MAVS) and RIG-I, in order to allow a fast recognition of extracellular viral material [228]. Interestingly, SIDT2 was shown to be able to transport DNA and work in a bidirectional fashion [229]. By actively exporting DNA from the lysosome into the cytoplasm, SIDT2 or related protein could contribute to the recognition of NET-fragments by cGAS.

Another possible mechanism that could allow the transport of NET components into the cytoplasm is the sampling machinery for the cross presentation of foreign antigens on major histocompatibility complex I (MHC-I) molecules. For the purpose of antigen presentation, molecules from the inside of the phagosome need to be exported by a channel into the cytoplasm [230]. Although the exact mechanism is still elusive, it is known that phagosomal content needs to be processed by the Endoplasmic reticulum-associated degradation (ERAD) in the cytoplasm to be further loaded on MHC-I [231]. During this process, NETs could have contact with cGAS.

3.3 ConA injection as a new *in vivo* model of systemic NET formation

The field of NET research lacks reliable *in vivo* systems to investigate the effect of NETs on other blood cells or endo- and epithelial cells. To date, most *in vivo* NET mouse models are based on injection of microbial components or infection of the animals. It is reported that a model of LPS-induced sepsis results in NET formation in the liver and induces thrombosis [173]. Also infections of mice with *S. flexneri*, *S. aureus* or *C. albicans* induce NET formation *in vivo* [33,174,186]. These models, however, have the constraint that NETs were only described at local sides of infection, like the lung in the case of *C. albicans* or the liver in case of *S. aureus*. In addition, injection of PAMPs or infections causes expression of inflammatory cytokines like TIIFN by activating various PRRs independently of the desired NET production. Investigating the contribution of a single receptor or signaling molecule might therefor be difficult. In order to investigate the effect of NET formation as it occurs in SLE for example, these models are less applicable. To circumvent this problem and mimic systemic NET formation, Lood et al. injected oxidized DNA, a component of NETs, i.v. together with DOTAP, a transfection reagent [85]. Although this approach is more closely related to pathological situations like in SLE, the co-injection of a transfection reagent might influence the outcome of the experiment.

In this thesis, I apply the model of ConA-induced autoimmune hepatitis as a systemic model of NET formation. ConA administration leads to the antigen-independent activation of cytotoxic T cells and hepatic Kupffer-cells, which release high amounts of TNF that is toxic for the endothelial layer and the hepatocytes residing below [175]. Only recently, ConA was shown to induce NETs i*n vitro* [174]. Here I report for the first time that ConA also induces NET formation *in vivo* (Fig. 2.14). This model has different advantages. Successful ConA injection can be verified by quantifying the liver enzymes AST and ALT, which serve as surrogate markers for liver damage. Since the resulting NET induction is systemic, an ELISA can be used to quantify NETs in serum and compare NET concentrations between different genotypes (Fig. 2.14). As presented in this study, systemic NET induction has an effect on the global expression of ISGs (Fig. 2.16), while, at least to my knowledge, no background TIIFN expression is reported in the literature. This notion is supported by my human cocultivation experiment of PBMCs

and neutrophils in the presence of ConA, where ConA treatment alone does not induce TIIFN, while neutrophils and ConA together induce TIIFN expression in PBMCs (Fig. 2.7). The experiments can be performed very rapidly compared to infection models. The system also has some drawbacks. The efficiency of ConA injection is variable between different animals (Fig. 2.14). Although ALT/AST values deviate between the different animals, all animals injected show significant ALT/AST release compared to uninjected animals. This variability is observed in multiple experiments and may result in differential levels of NET production that ultimately leads to different levels of ISG expression. The reason for this variability is not clear. Since the mice in one group are of the same background, sex and age, the experimental variability has to be attributed to the ConA injection procedure. Another drawback is that ConA induces massive liver damage and hepatocyte death, which results in the release of DAMPs like nucleosomes into the extracellular space. Although the NET ELISA allows accurate quantification of NETs and also a distinction between NETs and other DAMPs (Fig. 2.14D and E), it is hard to estimate the bias introduced by DAMPs from other dying cells or neutrophils undergoing degranulation.

The depletion of neutrophils did not result in an effect on ISG expression in this model (Fig. 2.17E-J). Although the FACS analysis showed that the antibody-mediated depletion was successful in blood (Fig. 2.17B), depleted mice still displayed NETs in their serum after ConA administration (Fig. 2.17C). This indicates that either there were enough remaining neutrophils to produce sufficient amount of NETs for cGAS activation or that the pool of depleted neutrophils is replenished during the experiment. In fact, during inflammatory conditions, like a systemic bacterial infection, the bone marrow is able to rapidly release tremendous amounts of neutrophils during a process called emergency granulopoiesis. This process is described both in humans and mice [232], and might very well be activated by ConA, either directly by its function as a mitogen or indirectly by causing hepatocyte death related cytokine production.

Interestingly, not all ISGs are regulated the same way when I compared different genotypes. Although the ISGs have in common that they are expressed upon IFNAR activation, they can also be induced by other signaling pathways independently of IFNAR engagement. CXCL10, for example, is the only ISG that is not downregulated in ConA stimulated Cybb$^{-/-}$ mice, when compared to Wildtype (Fig. 2.18 A). Apart from being activated by TIIFN signaling, CXCL10 is also upregulated by NFκB signaling (nuclear factor 'kappa-light-chain-enhancer' of activated B-cells), a transcription factor induced by a variety of other pathways, including TNF signaling. This could provide the explanation for the missing phenotype in Cybb$^{-/-}$ mice, because the TNF induced by the liver damage could upregulate CXCL10 independently of TIIFN [233].

Taken together, the applied ConA model combined with the NET ELISA allows a quantifiable systemic NET induction and opens the opportunity to investigate the effects of NETs on other immune cells.

3.4 Interaction of cGAS with other receptors

A group of innate DNA sensors execute the recognition of dsDNA in the cytoplasm that comprises, among others, cGAS, IFI16 and AIM2. Although each of them is a DNA sensor *per se*, they do not work as separated entities, but rather interact and regulate each other [234].

IFI16, a DNA sensor structurally related to AIM2, has a high binding affinity towards dsDNA. Two publications describe IFI16 as a co-factor required for potent cGAS activation in both human macrophages and keratinocytes [183,235]. The papers suggest that IFI16 is both important for cGAS binding to DNA but also for activation of STING by cGAMP. My results, achieved by stimulation of PMA-differentiated THP-1 cells as in Almine et al., do not support this observation (Fig. 2.5E). In my hands, IFI16$^{-/-}$ clones and cells of the positive control produced comparable amounts of TIIFN. This might be due to the different stimulus that is applied. While the Cytomegalovirus infection used in the publication transfers only a small amount of DNA into the target cells, the NET treatment used in my study might introduce larger amounts of DNA, and a supporting co-factor for enhanced DNA binding is no longer required. There is no direct ortholog of IFI16 in mice, but a mouse with depleted PYHIN-encoding genes (a domain also found in IFI16) does not show alterations in DNA sensing [236], supporting my observation that IFI16 is dispensable for cGAS activation.

Another DNA receptor undergoing mutual regulation with cGAS is AIM2. In primary murine BMM I observed increased TIIFN production following NET stimulation after silencing of the AIM2 inflammasome pathway. This occurred independently of whether the priming (MyD88$^{-/-}$), the DNA sensor (AIM2$^{-/-}$) or the executing caspases (CASP1/11$^{-/-}$) were affected (Fig. 2.6D). This result indicates that AIM2 is a negative regulator of cGAS activation, a result supported by recent literature. Banerjee et al. describe that AIM2 activation results in GSDMD pore formation and a subsequent K^+ efflux from the cell that has an inhibitory effect on cGAS activation [237]. Another publication reports an overproduction of IFNβ in a *M. tuberculosis* infection model in an AIM2$^{-/-}$ background. They show that apoptosis-associated speck-like protein (ASC) interferes with the interaction of TBK1 and STING, downstream of cGAS [238]. Lastly, AIM2 activation induces caspase1 dependent cleavage of cGAS, resulting in decreased TIIFN production [239]. In addition to the mechanisms mentioned above, blocking of pyroptosis by inflammasome inhibition generally results in a prolonged life-span and allows increased production of TIIFN.

I also observed increased AIM2-mediated IL1β production in cGAS$^{-/-}$ BMM when compared to Wildtype, while NLRP3 activation remained unchanged (Fig. 2.6E). This indicates that cGAS is a negative regulator of AIM2, a notion that is in opposition with the recent literature. Different papers show that activation of the cGAS-STING pathway has a priming effect on inflammasome activation. This occurs either directly by driving IFNβ production, which is an external priming signal for inflammasome activation or by producing cGAMP, which induces IL1β production by a AIM2-dependent mechanism [240].

Taken together, these findings indicate that cGAS activation by NETs is not an isolated immunological signaling event, but rather incorporates into a complex signaling network of different receptors and pathways.

3.5 Conclusion and Outlook

The results presented in this thesis contribute to answering the central question of how a specific form of neutrophil cell death can contribute to the development and progression of autoinflammatory diseases. It closes the gap between the undesired production of NETs and the expression of TIIFN, a group of pro-inflammatory cytokines that are involved in a plethora of different diseases by showing that NETs are recognized by the cytosolic DNA sensor cGAS, which controls TIIFN expression. My data describe a hitherto unknown process by which cGAS is activated in the cytoplasm of an intact phagocytic cell that has feasted upon NETs. In doing so, I am the first to present NETs as a self-ligand of an extracellular source that is able to activate cGAS leading to the production of TIIFN. These findings have implications for a growing list of NET-associated diseases, because it helps on the one hand to understand their etiology and on the other hand it opens a window for the development of new treatment strategies, which hopefully will bring improvement to the affected patients.

A possible next step would be to investigate the role of cGAS activation by NETs in murine models for SLE like the DNAse1L3$^{-/-}$ mouse, which spontaneously develops a lupus-like phenotype. To test the effect of cGAS in this model, the mice could be treated with pharmacological inhibitors of cGAS like RU.521 or they can be crossed onto a cGAS$^{-/-}$ background. Furthermore, I would address the question how NETs escape from the phagosome, by inhibiting the HMGB1-RAGE pathway or SIDT2 with small molecule inhibitors.

4 Material and Methods

4.1 Material

4.1.1 Eukaryotic and prokaryotic Cells

Eukaryotic cells – cell lines

Name	Origin	Medium and culture conditions
HEK-Blue™ IFN-α/β Cells (Invivogen)	human, embryonic kidney cell line carrying SV40-large T antigen	DMEM basic medium, 37°C, 5 % CO_2 split every 3 days at ratio 1:5
HEK293T	human, embryonic kidney cell line carrying SV40-large T antigen	DMEM basic medium, 37°C, 5 % CO_2 split every 3 days at ratio 1:5
THP-1	human, monocytic leukemia	RPMI basic medium, 37°C, 7 % CO_2 split every 3 days at ratio 1:5
L929 ISRE luc	murine, fibroblast	DMEM basic medium, 37°C, 5 % CO_2 split every 3 days at ratio 1:5
Immortalized Balb/C Macrophages	Murine, macrophage	DMEM basic medium, 37°C, 5 % CO_2 split every 3 days at ratio 1:5

Eukaryotic cells – primary cells

Genotype	Origin	Medium and culture conditions
Wildtype	murine, primary cells from bone marrow	DMEM with 10 % FCS, Q, P/S and 20 % L-cell supernatant containing mMCSF
$AIM2^{-/-}$	murine, primary cells from bone marrow	DMEM with 10 % FCS, Q, P/S and 20 % L-cell supernatant containing mMCSF
$CASP1/11^{-/-}$	murine, primary cells from bone marrow	DMEM with 10 % FCS, Q, P/S and 20 % L-cell supernatant containing mMCSF
$cGAS^{-/-}$	murine, primary cells from bone marrow	DMEM with 10 % FCS, Q, P/S and 20 % L-cell supernatant containing mMCSF
$MyD88^{-/-}$	murine, primary cells from bone marrow	DMEM with 10 % FCS, Q, P/S and 20 % L-cell supernatant containing mMCSF

Prokaryotic cells

Name	Genotype	Application	Source
E. coli DH5α	F-ϕ80lacZΔM15 Δ(lacZYAargF)U169 recA1 end A1hsdR17 (rk-,mk-) phoAsupE44 thi-1 gyrA96 relA1 λ-	Chemically competent bacteria for plasmid amplification	Invitrogen (Carlsbad, CA, USA)

4.1.2 Mouse strains

Strain	Short name	Description	Source
C57BL/6	Wildtype	Wildtype mice in C57BL/6 background	The Jackson Laboratory
Mb21d1$^{tm1a(EUCOMM)Hmgu}$	cGAS$^{-/-}$	Strain carrying a knockout of the cytosolic DNA sensor cGAS	Kindly provided by Veit Hornung, Genzentrum München, Germany
B6.129S6-Cybb tm1Din /J	Cybb$^{-/-}$ KO	Strain carrying a knockout in the Cybb subdomain of NADPH oxidase	The Jackson Laboratory
B6.129X-Ctsb^{tm1Vil} Ctsc^{tm1Ley} Ctss^{tm1Cha}/J	CtsBCS TKO	Strain carrying a tripple knockout for the Cathepsins B, C and S.	Kindly provided by Kenneth Rock, University of Massachusetts, USA

4.1.3 Media

Name	Ingredients
DMEM basic	DMEM with 10 % (v/v) FCS, 2 mM L-glutamine, 100 U/ml Penicillin, 100 µg/ml streptomycin
RPMI basic	RPMI with 10 % (v/v) FCS, 2 mM L-glutamine, 100 U/ml Penicillin, 100 µg/ml streptomycin
RPMI neutrophil medium	RPMI w/o phenol red, 0,2 % HSA, 5 mM HEPES
DMEM BMM	DMEM with 10 % (v/v) FCS, 2 mM L-glutamine, 100 U/ml Penicillin, 100 µg/ml Streptomycinand 20% L-cell supernatant containing mMCSF
freezing medium	90 % FCS and 10 % DMSO

4.1.4 CRISPR gRNA

Target gene	number of guide	gRNA sequence (no PAM) 5'→3'
hcGAS	1	GGCCATGCAGAGAGCTTCCG
hcGAS	2	CTGCCCCCAAGGCTTCCGCA
hDAI	1	CCTTGAACAAAGAATCCTGC
hDAI	2	AGGAATGCCAAGCACCCAAG
hIFI16	1	GACCAGCCCTATCAAGAAAG
hIFI16	2	CAAGCAGCACTGTCAAAACT
hIRF3	1	GGGCAGGATCCGTGGCTTTG
hIRF3	2	TGGTGTCGCAGCTGGACCTG
hNE	1	ACTCGCGTGTCTTTTCCTCG
hNE	2	TGCGCCCAACTTCGTCATGT
hSTING	1	CACTCCAGCCTGCATCCATC
hSTING	2	CTCCAGCCTGCATCCATCCA
hTLR9	1	CCGGACTGCCACACTTCACC
hTLR9	2	GCTCCGAAGCTCCGCTGATG
mcGAS	1	AGATCCGCGTAGAAGGACGA
mcGAS	2	GCGAGGGTCCAGGAAGGAAC
mNE	1	AGAGATTGTTGGTGGCCGGC
mNE	2	TGACCTGCGGCGACAGGAGC
mSTING	1	GATGATCCTTTGGGTGGCAA
mSTING	2	CTCCAAATATGTAGCCCTCA

4.1.5 Oligonucleotides

Primer for qPCR

species	gene	orientation	sequence 5'→3'
human	hIFNA1	fwd	TGGAAGCCTGTGTGAT
		rev	ATGATTTCTGCTCTGACA
	hIFNB	fwd	GTCAGAGTGGAAATCCTAAG
		rev	CTGTAAGTCTGTTAATGAAG
	hB2M	fwd	CTCCGTGGCCTTAGCTGTG
		rev	TTTGGAGTACGCTGGATAGCCT
mouse	mCXCL10	fwd	CCAAGTGCTGCCGTCATTTT
		rev	CTCAACACGTGGGCAGGATA
	mGAPDH	fwd	AACTTTGGCATTGTGGAAG
		rev	ACACATTGGGGGTAGGAAC
	mIFIH1	fwd	ATGGACGCAGATGTTCGTGG
		rev	TCCCTTCTCGAAGCAAGTGTC
	mIFIT1	fwd	TGCTGAGATGGACTGTGAGG
		rev	CTCCACTTTCAGAGCCTTCG
	mIFIT2	fwd	GGAGAGCAATCTGCGACAG
		rev	GCTGCCTCATTTAGACCTCTG
	mMX1	fwd	GATCCGACTTCACTTCCAGATGG
		rev	CATCTCAGTGGTAGTCAACCC
	mOAS1A	fwd	GCCTGATCCCAGAATCTATGC
		rev	GAGCAACTCTAGGGCGTACTG

Primer for Outknocker

To validate the efficiency of the knock out, the target locus was amplified with the primers indicated below, which were fused to the following adapter sequences:

Adapter for Fwd-primer: ACACTCTTTCCCTACACGACGctcttccgatct-primer
Adapter for Rev-primer: TGACTGGAGTTCAGACGTGTGctcttccgatct-primer

Target	guide	fwd primer 5'→3'	rev primer 5'→3'
hcGAS	1	TGTGCCCGCCAGTAGTGCTTGGT	TTTTCTGCCGGGATCCCGACTTC
hcGAS	2	GCTGCTGCTGGCTCTTCCTCTTG	GGCGCTCTTTTTCTGCCGGGATC
hDAI	1	TTGCCCTTTCCTCTGCCCTGGAC	TGTGAGGGAGACTTTCAACTCCT
hDAI	2	TGGGGACCTGGGAGACTCAGTTC	CAAGGCCAGCTCTGCAGGACCCT
hIFI16	1	GAACCCTCAAGCAGGAACTGAGA	GGACTTGAAGCCTGCTCCTCTTC
hIFI16	2	CTGCTTCAGCTGTCGGAGATCGT	AGAAATAACTGCCTGCTGGAGAG
hIRF3	1	AAAATATGGGTGAAGGACCTGTG	GAAATCCTCCTGCTGTGCATCCT
hIRF3	2	AGGAGGTCTGGGTGCGGAAACTC	CGTCGCACGCACCTGGAAGATTC
hNE	1	GTGCCAGGGGAGAGGAAGTGGAG	AGGATGAGGGACCCACACTGGTG
hNE	2	CAGGCTCCTTGGCAGGCACTCAG	GCCTGAGGGCGAAGGTGCTCGAG
hSTING	1	TGGGAGTGGCTGGGCACCAGGGA	TGGAGCACCAGGTACCGGAGAGT
hSTING	2	GAGTGGCTGGGCACCAGGGAAAG	TAGGTGGAGCACCAGGTACCGGA
hTLR9	1	CAAGACAGTGGACCACTCCTGGT	TGATGCAGCATGGGCACACCCAG
hTLR9	2	CTTCCGCTCACTCGATGAGACCA	TGAAGTTGAGGGTGCTGCAGTTG
mcGAS	1	GCGGATACTGACCGGCTACGTTC	TCCGTGGTGTCCCCGTCACGCTC
mcGAS	2	AGGCCATCCTGGATCCGGAGCTG	CCGACTCCCGTTTCTGCATTCTG
mNE	1	GGCTAGGTCCCTTGTCTTTTCTC	ACTCACAGGCCGTTCACACAGTG
mNE	2	GCCCTCAATGTCCATGCGGGTCA	TTGCACGAGGCTCAGGTTCCTGA
mSTING	1	CAGAAGCATAGCTGTGGATTTCT	GTTACCTGGACTGGACATGGCAC
mSTING	2	CTAGTCAGGACCTTAGGCCCTGA	CAGCAGAGGTTTTTCAACAGTAG

For the subsequent sequencing analysis, a second PCR step was performed. The used primers contained the binding sites for the sequencing chamber and Illumina barcode indices. The combination of a barcoded fwd- and rev-primer allowed to trace back in which well which clone was frozen, once the sequencing results were received.

primer	sequence	Illumina Barcode Index
Barcode fwd 1	AATGATACGGCGACCACCGAGATCTACACTATAGCCTACACTCTTTCCCTACACGACGCT	D501
Barcode fwd 2	AATGATACGGCGACCACCGAGATCTACACATAGAGGCACACTCTTTCCCTACACGACGCT	D502
Barcode fwd 3	AATGATACGGCGACCACCGAGATCTACACCCTATCCTACACTCTTTCCCTACACGACGCT	D503
Barcode fwd 4	AATGATACGGCGACCACCGAGATCTACACGGCTCTGAACACTCTTTCCCTACACGACGCT	D504
Barcode fwd 5	AATGATACGGCGACCACCGAGATCTACACAGGCGAAGACACTCTTTCCCTACACGACGCT	D505
Barcode fwd 6	AATGATACGGCGACCACCGAGATCTACACTAATCTTAACACTCTTTCCCTACACGACGCT	D506
Barcode fwd 7	AATGATACGGCGACCACCGAGATCTACACCAGGACGTACACTCTTTCCCTACACGACGCT	D507
Barcode fwd 8	AATGATACGGCGACCACCGAGATCTACACGTACTGACACACTCTTTCCCTACACGACGCT	D508
Barcode rev 1	CAAGCAGAAGACGGCATACGAGATCGAGTAATGTGACTGGAGTTCAGACGTGTGCT	D701
Barcode rev 2	CAAGCAGAAGACGGCATACGAGATTCTCCGGAGTGACTGGAGTTCAGACGTGTGCT	D702
Barcode rev 3	CAAGCAGAAGACGGCATACGAGATAATGAGCGGTGACTGGAGTTCAGACGTGTGCT	D703
Barcode rev 4	CAAGCAGAAGACGGCATACGAGATGGAATCTCGTGACTGGAGTTCAGACGTGTGCT	D704
Barcode rev 5	CAAGCAGAAGACGGCATACGAGATTTCTGAATGTGACTGGAGTTCAGACGTGTGCT	D705
Barcode rev 6	CAAGCAGAAGACGGCATACGAGATACGAATTCGTGACTGGAGTTCAGACGTGTGCT	D706
Barcode rev 7	CAAGCAGAAGACGGCATACGAGATAGCTTCAGGTGACTGGAGTTCAGACGTGTGCT	D707
Barcode rev 8	CAAGCAGAAGACGGCATACGAGATGCGCATTAGTGACTGGAGTTCAGACGTGTGCT	D708
Barcode rev 9	CAAGCAGAAGACGGCATACGAGATCATAGCCGGTGACTGGAGTTCAGACGTGTGCT	D709
Barcode rev 10	CAAGCAGAAGACGGCATACGAGATTTCGCGGAGTGACTGGAGTTCAGACGTGTGCT	D710
Barcode rev 11	CAAGCAGAAGACGGCATACGAGATGCGCGAGAGTGACTGGAGTTCAGACGTGTGCT	D711
Barcode rev 12	CAAGCAGAAGACGGCATACGAGATCTATCGCTGTGACTGGAGTTCAGACGTGTGCT	D712

4.1.6 Plasmids

Designation	Insert	Application	Source
plentiCRISPRv2ccdB	CRISPR gRNA	targeted CRISPR knock outs, carries Cas0, gRNA and Puromycin selection cassette	Addgene [155]
pMD.2G	-	Envelope plasmid for production of lentiviral particles	Kindly provided by Achim Kramer, Charité Berlin, Germany
psPAX2	-	Packaging plasmid for production of lentiviral particles	Kindly provided by Achim Kramer, Charité Berlin, Germany

4.1.7 Enzymes and buffers

Enzyme	Company	Catalog#
BsmBI	New England Biolabs	R0580L
DNAse1	New England Biolabs	M0303S
DNAse1 reaction buffer	New England Biolabs	B0303S
Horseradish peroxidase	Sigma-Aldrich	77332
Proteinase K	New England Biolabs	P8107S
T4 DNA Ligase	Promega	M180
T4 DNA ligase buffer	Promega	C126

4.1.8 Kits

ELISAs

Kit	Target	Company	Catalog#
Interferon α All Subtype ELISA Kit	human IFN α	PBL Assay Science	41115-1
Human CXCL10/IP-10 DuoSet ELISA	human CXCL10	R&D Systems	DY266
VeriKine Mouse Interferon β ELISA Kit	murine IFN β	PBL Assay Science	42400-1
Cell Death Detection ELISA^{PLUS}	nucleosomes	Sigma-Aldrich	11774425001
Human Complement C1q ELISA Kit	Human C1q	Abcam	ab170246
Human Anti-Nuclear Antibodies (ANA) ELISA Kit	ANA Autoantibodies	Alpha Diagnostics	3205

Other Kits

Kit	Company	Catalog#
A&B Fast SYBR Green Master mix	Thermo Fisher Scientific	4385612
AlamarBlue™ Cell Viability Reagent	Thermo Fisher Scientific	DAL1025
Bright-Glo™ Luciferase Assay System	Promega	E2610
CD14 MicroBeads	Miltenyi Biotec	130-050-201
Giemsa Stain Kit	Abcam	ab150670
High-Capacity cDNA reverse transcription Kit	Thermo Fisher Scientific	4368814
Low input Quick-Amp Labeling Kit, one color	Agilent Technologies	5190-2305
Mitochondria Isolation Kit for Mammalial cells	Thermo Fisher Scientific	89874
Phusion® High-Fidelity PCR Kit	New England Biolabs	E0553L
Plasmacytoid Dendritic Cell Isolation Kit II	Miltenyi Biotec	130-097-415
Quant-iT™ PicoGreen ® dsDNA Kit	Thermo Fisher Scientific	P11496
Whole mouse genome 4x44K microarray kit	Agilent Technologies	G4122F
Zymoclean Gel DNA recovery Kit	Zymo Research	D4007
Zyppy Plasmid Miniprep Kit	Zymo Research	D4020

4.1.9 Buffers

Buffer/Solution	Ingredients
FACS buffer (mouse samples)	PBS, 2,5 % /v/v) FCS, 0,1 % (w/v) NaN_3
MACS buffer	PBS, 0,2 % (w/v) HSA, 5 mM EDTA
IFA buffer	PBS, 3 % (v/v) serum (depending on primary antibody), 3 % (v/v) cold water fish gelatine, 1 % (w/v) BSA , 0,5 % Tween 20 (v/v)
ELISA dilution buffer	PBS-T, 1 % (w/v) BSA
PBS/HSA	PBS, 0,02 % (w/v) HSA
RBC lysis buffer	dH_2O, 15,4 mM NH_4Cl, 1 mM $KHCO_3$, 127,3 µM EDTA
Outknocker lysis buffer	dH_2O, 0,2 mg/ml Proteinase K, 1 mM $CaCl_2$, 3 mM $MgCl_2$, 1 mM EDTA, 1 % Triton X100, 10 mM Tris (ph7.5)
PBS-T	PBS, 0,05 % Tween 20
PBS	Dulbecco's PBS (Gibco Cat.# 14190094)
dH_2O	UltraPureTM Distilled Water (Invitrogen Cat.# 10977-035)
TE	dH_2O, 10 mM Tris (pH 8.0), 1 mM EDTA
Lavage solution	PBS, 0,02 % (v/v) EDTA
Casein solution	PBS, 7 % (w/v) Casein

4.1.10 Antibodies and Dyes

FACS antibodies

Antigen	target-species	Fluorochrome	Company	Dilution	Catalog#
CD115	mouse	PE	BD	1:100	562249
CD3	mouse	FITC	BD	1:100	561798
CD4	mouse	Pe-Cy7	BD	1:100	552775
CD45	mouse	V500	BD	1:100	561487
CD8a	mouse	APC	BD	1:100	561093
Gr1	mouse	PerCP-Cy5.5	Biolegend	1:100	108428
CD14	human	PE	Miltenyi Biotec	1:100	170-078-013
CD15	human	FITC	Miltenyi Biotec	1:40	170-078-051
CD66b	human	APC-Vio770	Miltenyi Biotec	1:40	130-104-399

Antibodies for other applications

Name	Target	Application	Company	Catalog#
MPO-Biotin	murine MPO	NET ELISA	Hycult Biotech	HM1051BT
pIRF3	human phosphorylated IRF3	FACS	Cell Signaling	D601M
1A8	Ly6G	neutrophil depletion	BioXcell	BP0075-1
2A3	isotype control	isotype control	BioXcell	BP0089
PL23	chromatin	Immunofluorescence	made in house	-
NE	human NE	Immunofluorescence	Calbiochem	481001

Secondary antibodies

Name	Reactivity	Origin	Fluorochrome	Company	Catalog#
anti-mouse Alexa568	mouse	goat	Alexa Fluor 568	Thermo Fisher Scientific	A-21124
anti-rabbit Alexa488	rabbit	goat	Alexa Fluor 488	Thermo Fisher Scientific	A-11008

Dyes and Probes

Name	Company	Catalog#
4',6-diamidino-2-phenylindole (DAPI)	Thermo Fisher Scientific	62247
Cell tracker™ Deep Red Dye	Thermo Fisher Scientific	C34565
Hoechst 33342	Thermo Fisher Scientific	62249
Lyso Tracker™ Red DND-99	Thermo Fisher Scientific	L7528
Syto™ Green Nucleic Acid Stain	Thermo Fisher Scientific	S7578
Sytox™ Orange Nucleic Acid Stain	Thermo Fisher Scientific	S11368

4.1.11 Chemicals

Chemical	Company	Catalog#
Agarose	Biozym	840004
Albutein (HSA)	Grifols	G4AFB05201
Amlexanox	Invivogen	inh-amx
Bafilomycin	Invivogen	tlrl-baf1
BSA	Carl Roth	8076.3
Calf-Thymus DNA	Thermo Fisher Scientific	15633019
Carbenecillin	Sigma-Aldrich	C1613
Casein Sodium salt	Sigma-Aldrich	C8654
CCCP	MedChemExpress	HY-100941
Chloroform	Honeywell	602-006-00-4
ConA	Sigma-Aldrich	C5275-5MG
Cytochalasin B	Sigma-Aldrich	C6762
DL-Dithiothreitol	Sigma-Aldrich	43815
DMSO	Sigma-Aldrich	D8418
DOTAP	Carl Roth	L787.2
EDTA	Sigma-Aldrich	E6758
Elastase inhibitor (NEi)	Biomol	AG-CR1-3632-M001
Ethanol	Merck	1.009.832.511
Ethidiumbromide	Thermo Fisher Scientific	15585011
FcR blocking reagent, human	Miltenyi Biotec	130-059-901
FCS	Merck	S0115
fMLP	Sigma-Aldrich	F3506
Gelatin from cold water fish skin	Sigma-Aldrich	G7765
Glycogen	Thermo Fisher Scientific	R0561
hIFNγ	Sigma-Aldrich	SRP3058

hIFNα universal	PBL Assay Science	11200-1
hIFNβ	PBL Assay Science	11415-1
Histopaque 1119	Sigma-Aldrich	11191-100ML
hMCSF	Miltenyi Biotec	130-096-485
Isopropanol	Fisher Chemical	P/7500/17
K777	Adipogen	AG-CR1-0158-M001
L-Glutamine	Gibco	25030-024
Lipofectamine 2000	Thermo Fisher Scientific	11668027
LPS	Enzo Life Science	ALX-581-011-L001
Luminol	AAT Bioquest	11050
MeOH	Merck	1.060.092.500
mGCSF	Peprotech	250-05
Nigericin	Sigma-Aldrich	N7143
Nystatin	Sigma-Aldrich	N6261
Paraformaldehyde	Sigma-Aldrich	P6148
pdAdT	Invivogen	tlrl-patn
Penicillin/Streptomycin	Gibco	15140-122
Percoll	GE Healthcare	17-0891-02
PMA	Sigma-Aldrich	P8139
Puromycin	Sigma-Aldrich	P8633
Quanti-Blue solution	Invivogen	rep-qb1
RU.521	Invivogen	inh-ru521
Sivelestat	Sigma-Aldrich	S7198
Sodiumacetate	Sigma-Aldrich	S2889
TRIS	Carl Roth	9090.3
TritonX 100	Sigma-Aldrich	X100
TRIZOL	Thermo Fisher Scientific	15596026
Trypsin	Promega	V5111
Tween 20	Sigma-Aldrich	P1379
zVAD-FMK	Invivogen	tlrl-vad

4.1.12 Material

Name	Company	Catalog#
12-well plate	Sarstedt	83.3921
15µ-Slide 8-well	IBIDI	80827
24-well plate	Sarstedt	83.3922
6-well plate	Sarstedt	83.3920
96-well plate	Sarstedt	83.3924
Cellscraper	Sarstedt	83.1832
Cover glasses 13mm	Thermo Fisher Scientific	0864
Eppendorf Tubes	Eppendorf	0030120086
FACS tubes	BD	352054
Falcon tubes 15 ml	Corning	430791
Falcon tubes 50 ml	Corning	430829

LS columns	Miltenyi Biotec	130-042-401
MicroAMP Fast Optical96-well Reaction plate	Applied Biosystems	4346906
MicroAMP 8-tube-Strip 200 µl	Applied Biosystems	N8010838
Microscope slide	Marienfeld	1010612
MidiMACS Separator	Miltenyi Biotec	130-042-302
Plastipak 1 ml Sub-Q syringe	BD	305501
S-Monovette K3E	Sarstedt	02.1066.001
S-Monovette Serum	Sarstedt	02.1063.100
Sterican needle 18 G x 1,5"	Braun	4658313
Steril filter system 500 ml	Corning	430758
Stuffed tips 10 µl	Thermo Fisher Scientific	2139
Stuffed tips 1000 µl	Corning	4140
Stuffed tips 200 µl	Corning	4136
Tissue culture Bottle T175	Sarstedt	83.3912.002
Tissue culture Bottle T25	Sarstedt	83.3910.002
Tissue culture Bottle T75	Sarstedt	83.3911.002

4.1.13 Machines

Machine	Company
Agilent 2100 Bioanalyzer	Agilent Technologies
Casy Cell Counter	OMNI Life Science
Centrifuge 5415D	Eppendorf
Compact Thermomixer	Eppendorf
EVOS FL Auto2	Thermo Fisher Scientific
Fluoroskan Ascent	Thermo Fisher Scientific
G2565CA High-resolution Laser Microarray Scanner	Agilent Technologies
Gel Doc XR+	BioRad
Innova 44R Bacterial shaker	New Brunswick Scientific
MACS Quant	Miltenyi Biotec
Microconcentrator 5301	Eppendorf
Multifuge 3S-R	Thermo Fisher Scientific
NanoDrop2000	Thermo Fisher Scientific
Optima L-90K Ultra Centrifuge	Beckmann Coulter
Orbitrap LC-MS	Thermo Fisher Scientific
QuantStudio 3	Thermo Fisher Scientific
Sonopuls Sonicator	Bandelin
TCS SP8 Confocal Microscope	Leica Microsystems
Thermo Cycler S1000	BioRad
Thermo Forma Cell Culture Incubator	Thermo Fisher Scientific
Versa Max microplate reader	Molecular devices
Victor X Light Luminescence Reader	Perkin Elmer

4.1.14 Software

Name	Version	Company
GraphPad PRISM	7.03	GraphPad Software
MACS Quantify	2.11	Miltenyi Biotec
FlowJo	10.2	FlowJo
ImageJ	1.52c	National Institute of Health, USA
Quant Studio Design & Analysis	1.4.1	Thermo Fisher Scientific
Perkin Elmer 2030 Workstation	4.0	Perkin Elmer
Rosetta Resolver Biosoftware	7.2.2	Rosetta Biosoftware

4.2 Methods

4.2.1 Human primary immune cells

Isolation of human neutrophils

The ethics council of the Charité Berlin (Germany) approved blood sampling and all donors gave informed consent according to the Declaration of Helsinki.

Human neutrophils were isolated by a two-step density separation as described before [35]. Heparinized blood (5 U/ml) was layered on an equal volume of histopaque 1119 and centrifuged at 800 g for 20 min. PBMCs and neutrophil layers were collected separately, washed with PBS 0,2 % HSA and pelleted at 300 g 10 min. The neutrophil pellet was resuspended in PBS 0,2 % HSA, layered on a discontinuous Percoll gradient (85 %-65 % in 2ml layers) and centrifuged at 800 g for 20 min. The neutrophil containing band was collected, washed in PBS 0,2 % HSA and pelleted for 10 min at 300 g. The cell number was determined using a CASY cell counter (OMNI Life Science).

Isolation of human monocytes and differentiation in macrophages

Monocytes were isolated by positive selection. The PBMC fraction generated during neutrophil isolation was washed again in MACS buffer and pelleted 10 min at 300 g. The cells were resuspended in MACS buffer and counted using the CASY cell counter (OMNI Life Science). After subsequent pelleting, 80 µl MACS buffer and 20 µl magnetic CD14-beads were added per 10^7 cells and the mixture was incubated for 15 min at 8°C. After another washing step, the cells were passed through a magnetic LS MACS column (Miltenyi) by gravity flow. The column was washed with 8 ml of MACS buffer and bound monocytes were subsequently eluted with 5 ml MACS buffer, washed and counted. The purity of the preparation was determined by FACS staining with an anti-CD14 antibody. Monocytes were cultivated in RPMI basic medium at 37°C, 7 % CO_2.

To generate monocyte-derived macrophages (MDM), monocytes were taken up in RPMI basic medium supplemented with 5 ng/ml hMCSF and incubated at 37°C and 7 % CO_2 for a total of 7 days, including a medium change after three days.

Isolation of human pDCs

pDCs were isolated by negative selection. The PBMC fraction was washed and counted as described above and incubated for 10 min with 100 µl non-pDC biotin-antibody cocktail II and 400 µl MACS buffer per 10^8 PBMCs. After subsequent washing, non-pDC microbead cocktail II was added at the same ratio and incubated for 15 min at 8°C. The cell suspension was added to a LS MACS column (Miltenyi) and allowed to pass by gravity flow. After washing the column with 8 ml of MACS buffer, the flow through was collected, pelleted and the cells were counted by CASY cell counter (OMNI Life Science). pDCs were cultivated in RPMI basic medium at 37°C, 7 % CO_2.

4.2.2 Murine primary immune cells

Isolation of murine neutrophils

Mice were injected i.p. with 1 ml of 7 % Casein solution in the evening and again after 12 h at the next morning. Three hours after the second injection, mice were sacrificed by rapid cervical dislocation. The peritoneal cavity was flushed with a total of 10 ml of lavage solution and the exiting liquid with the cells was collected. The cells were pelleted by centrifugation at 200 g for 10 min and washed three times with PBS. After washing the cells were resuspended in 1 ml of PBS and mixed with 9 ml Percoll gradient. Neutrophils were separated by continuous density centrifugation for 20 min at 60000 g and the upper band containing the neutrophils was collected. Subsequently neutrophils were washed and counted in the CASY cell counter (OMNI Life Science). To assess cell purity, a cytospin with $1x10^5$ cells was stained with Gimsa and analyzed by microscopy. Neutrophils were identified by their nuclear morphology.

Generation of bone-marrow derived macrophages (BMM)

The mice were sacrificed by rapid cervical dislocation and the femurs of their hind legs were collected. The bones were rinsed with 70 % EtOH and washed in PBS. The bone-marrow was flushed out with PBS. The cells were pelleted at 300 g for 10 min and red blood cells were lysed using 3 ml RBC lysis buffer for 3 min on ice. The cells were resuspended in DMEM with 10 % FCS, Q, P/S and 20 % L-cell supernatant containing mMCSF. Cells differentiated for 7 days at 37°C, 5 % CO_2.

4.2.3 Generation of gene specific CRISPR knockouts in human and murine cell lines

Cultivation of cell lines

For generation of CRISPR knockouts a human and a murine cell line were chosen. The human monocyte-like cell line THP1 was cultured in RPMI basic medium at 37°C, 7 % CO_2. Murine immortalized Balb/C macrophages were cultured in DMEM basic medium at 37°C, 5 % CO_2.

gRNA design

gRNA sequences targeting all possible transcript variants were obtained from ChopChop (https://chopchop.rc.fas.harvard.edu) and tested for sequence specificity using NCBI Nucleotide Basic local alignment search tool (BLAST, https://blast.ncbi.nlm.nih.gov/Blast.cgi). Oligonucleotides consisting of the gRNA (20 bp, without PAM-sequence) flanked by adapter sequences were generated that had the following structure:

5'-GT CGTCTC C CACC G – 20 bp-gRNA – GTTT C GAGACG TG-3'

The reverse complement oligonucleotide was generated using an online tool (http://reverse-complement.com/). The oligonucleotides were synthetized by Sigma-Aldrich (Darmstadt, Germany).

Oligo-annealing, ligation into plentiCRISPRv2ccdB and transformation into chemo-competent E.Coli

The oligonucleotides were resuspended in 1 µl dH_2O (100 µM) of forward and reverse oligonucleotide were combined with 98 µl TE buffer, heated to 99°C for 5 min and allowed to cool down to room temperature (RT). Using a Golden gate cloning strategy, the annealed oligonucleotides were ligated into the plentiCRISPRv2ccdB target vector.

Cloning mix		Cloning reaction		
component	amount	temperature	time	
plentiCRISPRv2ccdB	50 ng	37°C	5 min	10x
T4 ligase buffer	2 µl	16°C	10 min	
T4 ligase	1 µl	55°C	5 min	
BsmBI	1 µl (10 U/µl)	80°C	5 min	
Annealed oligonucleotides	1 µl	4°C	∞	
dH_2O	Ad 20 µl			

10 µl of the ligation mix were added to recA-deficient *E. coli* DH5α and incubated for 10 min on ice. After a 45 sec heat shock to 42°C, bacteria were stored for 1 min on ice. 1 ml LB medium was added

and the bacteria were incubated for 1 h rotating at 37°C. The cells were pelleted for 5 min at 1000 g and plated on selective agar plates containing Carbenicilin (100 µg/ml).

Isolation of plasmid DNA from bacteria

5 ml LB were inoculated with a single colony and incubated shaking o.n. at 37°C under selective conditions. Bacteria were pelleted and plasmid DNA was isolated using the Zyppy Plasmid Miniprep Kit (Zymo research) according to manufacturers instructions. The DNA concentration was determined with the NanoDrop2000 (Thermo Fisher Scientific). The plasmids were sent for sequencing (Eurofins Genomics, Anzinger Str. 7a, 85560 Ebersberg, Germany) using the hU6-F primer (5'-GAGGGCCTATTTCC CATGATT-3').

Lentivirus production

$8x10^5$ HEK 293T cells were seeded in a 6-well plate the day before transfection. On the day of transfection, the medium was replaced with 1 ml OptiMEM medium. 2 µg plentiCRISPRv2ccdB, 0,5 µg psPAX, 1,5 µg pMD2.G and 7 µl Lipofectamine were combined in 500 µl OptiMEM and incubated for 15 min at RT. The transfection mix was added carefully to the HEK 293T cells and cells were incubated at 37°C and 5 % CO_2. The medium was replaced with DMEM basic medium after 24 h, virus was harvested after 72 h and 96 h and stored at -80°C.

Transduction and selection of target cells

$1x10^6$ target cells were seeded in 1 ml of their respective medium in a 6-well plate. 1 ml of viral supernatant was added and cells were incubated for 4 h at 37°C, then 3 ml fresh medium were added. After 48 h, the medium was replaced and cells were kept under selective conditions with 5 µg/ml Puromycin for 72 h.

Generation of single clones by limited dilution cloning

The cells were counted by CASY cell counter (OMNI Life Science). For each construct 500 wells with 0,8 cells/well in 200 µl medium were seeded. The cells were cultivated for approx. two weeks until colonies appeared. 32 clones of each constructs were transferred into a new plate and cultivated for another two days. The cells were split in two plates; one was frozen in mammalian cell freezing medium and the other further processed for DNA isolation.

Verification of target gene mutation by Outknocker

The verification of the knockouts was performed as described before [156]. In brief, the cells were lysed in 30 µl Outknocker lysis buffer for 10 min at 65°C and subsequently inactivated for 15 min at 95°C. The isolated genomic DNA was used as template for two consecutive PCR reactions. In the first PCR, the target locus of the gRNA was amplified using site-specific primers (N23) with attached adapter sequences:

Fwd: ACACTCTTTCCCTACACGACGctcttccgatct-N23

Rev: TGACTGGAGTTCAGACGTGTGctcttccgatct-N23

In the second PCR the samples of the first PCR were labeled with barcodes in an arrayed fashion and sequencing adapters were attached. The second PCR used the same reaction conditions as the first PCR.

PCR components		PCR programm		
DNA	1 µl	98°C	30 sec	
Phusion pol.	0,0625 µl	98°C	10 sec	19x
dNTPs	0,125 µl	60°C	30 sec	
primer fwd	0,3125 µl	72°C	30 sec	
primer rev.	0,3125 µl	72°C	3 min	
5x buffer	1,25 µl	12°C	∞	
DMSO	0,1875 µl			
dH_2O	3 µl			

After the PCRs were finished, 3 µl of the 2nd PCR step were collected and pooled. The samples were separated on a 1,5 % agarose gel at 100 V and bands between 300 to 450 bp were collected. They were eluted from the gel using the Zymoclean Gel DNA Recovery kit (Zymo Research) according to manufacturers specifications and DNA was precipitated using 0,1 volume 3 M NaOAc (pH 5.2) and 1,1 volume isopropanol. After 15 min centrifugation at full speed, the pellet was washed with 70 % EtOH, air dried and resuspended in 30 µl H_2O. The concentration was determined by NanoDrop2000 (Thermo Fisher Scientific).

Illumina MiSeq 250bp single-end sequencing was performed by ATLAS Biolabs GmbH (Friedrichstraße 147, 20117 Berlin, Germany). The received FASTA-files were analyzed with the Outknocker web tool (http://www.outknocker.org/). Outknocker provided an alignment of the sequencing results with the target locus of the gRNA, showing if there was a mutation, how many sequencing reads span the area

of interest and how many indels were detected. For further experiments, we selected clones with a sufficient number of reads and a clear out-of-frame mutation.

4.2.4 Induction, isolation and quantification of human and murine NETs

Induction, visualization and quantification of human NETs

1x10^5 neutrophils were seeded in a 24-well plate in RPMI neutrophil medium on a glass coverslip. The cells were stimulated with 100 nM PMA for 4 h at 37°C, 7 % CO_2. The cells were fixed 2 % para-formaldehyde (PFA) (w/v) for 15 min at RT, subsequently washed twice with PBS and stored at 4°C.

For NET staining, the samples were permeabilized for 5 min with 0,1 % TritonX100 in PBS at RT and subsequently blocked for 20 min with IFA blocking buffer. Afterwards the samples were incubated with the primary antibodies mouse α-human chromatin (PL2.3, 1 µg/ml) and rabbit α-human NE (10 µg/ml) for 1 h at RT. After three subsequent washes with PBS, the according secondary antibodies (10 µg/ml) and Hoechst (100 ng/ml) were added for 30 min. Finally, the samples were washed twice with PBS and once with water and then mounted on glass slides.

Five random images of the separate channels were taken with the 10x objective, using the EVOS FL Auto2 imaging system (Thermo Fisher Scientific). The images were analyzed as described before using ImageJ [241]. In brief, the number of cells was determined using the Hoechst images with the Bernsen automatic local threshold function with diameter set to 15 and the threshold to 35. Particles larger than 20 pixels were counted. For NET-positive cells the PL23 channel was used. The threshold was set interactively, controlling both unstimulated and stimulated samples, and objects larger than 75 pixels were counted. Percentage of NET formation was calculated by the following formula:

$$\%\ NETosis = \frac{count\ PL23^{+}\ cells}{count\ Hoechst^{+} cells} * 100$$

Isolation and quantification of human NETs

For NET isolation 3x10^6 neutrophils were seeded in a 6-well plate and stimulated for 4 h with 100 nM PMA in RPMI neutrophil medium. After 4 h the medium was removed, the NETs were washed three times with PBS and 300 µl PBS were added. The NETs were scraped off the plate and transferred into an Eppendorf tube. The NETs were either directly frozen or sonicated with the Bandelin Sonopuls stick-sonicator with three pulses (70 % power) of three seconds each.

For the stimulation of recombinant cGAS, samples were further processed. NETs were digested with either DNAse1 (10 U/ml) for 2 h a 37°C or with Proteinase K (10 U/ml) for 2h at 56°C. To stop the

enzymatic reactions, the mix was inactivated for 10 min at 85°C. Furthermore, NETs were separated into DNA and protein components using phenol-chloroform extraction.

To quantify NETs the Quant-iT™ PicoGreen ® dsDNA Kit was used according to manufacturers specification. Calf thymus DNA was used as a standard, starting from 1 mg/ml following a 1:1 serial dilution.

Induction, visualization and quantification of murine NETs

10^5 neutrophils were seeded in a 24-well plate in 500 µl RPMI with 1 % serum of DNAse1$^{-/-}$ mice and recombinant mGCSF (100 ng/ml) and stimulated for 12 h with 100 nM PMA. Sytox orange (50 µM) and syto green (12,5 µM) were added 1:100 to the samples and incubate for 15 min at 37°C. Three images per sample were taken at a 20x magnification and analyzed by manual counting. The cell number was determined by sytox orange positive cells, whereas the NET number was determined by large syto green particles. Percentage of NET formation was calculated by the following formula:

$$\%\ NETosis = \frac{count\ sytox\ orange^{+} cells}{count\ syto\ green^{+} cells} * 100$$

Analysis of the NET proteome by mass spectrometry

NETs were generated and harvested as described above in the absence of HSA. NETs were finally resuspended in 200 µl PBS and sonicated. 90 µl sample were reduced with 15 µl 45 mM Dithiothreitol (DTT) for 15 min at 60°C and subsequently alkylated with 15 µl 100 mM Iodoacetamide (IAA) for 15 min at RT. The sample was further diluted with 4 volumes of 50 mM Ammonium bicarbonate / 5 % Acetonitrile (ACN) and digested o.n. at 37°C with 0,5 µg trypsin (Promega). The digestion was stopped by adding 12 µl of 20 % trifluoroacetic acid (TFA). The sample was desalted with a ZipTip C18 (Millipore, 0,6 µl bed volume) that was wetted with 50 µl 100 % ACN and equilibrated with 50 µl 0,1 % TFA. After the sample ran through the tip, it was washed twice with 50 µl 0,1 % TFA. Peptides were eluted in two consecutive steps with 5 µl of 60 and 80 % ACN 0,1 % TFA. Eluted peptides were combined and dried at 45°C using a microconcentrator (Eppendorf). For LC-MS/MS analysis the peptides were analyzed using a QExactive Plus mass spectrometer (Thermo Fisher Scientific) coupled on line to a Dionex UltiMate 3000 RSLC nano system (Thermo Fisher Scientific). After solubilization in 23 µl 2 % ACN /0,1 % TFA, 10 µl of the sample was loaded on a C18 PepMap 100 trap column (300 µm x 5mm; 5 µm particle size 100 Å pore size; Thermo Fisher Scientific) at a flow rate of 20 µl/min 2 % ACN /0,1 % TFA for pre-concentration and desalting. Separation was performed using a PicoChip (H354 Reprosil-Pur C18-AQ3; 75 µm i.d. x 105 mm; 120 Å pore size; TipSize 15 µm; New Objective) at a flow rate of 300 nl/min. HPLC

solvent A was 0,1 % formic acid (FA) and peptides were eluted from the column using HPLC solvent B 80 % ACN / 0,1 % FA starting from 3 %, increasing to 40 % in 45 minutes, and to 98 % in 5 minutes. The peptides were analyzed in data-dependent acquisition mode that alternated between one MS scan and 10 MS/MS scans for the most abundant precursor ions. MS scans were acquired over a mass range of m/z 350–1600 and resolution was set to 70000. Peptides were fragmented using HCD at 27 % normalized collision energy and measured in the Orbitrap at a resolution of 17500.

Proteins were identified using an in-house version of Mascot (version 2.6). Peak lists were searched against the SwissProt_human data base (20,214 sequences; 11,330,251 residues) Mass accuracy was set to 5 ppm for MS mode and to 0,03 Da for MS/MS mode and two missed tryptic cleavage sites were allowed. Methionine oxidation, acetylation at protein N-terminus, pyroglutamate formation of N-terminal glutamine and carbamidomethylation of cysteines were allowed as variable modifications. The false discovery rate was set to 1 %.

Isolation of mitochondrial DNA

HEK 293 T cells were harvested and mitochondria were isolated using the Mitochondria Isolation Kit (Thermo Fisher Scientific) according to manufacturers instructions. DNA was isolated with the Zyppy Plasmid Miniprep Kit (Zymo Research) and quantified using the Nanodrop 2000.

4.2.5 Stimulation of target cells with isolated NETs

Generation human serum from SLE patients

Blood was collected in S-Monovette serum tubes and stored rolling for 30 min at RT. The tubes were centrifuged at 2000 g for 10 min and the serum was collected, aliquoted and shock frozen in liquid nitrogen.

Stimulation human and murine cells

10^5 cells/well were seeded 100 µl in 96-well plate in their according medium. NETs were added at a final concentration of 100 µg/ml, either with or without DOTAP (5 µl/well). As a positive control for interferon induction pdAdT (2 µg /ml) was transfected using DOTAP. Human serum was applied at a final concentration of 10 %. The cells were incubated for 15 h at 37°C and supernatants were collected and frozen at -80°C. The inhibitors NEi (20 µM) and Sivelestat (1 µM), K777 (10 µM) and zVAD-FMK (20 µM) were added in 50 µl at 4x concentration before the NETs were added.

For inflammasome stimulation, 10^5 murine BMM were seeded per well 100 µl in 96-well plate in BMM medium. If required, cells were primed with 500 ng/ml LPS for 3 h at 37°C. For Activation of the NLRP3

inflammasome, the cells were treated for 1h with 15 µM Nigericin. For activation of the AIM2 inflammasome cells were stimulated with pdAdT (2 µg/ml) or NETs (100 µg/ml) in the presence of lipofectamine or DOTAP for 4 h.

If different CRISPR clones or primary cells of different genotype were seeded for comparison, the cell number was compared using the Alamar Blue assay according to manufacturers specifications. In brief, 10 µl Alamar Blue solution were added to 100 µl cell solution and incubated for 30 min at 37°C. Subsequently, the fluorescence was measured using a fluorescent plate-reader at 514/590 (ex/em). The cell count data was used for normalization of the interferon data.

4.2.6 Cocultivation

$3x10^6$ target cells (PBMCs, monocytes or pDCs) were combined with neutrophils at a 1:1 ratio in 1 ml RPMI basic medium. They were either left untreated or stimulated with PMA (final concentration 100 nM) or ConA (final concentration 50 µg/ml) in a final volume of 1,5 ml. The inhibitors NEi (20 µM), RU.521 (10 µM), Amlexanox (10 µg/ml), CCCP (10 µM), Nystatin (10 µg/ml), Cyto B (5 µg/ml) or DNAse1 (5 U/ml) were added before PMA stimulation. The cells were cocultivated rotating for at 37°C at 5 % CO_2. After 15 h, the cells were pelleted at 1000 g for 5 min on 4°C. The supernatant was collected and frozen at -80°C and the cells were resuspended in 1 ml TRIZOL and frozen as well.

4.2.7 RNA isolation and reverse transcription

The TRIZOL samples were defrosted at RT and 200 µl chloroform were added. The samples were mixed by inverting the tubes and incubated for 5 min at RT. After 15 min centrifugation at 10000 g at 4°C the aqueous phase was collected in RNAse free tubes and mixed with 1 µl glycogen (20 mg/ml) and 500 µl isopropanol. The mix was incubated for at least 1 h at -20°C, in most of the cases over night to allow optimal precipitation. The mix was centrifuged at 16100 g for 10 min at 4°C, the supernatant was discarded and the pellet was washed twice with 500 µl cold 70 % EtOH. Finally, the pellet was air dried and resuspended in 30 µl dH_2O and stored at -80°C. The RNA concentration was measured with the NanoDrop2000 (Thermo Fisher Scientific).

2 µg of RNA were reverse transcribed using the High-Capacity cDNA reverse Transcription Kit (Thermo Fisher Scientific) according to manufacturers instructions.

reaction mix		PCR program	
RNA	2 µg		
25x dNTPs	0,8 µl	25°C	10 min
10x RT buffer	2 µl	37°C	120 min
10x random primers	2 µl	85°C	5 min
Reverse transcriptase	1 µl	12°C	∞
dH_2O	ad 20 µl		

4.2.8 Detection of TIIFN

Expression analysis by quantitative polymerase chain reaction (qPCR)

Primers for qPCR were chosen from selected publications and checked for their specificity using the NCBI primer designing tool (https://www.ncbi.nlm.nih.gov/tools/primer-blast/). Primer functionality was tested by serial dilution of the cDNA and by melt curve analysis of the qPCR products. qPCR was performed using the Quant Studio 3 qPCR system with the following specifications:

qPCR reaction		qPCR programm	
10 µl	A&B Fast SYBR Green Master mix		
1 µl	primer fwd (20 µM)	95°C	
1 µl	primer rev (20 µM)	95°C	50 cycles
1 µl	cDNA	60°C	
7 µl	dH_2O		

The cycle of threshold (C_t) values were analyzed using Quant Studio Design & Analysis software, at an normalized reporter value (ΔRn) of 0,1. Human β2-microglobulin (B2M, Gene ID 567) and murine glyceraldehyde-3-phosphate dehydrogenase (GAPDH, Gene ID 14433) were used as references genes for sample loading control.

For human cocultivation experiments, the data were analyzed using the $\Delta\Delta C_t$ method. The C_t value of the reference gene was substracted from the C_t value of the gene of interest to normalize for equal loading. The resulting ΔC_t value was substracted from the ΔC_t value of the unstimulated control. The fold change was calculated using the formula $FC = 2^{(-\Delta\Delta Ct)}$. In cases where inhibitors were used, samples were normalized to cocultivations of PBMCs with neutrophils stimulated with PMA without inhibitor.

In murine ConA *in vivo* experiments the ΔC_t value was calculated the same way as described for human samples. To make the different mice comparable, the relative expression was calculated by using the formula $RE = 2^{-\Delta Ct}$.

Reporter cell assay for human TIIFN

For the detection of human TIIFN HEK Blue reporter cells were used. 0,8x10^5 cells were seeded in 100 µl DMEM basic medium in 96-well plates and combined with 100 µl undiluted supernatant of stimulated cells and incubated for 24 h at 37°C. After 24 h, 100 µl of the HEK Blue cell supernatant were transferred into a new plate, combined with 100 µl Quanti-Blue solution and incubated at 37°C until a color change from pink to blue was visible that correlated with the presence of TIIFN. The color change was measured at OD655nm using a spectrophotometer.

Reporter cell assay for murine TIIFN

0,5x10^5 L929 ISRE Luc cells were seeded in 100 µl DMEM in white 96-well plates and incubated o.n. at 37°C. The next day, 100 µl undiluted culture supernatant was added and incubated for 6 h at 37°C. Subsequently, the supernatant was aspirated and replaced with 100 µl Bright-Glo luciferase substrate (Promega). After 2 min incubation at RT, luciferase activity was quantified with the Victor X Light reader (Perkin Elmer).

ELISAs

ELISAs for human universal IFNα, humane CXCL10, ANCA antibodies, human C1q, nucleosomes, and murine IFNβ were conducted according to the instructions of the manufacturers. The supernatants of stimulated cells were used undiluted. For blocking of plates and dilution of standard curves, ELISA dilution buffer was used, unless it was specified differently in the instructions. ELISA plate were washed with PBS-T.

4.2.10 Uptake of NETs by human macrophages

Cocultivation of macrophages and neutrophils undergoing NETosis

Human monocytes were isolated and differentiated into macrophages in 8-well IBIDI chambers as described above. At day seven, the supernatant was removed and replaced with 150 µl fresh medium. In case of live cell imaging, neutrophils were pre-stained with cell-tracker according to manufacturers instructions. Neutrophils were added to the macrophages at a ratio of 1:1 in the presence of Hoechst and stimulated with 100 nM PMA. For live cell imaging cell were recorded for 6 h at 20x magnification. Alternatively, cells were incubated for 4 h at 37°C and subsequently treated with 20 U DNAse1 for 15 min to remove extracellular NETs. Afterwards the samples were fixed for 15 min at RT with 2 % PFA.

Staining of uptake samples

Cells were permeabilized with 0,5 % Triton X100 in PBS for 5 min at RT and subsequently blocked for 20 min at RT with IFA-blocking buffer. The samples were incubated with the primary antibodies for 1 h at RT and washed three times with PBS. The corresponding secondary antibodies and Hoechst (100 ng/ml) were added for 30 min at RT. After three subsequent washes with PBS, the samples were stored in PBS at 4°C and imaged as soon as possible. The samples were imaged using the SP8 confocal (Leica) microscope with the 63x objective.

4.2.11 FACS staining

FACS human neutrophils

Human cells were resuspended in PBS and incubated with FcR-blocking solution (Miltenyi) for 5 min at RT. Subsequently fluorochrome-labeled antibodies were added and the samples were incubated for 30 min on ice. The cells were washed three times with PBS and analyzed using the MACS Quant system. To test viability DAPI (500 ng/ml) was added directly before acquisition. The data was analyzed by FlowJoX.

FACS murine immune cells

100 µl of full blood were transferred into a FACS tube and mixed with 100 µl FACS buffer containing the fluorochrome-labeled antibodies in 2x concentration. The samples were vortexed gently and incubated for 1 h in the dark at RT. Subsequently 3 ml of 1x one step lyse/fix solution (Invitrogen) was added and incubate for 30 min in the dark at RT. The cells were pelleted at 500 g for 5 min and washed three times with FACS buffer. Finally, the cells were resuspended in 300 µl PBS and 50 µl were measured using the MACS Quant system.

FACS for phosphorylation of IRF3

Monocytes were stimulated for 6 h with 100 µg/ml NETs and 25 µl DOTAP. Subsequently the cells were fixed with 4 % PFA (w/v) for 10 min at RT. After centrifugation for 5 min at 300g and 4°C, cells were stored o.n in 90 % MeOH at -20°C. At the next day, the cells were harvested by centrifugation, resuspended in 100 µl 0,5 % (w/v) BSA in PBS and incubated with the primary antibody (1:50, concentration not specified by company) for 1 h at RT. The cells were centrifuged and washed three times in 500 µl 0,5 % BSA in PBS. Subsequently the cells were incubated for 30 min with the secondary

antibody (10 µg/ml) at RT. After three additional washing steps the cells were resuspended in 200 µl PBS and analyzed with the flow cytometer.

4.2.12 Murine *in vivo* experiments

All animal experiments were officially approved by Landesamt für Gesundheit und Soziales (Berlin, Germany) and are conducted in compliance with the German animal protection law.

Concanavalin A injection

Mice of different genotypes were injected i.v. with ConA (15 mg/kg bodyweight). After 12 h, mice were anesthetized with isoflurane and bled by cardiac puncture, resulting in painless death due to blood loss. The blood was collected in syringes with EDTA (final concentration 50 µM) to prevent coagulation and immediately stored on ice. To generate plasma the blood was centrifuged 10 min at 4°C at 10000 g. The plasma was collected and shock frozen in liquid nitrogen. The cells were resuspended in 1 ml RBC lysis buffer and incubated for 3 min on ice. The cells were pelleted at 500 g for 5 min at 4°C, resuspended in 1 ml TRIZOL and stored for RNA isolation at -80°C.

ALT/AST measurement

The hepatocyte specific enzymes alanine-aminotransferase (ALT) and asparatate-aminotransferase (AST) that were used as markers for liver damage were quantified by the routine veterinarian service laboratory SYNLAB.vet GmbH (Turmstraße 21, 10559 Berlin, Germany).

NET ELISA

Biotin-coated ELISA plates were labeled with 50 µl MPO-streptavidin (1 µg/ml) o.n. at 4°C. At the next day, the plates were washed in PBS-T and blocked for 2 h at RT with 5 % BSA in PBS. 50 µl sample or 50 µl standard were added to the wells and incubated 2h at RT under constant shaking. Murine NETs were used as a standard, starting with 1 µg/ml as a highest concentration being diluted 1:1. The serum samples were used undiluted. Subsequently, the plate was washed three times with PBS-T and the anti-DNA antibody (1:50) coupled to a peroxidase of the ROCHE cell death ELISA Kit was added for 2 h. Finally, the plate was washed, 100 µl TMB substrate were added and the reaction was stopped using 50 µl 2N H_2SO_4 when the desired color change was visible. The signal was quantified at OD405nm using a spectrophotometer.

Neutrophil depletion

Wildtype mice were injected i.p. with the neutrophil-depleting Ly6G antibody or an isotype control (20 mg/kg bodyweight). After 24 h mice were treated with PBS or ConA as described before. To verify the successful depletion, neutrophils were quantified in full blood as described above.

Chemiluminescence assay for detection of ROS production

10^5 neutrophils were seeded in 100 µl medium in a white 96-well plate. HRP (1200 U/ml) and luminol (50 mM) were diluted 1:200 in medium and 11 µl of the mix were added to the cells. The cells were incubated for 15 min at 37°C and subsequently stimulated with PMA (100 nM) or left untreated. Chemiluminscence was recorded using the Victor X Light reader (Perkin Elmer) for a total of 3 h in 2,5 minute intervals.

4.2.13 Microarray for ConA injected mice

Total RNA quality and quantity was analyzed using an Agilent 2100 Bioanalyzer (Agilent Technologies) and a NanoDrop 1000 UV-Vis spectrophotometer (Thermo Fisher Scientific). Microarray experiments were performed as single-color hybridization. Total RNA was amplified and labeled with the low input Quick-Amp Labeling Kit (Agilent Technologies). In brief, mRNA was reverse transcribed and amplified using an oligo-dT-T7 promoter primer and labeled with cyanine 3-CTP. After precipitation, purification, and quantification, 1,25 µg of each labeled cRNA was fragmented and hybridized to whole genome mouse 4 × 44k multipack microarrays (Agilent-014868, whole mouse genome 4x44K microarray kit) according to the supplier's protocol (Agilent Technologies). Scanning of microarrays was performed with 5 µm resolution using a G2565CA high-resolution laser microarray scanner (Agilent Technologies) with extended dynamic range (XDR). Microarray image data were processed with the Image Analysis/Feature Extraction software G2567AA v. A.11.5.1.1 (Agilent Technologies) using default settings and the GE1_1105_Oct12 extraction protocol. The extracted MAGE-ML files were analyzed further with the Rosetta Resolver Biosoftware, Build 7.2.2 SP1.31 (Rosetta Biosoftware) and the extracted txt files were further analyzed with R scripts and the associated BioConductor limma package [242].

To generate the scatter plot, fold changes detected by microarray after ConA stimulations were plotted from Wildtype versus $cGAS^{-/-}$ mice. Genes were colored by significance of their different regulation in Wildtype compared to $cGAS^{-/-}$ mice. Labeled genes are significant genes that are contained in either GO-term „cytokine activity" (GO:005125) or „response to type I interferon" (GO:0034340).

Select GO-terms from microarray were plotted using the R tmod package [243].

4.2.14 *In vitro* stimulation of recombinant cGAS

Constructs and cloning

The plasmids encoding catalytic domains of human (h) and mouse (m) cGAS (aa 155–522 and aa 141–507, respectively) for an N-terminal His_6–MBP (maltose-binding protein) fusion protein expression were described before[244].

Protein expression and purification

Proteins were expressed and purified as described before [227]. Proteins were flash-frozen in liquid nitrogen and stored at −80 °C.

Radio-labelled cGAS activity assays

Radiolabelled cGAS activity assays were performed analogously to previously described [244]. Briefly, 10 ng/µl sonified NETs (defined by absorption at 260nm) were mixed with 4 µM mcGAS. The reaction was started by adding 100 µM ATP and 100 µM GTP in buffer containing 40 mM Tris pH 7.5, 100 mM NaCl, 10 mM $MgCl_2$, and 1:600 [α^{32}P]ATP (3,000 Ci/mmol, Hartman Analytic). Following the incubation at 35°C for indicated time the reactions were stopped by plotting on PEI-Cellulose F plates (Merck) and analysed by thin-layer chromatography with 1 M $(NH_4)_2SO_4$/1,5 M KH_2PO_4 as running buffer. The radiolabelled products were visualized with a Typhoon FLA 9000 phosphor imaging system.

For DNaseI-treated NETs 6 ng/µl NETs and 6 µM hcGAS were used. NETs components and proteinase-treated NETs were prepared as described above and tested by using 8 ng/µl NETs and 4 µM hcGAS. In all control experiments pET28M–SUMO1–GFP vector (EMBL) (6,2 kbp, plasmid) was used in corresponding concentrations.

NET Electrophoresis

300 ng of DNAseI-treated NETs were analysed in 1,5 % agarose gel prepared with Ethidiumbromide (1 µg/ml), in running buffer containing 40 mM Tris, 20 mM acetic acid and 1 mM EDTA, pH 8,3. For analysis of the separate NETs components and proteinase-treated NETs 170 ng of material were used. The gel images were obtained with Gel Doc XR+ Imager (BioRad).

4.2.15 Statistical analysis

The number of replicates for each experiment is indicated below the figures. The compiled data was analyzed by GraphPad PRISM, using the indicated test. To assess if a parametric or non-paramatric test has to be used, the data sets were tested using the Shapiro-Wilk-Test, α=0,05. The statistical significance is indicated in the figures as follows: *p<0,05, **p<0,01, ***p<0,001, ****p<0,0001, values indicate exact p-values.

5 References

1. Buchmann, K. Evolution of Innate Immunity: Clues from Invertebrates via Fish to Mammals. *Front. Immunol.* **5,** 459 (2014).
2. Medzhitov, R. Origin and physiological roles of inflammation. *Nature* **454,** 428–435 (2008).
3. Schett, G. & Neurath, M. F. Resolution of chronic inflammatory disease: universal and tissue-specific concepts. *Nat. Commun.* **9,** 3261 (2018).
4. Bianchi, M. E. DAMPs, PAMPs and alarmins: all we need to know about danger. *J. Leukoc. Biol.* **81,** 1–5 (2007).
5. Pisetsky, D. S. The origin and properties of extracellular DNA: From PAMP to DAMP. *Clin. Immunol.* **144,** 32–40 (2012).
6. Gallucci, S. & Maffei, M. E. DNA Sensing across the Tree of Life. *Trends Immunol.* **38,** 719–732 (2017).
7. Motta, V., Soares, F., Sun, T. & Philpott, D. J. NOD-Like Receptors: Versatile Cytosolic Sentinels. *Physiol. Rev.* **95,** 149–178 (2015).
8. Kawai, T. & Akira, S. Toll-like Receptors and Their Crosstalk with Other Innate Receptors in Infection and Immunity. *Immunity* **34,** 637–650 (2011).
9. Hoving, J. C., Wilson, G. J. & Brown, G. D. Signalling C-Type lectin receptors, microbial recognition and immunity. *Cell. Microbiol.* **16,** 185–194 (2014).
10. Sharma, S., Fitzgerald, K. A., Cancro, M. P. & Marshak-Rothstein, A. Nucleic Acid-Sensing Receptors: Rheostats of Autoimmunity and Autoinflammation. *J. Immunol.* **195,** 3507–12 (2015).
11. Brubaker, S. W., Bonham, K. S., Zanoni, I. & Kagan, J. C. Innate Immune Pattern Recognition: A Cell Biological Perspective. *Annu. Rev. Immunol.* **33,** 257–290 (2015).
12. Ortega-Gómez, A., Perretti, M. & Soehnlein, O. Resolution of inflammation: an integrated view. *EMBO Mol. Med.* **5,** 661–74 (2013).
13. Newburger, P. E. & Dale, D. C. Evaluation and management of patients with isolated neutropenia. *Semin. Hematol.* **50,** 198–206 (2013).
14. Borregaard, N. Neutrophils, from Marrow to Microbes. *Immunity* **33,** 657–670 (2010).
15. McCracken, J. M. & Allen, L.-A. H. Regulation of human neutrophil apoptosis and lifespan in health and disease. *J. Cell Death* **7,** 15–23 (2014).
16. Strydom, N. & Rankin, S. M. Regulation of circulating neutrophil numbers under homeostasis and in disease. *J. Innate Immun.* **5,** 304–14 (2013).

17. Thomas, C. J. & Schroder, K. Pattern recognition receptor function in neutrophils. *Trends Immunol.* **34,** 317–328 (2013).
18. Scapini, P., Lapinet-Vera, J. A. & Cassatella, M. A. The neutrophil as a cellular source of chemokines. *Immunol. Rev.* 195–203 (2000).
19. Wozniak, A., Betts, W. H., Murphy, G. A. & Rokicinski, M. Interleukin-8 primes human neutrophils for enhanced superoxide anion production. *Immunology* **79,** 608–15 (1993).
20. Tecchio, C., Micheletti, A. & Cassatella, M. A. Neutrophil-derived cytokines: facts beyond expression. *Front. Immunol.* **5,** 508 (2014).
21. Dinarello, C. A. Proinflammatory Cytokines. *Chest* **118,** 503–508 (2000).
22. DeCoursey, T. E. & Ligeti, E. Regulation and termination of NADPH oxidase activity. *Cell. Mol. Life Sci.* **62,** 2173–2193 (2005).
23. Winterbourn, C. C., Kettle, A. J. & Hampton, M. B. Reactive Oxygen Species and Neutrophil Function. *Annu. Rev. Biochem.* **85,** 765–792 (2016).
24. Nguyen, G. T., Green, E. R. & Mecsas, J. Neutrophils to the ROScue: Mechanisms of NADPH Oxidase Activation and Bacterial Resistance. *Front. Cell. Infect. Microbiol.* **7,** 373 (2017).
25. Mittal, M., Siddiqui, M. R., Tran, K., Reddy, S. P. & Malik, A. B. Reactive oxygen species in inflammation and tissue injury. *Antioxid. Redox Signal.* **20,** 1126–67 (2014).
26. Marciano, B. E. *et al.* Common severe infections in chronic granulomatous disease. *Clin. Infect. Dis.* **60,** 1176–83 (2015).
27. Amulic, B., Cazalet, C., Hayes, G. L., Metzler, K. D. & Zychlinsky, A. Neutrophil function: from mechanisms to disease. *Annu. Rev. Immunol.* **30,** 459–489 (2012).
28. Faurschou, M. & Borregaard, N. Neutrophil granules and secretory vesicles in inflammation. *Microbes Infect.* **5,** 1317–1327 (2003).
29. Borregaard, N., Sørensen, O. E. & Theilgaard-Mönch, K. Neutrophil granules: a library of innate immunity proteins. *Trends Immunol.* **28,** 340–345 (2007).
30. Nordenfelt, P. & Tapper, H. Phagosome dynamics during phagocytosis by neutrophils. *J. Leukoc. Biol.* **90,** 271–284 (2011).
31. Pauwels, A.-M., Trost, M., Beyaert, R. & Hoffmann, E. Patterns, Receptors, and Signals: Regulation of Phagosome Maturation. *Trends Immunol.* **38,** 407–422 (2017).
32. Richards, D. M. & Endres, R. G. The mechanism of phagocytosis: Two stages of engulfment. *Biophys. J.* **107,** 1542–1553 (2014).
33. Brinkmann, V. *et al.* Neutrophil Extracellular Traps Kill Bacteria Brinkmann Science 2004.pdf. *Science* **303,** 1532–5 (2004).
34. Urban, C. F. *et al.* Neutrophil extracellular traps contain calprotectin, a cytosolic protein

complex involved in host defense against Candida albicans. *PLoS Pathog.* **5,** (2009).

35. Fuchs, T. A. *et al.* Novel cell death program leads to neutrophil extracellular traps. *J. Cell Biol.* **176,** 231–241 (2007).
36. Wen, F., White, G. J., VanEtten, H. D., Xiong, Z. & Hawes, M. C. Extracellular DNA is required for root tip resistance to fungal infection. *Plant Physiol.* **151,** 820–9 (2009).
37. Sousa-Rocha, D. *et al.* Trypanosoma cruzi and Its Soluble Antigens Induce NET Release by Stimulating Toll-Like Receptors. *PLoS One* **10,** e0139569 (2015).
38. Kenny, E. F. *et al.* Diverse stimuli engage different neutrophil extracellular trap pathways. *Elife* **6,** (2017).
39. Papayannopoulos, V., Metzler, K. D., Hakkim, A. & Zychlinsky, A. Neutrophil elastase and myeloperoxidase regulate the formation of neutrophil extracellular traps. *J. Cell Biol.* **191,** 677–91 (2010).
40. Munafo, D. B. *et al.* DNase I Inhibits a Late Phase of Reactive Oxygen Species Production in Neutrophils. *J. Innate Immun.* **1,** 527–542 (2009).
41. Ramos-Kichik, V. *et al.* Neutrophil extracellular traps are induced by Mycobacterium tuberculosis. *Tuberculosis* **89,** 29–37 (2009).
42. Urban, C. F., Reichard, U., Brinkmann, V. & Zychlinsky, A. Neutrophil extracellular traps capture and kill Candida albicans yeast and hyphal forms. *Cell. Microbiol.* **8,** 668–676 (2006).
43. Schönrich, G. & Raftery, M. J. Neutrophil Extracellular Traps Go Viral. *Front. Immunol.* **7,** 366 (2016).
44. Branzk, N. *et al.* Neutrophils sense microbe size and selectively release neutrophil extracellular traps in response to large pathogens. *Nat. Immunol.* **15,** 1017–1025 (2014).
45. Clark, S. R. *et al.* Platelet TLR4 activates neutrophil extracellular traps to ensnare bacteria in septic blood. *Nat. Med.* **13,** 463–469 (2007).
46. Yousefi, S., Mihalache, C., Kozlowski, E., Schmid, I. & Simon, H. U. Viable neutrophils release mitochondrial DNA to form neutrophil extracellular traps. *Cell Death Differ.* **16,** 1438–44 (2009).
47. Kessenbrock, K. *et al.* Netting neutrophils in autoimmune small-vessel vasculitis. *Nat. Med.* **15,** 623–625 (2009).
48. Mitroulis, I. *et al.* Neutrophil Extracellular Trap Formation Is Associated with IL-1β and Autophagy-Related Signaling in Gout. *PLoS One* **6,** e29318 (2011).
49. Amulic, B. *et al.* Cell-Cycle Proteins Control Production of Neutrophil Extracellular Traps. *Dev. Cell* **43,** 449–462.e5 (2017).
50. Bianchi, M. *et al.* Restoration of NET formation by gene therapy in CGD controls aspergillosis. *Blood* **114,** 2619–2622 (2009).

51. Hakkim, A. *et al.* Activation of the Raf-MEK-ERK pathway is required for neutrophil extracellular trap formation. *Nat. Chem. Biol.* **7,** 75–77 (2011).
52. Metzler, K. D., Goosmann, C., Lubojemska, A., Zychlinsky, A. & Papayannopoulos, V. A Myeloperoxidase-Containing Complex Regulates Neutrophil Elastase Release and Actin Dynamics during NETosis. *Cell Rep.* **8,** 883–896 (2014).
53. Sollberger, G. *et al.* Gasdermin D plays a vital role in the generation of neutrophil extracellular traps. *Sci. Immunol.* **3,** eaar6689 (2018).
54. Pilsczek, F. H. *et al.* A Novel Mechanism of Rapid Nuclear Neutrophil Extracellular Trap Formation in Response to Staphylococcus aureus. *J. Immunol.* **185,** 7413–7425 (2010).
55. Beiter, K. *et al.* An Endonuclease Allows Streptococcus pneumoniae to Escape from Neutrophil Extracellular Traps. *Curr. Biol.* **16,** 401–407 (2006).
56. Halverson, T. W. R., Wilton, M., Poon, K. K. H., Petri, B. B. & Lewenza, S. DNA is an antimicrobial component of neutrophil extracellular traps. *PLoS Pathog.* **11,** e1004593 (2015).
57. Guimaraes-Costa, A. B. *et al.* Leishmania amazonensis promastigotes induce and are killed by neutrophil extracellular traps. *Proc. Natl. Acad. Sci.* **106,** 6748–6753 (2009).
58. Juneau, R. A., Pang, B., Weimer, K. E. D., Armbruster, C. E. & Swords, W. E. Nontypeable *Haemophilus influenzae* Initiates Formation of Neutrophil Extracellular Traps. *Infect. Immun.* **79,** 431–438 (2011).
59. Bhattacharya, M. *et al. Staphylococcus aureus* biofilms release leukocidins to elicit extracellular trap formation and evade neutrophil-mediated killing. *Proc. Natl. Acad. Sci.* **115,** 7416–7421 (2018).
60. Park, J. *et al.* Cancer cells induce metastasis-supporting neutrophil extracellular DNA traps. *Sci. Transl. Med.* **8,** 361ra138 (2016).
61. Wong, S. L. *et al.* Diabetes primes neutrophils to undergo NETosis, which impairs wound healing. *Nat. Med.* **21,** 815–819 (2015).
62. Camicia, G., Pozner, R. & de Larrañaga, G. Neutrophil Extracellular Traps in Sepsis. *Shock* **42,** 286–294 (2014).
63. Martinod, K. & Wagner, D. D. Thrombosis: tangled up in NETs. *Blood* **123,** 2768–2776 (2013).
64. Warnatsch, A., Ioannou, M., Wang, Q. & Papayannopoulos, V. Neutrophil extracellular traps license macrophages for cytokine production in atherosclerosis. *Science (80-.).* **349,** 316–320 (2015).
65. Gupta, S. & Kaplan, M. J. The role of neutrophils and NETosis in autoimmune and renal diseases. *Nat Rev Nephrol* **12,** 402–413 (2016).
66. Momohara, S., Kashiwazaki, S., Inoue, K., Saito, S. & Nakagawa, T. Elastase from

polymorphonuclear leukocyte in articular cartilage and synovial fluids of patients with rheumatoid arthritis. *Clin. Rheumatol.* **16,** 133–40 (1997).

67. Denny, M. F. *et al.* A distinct subset of proinflammatory neutrophils isolated from patients with systemic lupus erythematosus induces vascular damage and synthesizes type I IFNs. *J. Immunol.* **184,** 3284–3297 (2010).
68. Rees, F., Doherty, M., Grainge, M. J., Lanyon, P. & Zhang, W. The worldwide incidence and prevalence of systemic lupus erythematosus: a systematic review of epidemiological studies. *Rheumatology* **56,** 1945–1961 (2017).
69. Al-Mayouf, S. M. *et al.* Loss-of-function variant in DNASE1L3 causes a familial form of systemic lupus erythematosus. *Nat. Genet.* **43,** 1186–1188 (2011).
70. Yasutomo, K. *et al.* Mutation of DNASE1 in people with systemic lupus erythematosus. *Nat. Genet.* **28,** 313–4 (2001).
71. Cojocaru, M., Cojocaru, I. M., Silosi, I. & Vrabie, C. D. Manifestations of systemic lupus erythematosus. *Maedica (Buchar).* **6,** 330–6 (2011).
72. Rahman, A. & Isenberg, D. A. Systemic lupus erythematosus. *N Engl J Med* **358,** 929–939 (2008).
73. Stojan, G. & Petri, M. Atherosclerosis in systemic lupus erythematosus. *J. Cardiovasc. Pharmacol.* **62,** 255–62 (2013).
74. Midgley, A. & Beresford, M. W. Cellular localization of nuclear antigen during neutrophil apoptosis: mechanism for autoantigen exposure? *Lupus* **20,** 641–6 (2011).
75. Friou, G. Clinical application of lupus serum-nucleoprotein reaction using fluorescent antibody technique. *J Clin Invest* **8,** 224–229 (1958).
76. Cervera, R. *et al.* Anti-chromatin antibodies in systemic lupus erythematosus: a useful marker for lupus nephropathy. *Ann. Rheum. Dis.* **62,** 431–4 (2003).
77. Nässberger, L., Jonsson, H., Sjöholm, A. G., Sturfelt, G. & Heubner, A. Circulating anti-elastase in systemic lupus erythematosus. *Lancet (London, England)* **1,** 509 (1989).
78. Fritzler, M. J. & Tan, E. M. Antibodies to histones in drug-induced and idiopathic lupus erythematosus. *J. Clin. Invest.* **62,** 560–7 (1978).
79. Spronk, P. E. *et al.* Antineutrophil cytoplasmic antibodies in systemic lupus erythematosus. *Br. J. Rheumatol.* **35,** 625–31 (1996).
80. Carmona-Rivera, C., Zhao, W., Yalavarthi, S. & Kaplan, M. J. Neutrophil extracellular traps induce endothelial dysfunction in systemic lupus erythematosus through the activation of matrix metalloproteinase-2. *Ann Rheum Dis* **74,** 1417–1424 (2015).
81. Lande, R. *et al.* Neutrophils activate plasmacytoid dendritic cells by releasing self-DNA-peptide complexes in systemic lupus erythematosus. *Sci. Transl. Med.* **3,** 73ra19 (2011).

82. Hirose, O., Itabashi, M., Takei, T., Honda, K. & Nitta, K. Antineutrophil cytoplasmic antibody-associated glomerulonephritis with immunoglobulin deposition. *Clin. Exp. Nephrol.* **21,** 643–650 (2017).

83. Waldman, M. & Madaio, M. P. Pathogenic autoantibodies in lupus nephritis. *Lupus* **14,** 19–24 (2005).

84. Garcia-Romo, G. S. *et al.* Netting neutrophils are major inducers of type I IFN production in pediatric systemic lupus erythematosus. *Sci. Transl. Med.* **3,** 73ra20 (2011).

85. Lood, C. *et al.* Neutrophil extracellular traps enriched in oxidized mitochondrial DNA are interferogenic and contribute to lupus-like disease. *Nat Med* **22,** 146–153 (2016).

86. Blanco, P., Palucka, A. K., Gill, M., Pascual, V. & Banchereau, J. Induction of dendritic cell differentiation by IFN-alpha in systemic lupus erythematosus. *Science (80-.).* **294,** 1540–1543 (2001).

87. Lande, R. *et al.* Plasmacytoid dendritic cells sense self-DNA coupled with antimicrobial peptide. *Nature* **449,** 564–569 (2007).

88. McNab, F., Mayer-Barber, K., Sher, A., Wack, A. & O'Garra, A. Type I interferons in infectious disease. *Nat. Rev. Immunol.* **15,** 87–103 (2015).

89. Crow, M. K. Type I interferon in the pathogenesis of lupus. *J Immunol* **192,** 5459–5468 (2014).

90. Banchereau, J. & Pascual, V. Type I Interferon in Systemic Lupus Erythematosus and Other Autoimmune Diseases. *Immunity* **25,** 383–392 (2006).

91. Bennett, L. *et al.* Interferon and granulopoiesis signatures in systemic lupus erythematosus blood. *J Exp Med* **197,** 711–723 (2003).

92. Baechler, E. C. *et al.* Interferon-inducible gene expression signature in peripheral blood cells of patients with severe lupus. *Proc. Natl. Acad. Sci. U. S. A.* **100,** 2610–5 (2003).

93. Amoura, Z. *et al.* Circulating plasma levels of nucleosomes in patients with systemic lupus erythematosus: correlation with serum antinucleosome antibody titers and absence of clear association with disease activity. *Arthritis Rheum.* **40,** 2217–25 (1997).

94. Telles, R. W., Ferreira, G. A., Silva, N. P. da & Sato, E. I. Increased plasma myeloperoxidase levels in systemic lupus erythematosus. *Rheumatol. Int.* **30,** 779–784 (2010).

95. Atamaniuk, J. *et al.* Analysing cell-free plasma DNA and SLE disease activity. *Eur. J. Clin. Invest.* **41,** 579–583 (2011).

96. Carli, L., Tani, C., Vagnani, S., Signorini, V. & Mosca, M. Leukopenia, lymphopenia, and neutropenia in systemic lupus erythematosus: Prevalence and clinical impact—A systematic literature review. *Semin. Arthritis Rheum.* **45,** 190–194 (2015).

97. Ren, Y. *et al.* Increased Apoptotic Neutrophils and Macrophages and Impaired Macrophage

Phagocytic Clearance of Apoptotic Neutrophils in Systemic Lupus Erythematosus. *Arthritis Rheum.* **48,** 2888–2897 (2003).

98. Villanueva, E. *et al.* Netting neutrophils induce endothelial damage, infiltrate tissues, and expose immunostimulatory molecules in systemic lupus erythematosus. *J. Immunol.* **187,** 538–552 (2011).
99. Hacbarth, E. & Kajdacsy-Balla, A. Low density neutrophils in patients with systemic lupus erythematosus, rheumatoid arthritis, and acute rheumatic fever. *Arthritis Rheum* **29,** 1334–1342 (1986).
100. Midgley, A. & Beresford, M. Increased expression of low density granulocytes in juvenile-onset systemic lupus erythematosus patients correlates with disease activity. *Lupus* **25,** 407–411 (2016).
101. Hakkim, A. *et al.* Impairment of neutrophil extracellular trap degradation is associated with lupus nephritis. *Proc Natl Acad Sci U S A* **107,** 9813–9818 (2010).
102. Wang, H., Li, T., Chen, S., Gu, Y. & Ye, S. Neutrophil extracellular trap mitochondrial DNA and its autoantibody in systemic lupus erythematosus and a proof-of-concept trial of metformin. *Arthritis Rheumatol.* **67,** 3190–3200 (2015).
103. Farrera, C. & Fadeel, B. Macrophage Clearance of Neutrophil Extracellular Traps Is a Silent Process. *J. Immunol.* **191,** 2647–2656 (2013).
104. Shao, W.-H. & Cohen, P. L. Disturbances of apoptotic cell clearance in systemic lupus erythematosus. *Arthritis Res. Ther.* **13,** 202 (2011).
105. Jacob, M., Napirei, M., Ricken, a, Dixkens, C. & Mannherz, H. Histopathology of lupus-like nephritis in Dnase1-deficient mice in comparison to NZB/W F1 mice. *Lupus* **11,** 514–527 (2002).
106. Sisirak, V. *et al.* Digestion of Chromatin in Apoptotic Cell Microparticles Prevents Autoimmunity. *Cell* **166,** 88–101 (2016).
107. Leffler, J. *et al.* Degradation of neutrophil extracellular traps co-varies with disease activity in patients with systemic lupus erythematosus. *Arthritis Res. Ther.* **15,** R84 (2013).
108. Lee-Kirsch, M. A. *et al.* Mutations in the gene encoding the 3'-5' DNA exonuclease TREX1 are associated with systemic lupus erythematosus. *Nat. Genet.* **39,** 1065–1067 (2007).
109. Fye, J. M., Orebaugh, C. D., Coffin, S. R., Hollis, T. & Perrino, F. W. Dominant Mutations of the TREX1 Exonuclease Gene in Lupus and Aicardi-Goutières Syndrome. *J. Biol. Chem.* **286,** 32373–32382 (2011).
110. Hu, Z. *et al.* Neutrophil extracellular traps induce IL-1?? production by macrophages in combination with lipopolysaccharide. *Int. J. Mol. Med.* **39,** 549–558 (2017).
111. Kahlenberg, J. M., Carmona-Rivera, C., Smith, C. K. & Kaplan, M. J. Neutrophil extracellular trap-

associated protein activation of the NLRP3 inflammasome is enhanced in lupus macrophages. *J. Immunol.* **190,** 1217–1226 (2013).

112. Mankan, A. K., Dau, T., Jenne, D. & Hornung, V. The NLRP3/ASC/Caspase-1 axis regulates IL-1beta processing in neutrophils. *Eur. J. Immunol.* **42,** 710–715 (2012).
113. Sabbione, F. *et al.* Neutrophil Extracellular Traps Stimulate Proinflammatory Responses in Human Airway Epithelial Cells. *J. Innate Immun.* **9,** 387–402 (2017).
114. Chamilos, G. *et al.* Cytosolic sensing of extracellular self-DNA transported into monocytes by the antimicrobial peptide LL37. *Blood* **120,** 3699–3707 (2012).
115. Caielli, S. *et al.* Oxidized mitochondrial nucleoids released by neutrophils drive type I interferon production in human lupus. *J Exp Med* **213,** 697–713 (2016).
116. Nickerson, K. M., Cullen, J. L., Kashgarian, M. & Shlomchik, M. J. Exacerbated autoimmunity in the absence of TLR9 in MRL.Fas(lpr) mice depends on Ifnar1. *J. Immunol.* **190,** 3889–94 (2013).
117. Lartigue, A. *et al.* Role of TLR9 in Anti-Nucleosome and Anti-DNA Antibody Production in lpr Mutation-Induced Murine Lupus. *J. Immunol.* **177,** 1349–1354 (2006).
118. Sun, L., Wu, J., Du, F., Chen, X. & Chen, Z. J. Cyclic GMP-AMP Synthase Is a Cytosolic DNA Sensor That Activates the Type I Interferon Pathway. *Science (80-.).* **339,** 786–791 (2013).
119. Lio, C.-W. J. *et al.* cGAS-STING Signaling Regulates Initial Innate Control of Cytomegalovirus Infection. *J. Virol.* **90,** 7789–7797 (2016).
120. Schoggins, J. W. *et al.* Pan-viral specificity of IFN-induced genes reveals new roles for cGAS in innate immunity. *Nature* **505,** 691–695 (2014).
121. Wu, J. J. *et al.* Inhibition of cGAS DNA Sensing by a Herpesvirus Virion Protein. *Cell Host Microbe* **18,** 333–344 (2015).
122. Ma, Z. *et al.* Modulation of the cGAS-STING DNA sensing pathway by gammaherpesviruses. *Proc Natl Acad Sci U S A* **112,** E4306-15 (2015).
123. Dansako, H. *et al.* The cyclic GMP-AMP synthetase-STING signaling pathway is required for both the innate immune response against HBV and the suppression of HBV assembly. *FEBS J.* **283,** 144–156 (2016).
124. Dai, P. *et al.* Modified Vaccinia Virus Ankara Triggers Type I IFN Production in Murine Conventional Dendritic Cells via a cGAS/STING-Mediated Cytosolic DNA-Sensing Pathway. *PLoS Pathog.* **10,** e1003989 (2014).
125. Lam, E., Stein, S. & Falck-Pedersen, E. Adenovirus Detection by the cGAS/STING/TBK1 DNA Sensing Cascade. *J. Virol.* **88,** 974–981 (2014).
126. Gao, D. *et al.* Cyclic GMP-AMP Synthase Is an Innate Immune Sensor of HIV and Other Retroviruses. *Science (80-.).* **341,** 903–906 (2013).

127. Watson, R. O. *et al.* The Cytosolic Sensor cGAS Detects Mycobacterium tuberculosis DNA to Induce Type I Interferons and Activate Autophagy. *Cell Host Microbe* **17,** 811–819 (2015).

128. Storek, K. M., Gertsvolf, N. A., Ohlson, M. B. & Monack, D. M. cGAS and Ifi204 cooperate to produce type I IFNs in response to Francisella infection. *J Immunol* **194,** 3236–3245 (2015).

129. Hartlova, A. *et al.* DNA damage primes the type I interferon system via the cytosolic DNA sensor STING to promote anti-microbial innate immunity. *Immunity* **42,** 332–343 (2015).

130. Glück, S. *et al.* Innate immune sensing of cytosolic chromatin fragments through cGAS promotes senescence. *Nat. Cell Biol.* **19,** 1061–1070 (2017).

131. West, A. P. *et al.* Mitochondrial DNA stress primes the antiviral innate immune response. *Nature* **520,** 553–557 (2015).

132. Ablasser, A. *et al.* RIG-I-dependent sensing of poly(dA:dT) through the induction of an RNA polymerase III–transcribed RNA intermediate. *Nat. Immunol.* **10,** 1065–1072 (2009).

133. Unterholzner, L. *et al.* IFI16 is an innate immune sensor for intracellular DNA. *Nat. Immunol.* **11,** 997–1004 (2010).

134. Sun, L., Wu, J., Du, F., Chen, X. & Chen, Z. J. Cyclic GMP-AMP synthase is a cytosolic DNA sensor that activates the type I interferon pathway. *Science (80-.).* **339,** 786–791 (2013).

135. Lee, A., Park, E.-B., Lee, J., Choi, B.-S. & Kang, S.-J. The N terminus of cGAS de-oligomerizes the cGAS:DNA complex and lifts the DNA size restriction of core-cGAS activity. *FEBS Lett.* **591,** 954–961 (2017).

136. Zhang, X. *et al.* The Cytosolic DNA Sensor cGAS Forms an Oligomeric Complex with DNA and Undergoes Switch-like Conformational Changes in the Activation Loop. *Cell Rep.* **6,** 421–430 (2014).

137. Gao, P. *et al.* Cyclic [G(2′,5′)pA(3′,5′)p] is the metazoan second messenger produced by DNA-activated cyclic GMP-AMP synthase. *Cell* **153,** 1094–1107 (2013).

138. Wu, J. *et al.* Cyclic GMP-AMP is an endogenous second messenger in innate immune signaling by cytosolic DNA. *Science (80-.).* **826,** 826–830 (2014).

139. Zhang, X. *et al.* Cyclic GMP-AMP containing mixed phosphodiester linkages is an endogenous high-affinity ligand for STING. *Mol Cell* **51,** 226–235 (2013).

140. Tanaka, Y. & Chen, Z. J. STING Specifies IRF3 Phosphorylation by TBK1 in the Cytosolic DNA Signaling Pathway. *Sci. Signal.* **5,** ra20-ra20 (2012).

141. Hiscott, J. Triggering the Innate Antiviral Response through IRF-3 Activation. *J. Biol. Chem.* **282,** 15325–15329 (2007).

142. West, A. P. *et al.* Mitochondrial DNA stress primes the antiviral innate immune response. *Nature* **520,** 553–557 (2015).

143. Stetson, D. B., Ko, J. S., Heidmann, T. & Medzhitov, R. Trex1 Prevents Cell-Intrinsic Initiation of Autoimmunity. *Cell* **134,** 587–598 (2008).

144. Ablasser, A. *et al.* TREX1 Deficiency Triggers Cell-Autonomous Immunity in a cGAS-Dependent Manner. *J. Immunol.* **192,** 5993–5997 (2014).

145. Gao, D. *et al.* Activation of cyclic GMP-AMP synthase by self-DNA causes autoimmune diseases. *Proc. Natl. Acad. Sci.* **112,** (2015).

146. Yoshida, H., Okabe, Y., Kawane, K., Fukuyama, H. & Nagata, S. Lethal anemia caused by interferon-beta produced in mouse embryos carrying undigested DNA. *Nat Immunol* **6,** 49–56 (2005).

147. Lan, Y. Y., Londono, D., Bouley, R., Rooney, M. S. & Hacohen, N. Dnase2a deficiency uncovers lysosomal clearance of damaged nuclear DNA via autophagy. *Cell Rep* **9,** 180–192 (2015).

148. Crow, Y. J. *et al.* Mutations in the gene encoding the 3'-5' DNA exonuclease TREX1 cause Aicardi-Goutières syndrome at the AGS1 locus. *Nat. Genet.* **38,** 917–920 (2006).

149. Kawane, K., Tanaka, H., Kitahara, Y., Shimaoka, S. & Nagata, S. Cytokine-dependent but acquired immunity-independent arthritis caused by DNA escaped from degradation. *Proc. Natl. Acad. Sci.* **107,** 19432–19437 (2010).

150. Kawane, K. *et al.* Chronic polyarthritis caused by mammalian DNA that escapes from degradation in macrophages. *Nature* **443,** 998–1002 (2006).

151. Jeremiah, N. *et al.* Inherited STING-activating mutation underlies a familial inflammatory syndrome with lupus-like manifestations. *J Clin Invest* **124,** 5516–5520 (2014).

152. Ablasser, A. *et al.* cGAS produces a 2'-5'-linked cyclic dinucleotide second messenger that activates STING. *Nature* **498,** 380–384 (2013).

153. Diner, E. J. *et al.* The innate immune DNA sensor cGAS produces a noncanonical cyclic dinucleotide that activates human STING. *Cell Rep* **3,** 1355–1361 (2013).

154. Mali, P. *et al.* RNA-Guided Human Genome Engineering via Cas9. **823,** 823–827 (2013).

155. Sanjana, N. E., Shalem, O. & Zhang, F. Improved vectors and genome-wide libraries for CRISPR screening. *Nat. Methods* **11,** 783–784 (2014).

156. Schmid-Burgk, J. L. *et al.* OutKnocker : a web tool for rapid and simple genotyping of designer nuclease edited cell lines. 1719–1723 (2014). doi:10.1101/gr.176701.114

157. Peng, K., Broz, P., Jones, J., Joubert, L.-M. & Monack, D. Elevated AIM2-mediated pyroptosis triggered by hypercytotoxic Francisella mutant strains is attributed to increased intracellular bacteriolysis. *Cell. Microbiol.* **13,** 1586–1600 (2011).

158. Prame Kumar, K., Nicholls, A. J. & Wong, C. H. Y. Partners in crime: neutrophils and monocytes/macrophages in inflammation and disease. *Cell Tissue Res.* **371,** 551–565 (2018).

159. Takaoka, A. *et al.* DAI (DLM-1/ZBP1) is a cytosolic DNA sensor and an activator of innate immune response. *Nature* **448,** 501–505 (2007).

160. Hemmi, H. *et al.* A Toll-like receptor recognizes bacterial DNA. *Nature* **408,** 740–745 (2000).

161. Tian, J. *et al.* Toll-like receptor 9-dependent activation by DNA-containing immune complexes is mediated by HMGB1 and RAGE. *Nat. Immunol.* **8,** 487–496 (2007).

162. Leffler, J. *et al.* Neutrophil extracellular traps that are not degraded in systemic lupus erythematosus activate complement exacerbating the disease. *J Immunol* **188,** 3522–3531 (2012).

163. Ahn, J., Gutman, D., Saijo, S. & Barber, G. N. STING manifests self DNA-dependent inflammatory disease. *Proc. Natl. Acad. Sci. U. S. A.* **109,** 19386–91 (2012).

164. Kerur, N. *et al.* CGAS drives noncanonical-inflammasome activation in age-related macular degeneration. *Nat. Med.* **24,** 50–61 (2018).

165. Gaidt, M. M. *et al.* The DNA Inflammasome in Human Myeloid Cells Is Initiated by a STING-Cell Death Program Upstream of NLRP3. *Cell* **171,** 1110–1124.e18 (2017).

166. Corkum, C. P. *et al.* Immune cell subsets and their gene expression profiles from human PBMC isolated by Vacutainer Cell Preparation Tube (CPT™) and standard density gradient. *BMC Immunol.* **16,** 48 (2015).

167. Connelly, K. L. *et al.* Longitudinal association of type 1 interferon-induced chemokines with disease activity in systemic lupus erythematosus. *Sci. Rep.* **8,** 3268 (2018).

168. Vincent, J. *et al.* Small molecule inhibition of cGAS reduces interferon expression in primary macrophages from autoimmune mice. *Nat. Commun.* **8,** 750 (2017).

169. Kuznik, A. *et al.* Mechanism of endosomal TLR inhibition by antimalarial drugs and imidazoquinolines. *J Immunol* **186,** 4794–4804 (2011).

170. Yoshimori, T., Yamamoto, A., Moriyama, Y., Futai, M. & Tashiro, Y. Bafilomycin A1, a specific inhibitor of vacuolar-type H(+)-ATPase, inhibits acidification and protein degradation in lysosomes of cultured cells. *J. Biol. Chem.* **266,** 17707–12 (1991).

171. Jiménez-Alcázar, M. *et al.* Host DNases prevent vascular occlusion by neutrophil extracellular traps. *Science (80-.).* **358,** (2017).

172. Glennon-Alty, L., Hackett, A. P., Chapman, E. A. & Wright, H. L. Neutrophils and redox stress in the pathogenesis of autoimmune disease. *Free Radic. Biol. Med.* 0–1 (2018). doi:10.1016/j.freeradbiomed.2018.03.049

173. Tanaka, K. *et al.* In vivo characterization of neutrophil extracellular traps in various organs of a murine sepsis model. *PLoS One* **9,** e111888 (2014).

174. Amulic, B. *et al.* Cell-Cycle Proteins Control Production of Neutrophil Extracellular Traps. *Dev.*

Cell **43,** 449–462.e5 (2017).

175. Heymann, F., Hamesch, K., Weiskirchen, R. & Tacke, F. The concanavalin A model of acute hepatitis in mice. *Lab. Anim.* **49,** 12–20 (2015).
176. Daley, J. M., Thomay, A. A., Connolly, M. D., Reichner, J. S. & Albina, J. E. Use of Ly6G-specific monoclonal antibody to deplete neutrophils in mice. *J. Leukoc. Biol.* **83,** 64–70 (2007).
177. Orlowski, G. M. *et al.* Multiple Cathepsins Promote Pro–IL-1β Synthesis and NLRP3-Mediated IL-1β Activation. *J. Immunol.* **195,** 1685–1697 (2015).
178. Bangalore, N., Travis, J., Onunka, V. C., Pohl, J. & Shafer, W. M. Identification of the primary antimicrobial domains in human neutrophil cathepsin G. *J. Biol. Chem.* **265,** 13584–8 (1990).
179. Chen, Y. T. *et al.* In Vitro and In Vivo Studies of the Trypanocidal Properties of WRR-483 against Trypanosoma cruzi. *PLoS Negl. Trop. Dis.* **4,** e825 (2010).
180. West, A. P. *et al.* Mitochondrial DNA stress primes the antiviral innate immune response. *Nature* **520,** 553–557 (2015).
181. Härtlova, A. *et al.* DNA damage primes the type I interferon system via the cytosolic DNA sensor STING to promote anti-microbial innate immunity. *Immunity* **42,** 332–343 (2015).
182. Du, M. & Chen, Z. J. DNA-induced liquid phase condensation of cGAS activates innate immune signaling. **1022,** 1–10 (2018).
183. Almine, J. F. *et al.* IFI16 and cGAS cooperate in the activation of STING during DNA sensing in human keratinocytes. *Nat. Commun.* **8,** 14392 (2017).
184. Marsman, G., Zeerleder, S. & Luken, B. M. Extracellular histones, cell-free DNA, or nucleosomes: differences in immunostimulation. *Cell Death Dis.* **7,** e2518 (2016).
185. Lee-Kirsch, M. A. *et al.* Familial Chilblain Lupus, a Monogenic Form of Cutaneous Lupus Erythematosus, Maps to Chromosome 3p. *Am. J. Hum. Genet.* **79,** 731–737 (2006).
186. Kolaczkowska, E. *et al.* Molecular mechanisms of NET formation and degradation revealed by intravital imaging in the liver vasculature. *Nat. Commun.* **6,** 6673 (2015).
187. Mitsios, A., Arampatzioglou, A., Arelaki, S., Mitroulis, I. & Ritis, K. NETopathies? Unraveling the dark side of old diseases through neutrophils. *Frontiers in Immunology* (2017). doi:10.3389/fimmu.2016.00678
188. Rodríguez-Carrio, J., Alperi-López, M., López, P., Ballina-García, F. J. & Suárez, A. Heterogeneity of the Type I Interferon Signature in Rheumatoid Arthritis: A Potential Limitation for Its Use As a Clinical Biomarker. *Front. Immunol.* **8,** 2007 (2017).
189. Oestreicher, J. L. *et al.* Molecular classification of psoriasis disease-associated genes through pharmacogenomic expression profiling. *Pharmacogenomics J.* **1,** 272–287 (2001).
190. Zhou, X. *et al.* Novel mechanisms of T-cell and dendritic cell activation revealed by profiling of

psoriasis on the 63,100-element oligonucleotide array. *Physiol. Genomics* **13,** 69–78 (2003).

191. Rönnblom, L. E., Alm, G. V. & Öberg, K. Autoimmune Phenomena in Patients with Malignant Carcinoid Tumors During Interferon-α Treatment. *Acta Oncol. (Madr).* **30,** 537–540 (1991).
192. Kiefer, K., Oropallo, M. A., Cancro, M. P. & Marshak-Rothstein, A. Role of type I interferons in the activation of autoreactive B cells. *Immunol. Cell Biol.* **90,** 498–504 (2012).
193. Hervas-Stubbs, S. *et al.* Direct effects of type I interferons on cells of the immune system. *Clin. Cancer Res.* **17,** 2619–27 (2011).
194. Ivashkiv, L. B. & Donlin, L. T. Regulation of type I interferon responses. *Nat. Rev. Immunol.* **14,** 36–49 (2014).
195. Bossaller, L. *et al.* TLR9 Deficiency Leads to Accelerated Renal Disease and Myeloid Lineage Abnormalities in Pristane-Induced Murine Lupus. *J. Immunol.* **197,** 1044–1053 (2016).
196. Patole, P. S. *et al.* G-Rich DNA Suppresses Systemic Lupus. *J. Am. Soc. Nephrol.* **16,** 3273–3280 (2005).
197. Summers, S. A. *et al.* TLR9 and TLR4 are required for the development of autoimmunity and lupus nephritis in pristane nephropathy. *J. Autoimmun.* **35,** 291–298 (2010).
198. An, J. *et al.* Expression of Cyclic GMP-AMP Synthase in Patients With Systemic Lupus Erythematosus. *Arthritis Rheumatol.* **69,** 800–807 (2017).
199. Khamashta, M. *et al.* Sifalimumab, an anti-interferon-α monoclonal antibody, in moderate to severe systemic lupus erythematosus: a randomised, double-blind, placebo-controlled study. *Ann. Rheum. Dis.* **75,** 1909–1916 (2016).
200. Kalunian, K. C. *et al.* A Phase II study of the efficacy and safety of rontalizumab (rhuMAb interferon-α) in patients with systemic lupus erythematosus (ROSE). *Ann. Rheum. Dis.* **75,** 196–202 (2016).
201. Furie, R. *et al.* Anifrolumab, an Anti-Interferon-α Receptor Monoclonal Antibody, in Moderate-to-Severe Systemic Lupus Erythematosus. *Arthritis Rheumatol.* **69,** 376–386 (2017).
202. Riggs, J. M. *et al.* Characterisation of anifrolumab, a fully human anti-interferon receptor antagonist antibody for the treatment of systemic lupus erythematosus. *Lupus Sci. Med.* **5,** e000261 (2018).
203. Morimoto, A. M. *et al.* Association of endogenous anti-interferon-α autoantibodies with decreased interferon-pathway and disease activity in patients with systemic lupus erythematosus. *Arthritis Rheum.* **63,** 2407–2415 (2011).
204. Hall, J. *et al.* Discovery of PF-06928215 as a high affinity inhibitor of cGAS enabled by a novel fluorescence polarization assay. *PLoS One* **12,** e0184843 (2017).
205. Rosenbaum, J. T., Mount, G. R., Youssef, J. & Lin, P. New Perspectives in Rheumatology:

Avoiding Antimalarial Toxicity. *Arthritis Rheumatol.* **68,** 1805–1809 (2016).

206. Ruiz-Irastorza, G., Ramos-Casals, M., Brito-Zeron, P. & Khamashta, M. A. Clinical efficacy and side effects of antimalarials in systemic lupus erythematosus: a systematic review. *Ann. Rheum. Dis.* **69,** 20–8 (2010).
207. Ponticelli, C. & Moroni, G. Hydroxychloroquine in systemic lupus erythematosus (SLE). *Expert Opin. Drug Saf.* **16,** 411–419 (2017).
208. Jang, C.-H., Choi, J.-H., Byun, M.-S. & Jue, D.-M. Chloroquine inhibits production of TNF-α, IL-1β and IL-6 from lipopolysaccharide-stimulated human monocytes/macrophages by different modes. *Rheumatology* **45,** 703–710 (2006).
209. Kuznik, A. *et al.* Mechanism of Endosomal TLR Inhibition by Antimalarial Drugs and Imidazoquinolines. *J. Immunol.* **186,** 4794–4804 (2011).
210. An, J. *et al.* A novel anti-malarial drug derivative inhibits cyclic GMP-AMP synthase in Trex1 deficient mice. *Arthritis Rheumatol.* (2018). doi:10.1002/art.40559
211. An, J., Woodward, J. J., Sasaki, T., Minie, M. & Elkon, K. B. Cutting Edge: Antimalarial Drugs Inhibit IFN-β Production through Blockade of Cyclic GMP-AMP Synthase–DNA Interaction. *J. Immunol.* **194,** 4089–4093 (2015).
212. Piscianz, E. *et al.* Reappraisal of Antimalarials in Interferonopathies: New Perspectives for Old Drugs. *Curr. Med. Chem.* **25,** 1–14 (2017).
213. Wang, Y., Su, G.-H., Zhang, F., Chu, J.-X. & Wang, Y.-S. Cyclic GMP-AMP Synthase Is Required for Cell Proliferation and Inflammatory Responses in Rheumatoid Arthritis Synoviocytes. *Mediators Inflamm.* **2015,** 192329 (2015).
214. Clark, I. A., Budd, A. C., Alleva, L. M. & Cowden, W. B. Human malarial disease: a consequence of inflammatory cytokine release. *Malar. J.* **5,** 85 (2006).
215. Sebina, I. & Haque, A. Effects of type I interferons in malaria. *Immunology* (2018). doi:10.1111/imm.12971
216. Gallego-Marin, C. *et al.* Cyclic GMP–AMP Synthase Is the Cytosolic Sensor of Plasmodium falciparum Genomic DNA and Activates Type I IFN in Malaria. *J. Immunol.* **200,** 768–774 (2018).
217. Feintuch, C. M. *et al.* Activated Neutrophils Are Associated with Pediatric Cerebral Malaria Vasculopathy in Malawian Children. *MBio* **7,** e01300-15 (2016).
218. Baker, V. S. *et al.* Cytokine-associated neutrophil extracellular traps and antinuclear antibodies in Plasmodium falciparum infected children under six years of age. *Malar. J.* **7,** 41 (2008).
219. Rocha, B. C. *et al.* Type I Interferon Transcriptional Signature in Neutrophils and Low-Density Granulocytes Are Associated with Tissue Damage in Malaria. *Cell Rep.* **13,** 2829–2841 (2015).
220. Abrams, S. T. *et al.* Circulating Histones Are Mediators of Trauma-associated Lung Injury. *Am. J.*

Respir. Crit. Care Med. **187,** 160–169 (2013).

221. Pereira, L. F. *et al.* Histones interact with anionic phospholipids with high avidity; its relevance for the binding of histone-antihistone immune complexes. *Clin. Exp. Immunol.* **97,** 175–80 (1994).
222. Lee, C.-C., Sun, Y., Qian, S. & Huang, H. W. Transmembrane pores formed by human antimicrobial peptide LL-37. *Biophys. J.* **100,** 1688–96 (2011).
223. Andersson, U., Yang, H. & Harris, H. High-mobility group box 1 protein (HMGB1) operates as an alarmin outside as well as inside cells. *Semin. Immunol.* 0–1 (2018). doi:10.1016/j.smim.2018.02.011
224. Xu, J. *et al.* Macrophage endocytosis of high-mobility group box 1 triggers pyroptosis. *Cell Death Differ.* **21,** 1229–1239 (2014).
225. Yanai, H. *et al.* HMGB proteins function as universal sentinels for nucleic-acid-mediated innate immune responses. *Nature* **462,** 99–103 (2009).
226. Sirois, C. M. *et al.* RAGE is a nucleic acid receptor that promotes inflammatory responses to DNA. *J. Exp. Med.* **210,** 2447–2463 (2013).
227. Andreeva, L. *et al.* cGAS senses long and HMGB/TFAM-bound U-turn DNA by forming protein–DNA ladders. *Nature* **549,** 394–398 (2017).
228. Nguyen, T. A. *et al.* SIDT2 Transports Extracellular dsRNA into the Cytoplasm for Innate Immune Recognition. *Immunity* **47,** 498–509.e6 (2017).
229. Aizawa, S. *et al.* Lysosomal membrane protein SIDT2 mediates the direct uptake of DNA by lysosomes. *Autophagy* **13,** 218–222 (2017).
230. Kovacsovics-Bankowski, M. & Rock, K. L. A phagosome-to-cytosol pathway for exogenous antigens presented on MHC class I molecules. *Science* **267,** 243–6 (1995).
231. Ackerman, A. L., Giodini, A. & Cresswell, P. A Role for the Endoplasmic Reticulum Protein Retrotranslocation Machinery during Crosspresentation by Dendritic Cells. *Immunity* **25,** 607–617 (2006).
232. Manz, M. G. & Boettcher, S. Emergency granulopoiesis. *Nat. Rev. Immunol.* **14,** 302–314 (2014).
233. Harris, D. P., Bandyopadhyay, S., Maxwell, T. J., Willard, B. & DiCorleto, P. E. Tumor Necrosis Factor (TNF)-α Induction of CXCL10 in Endothelial Cells Requires Protein Arginine Methyltransferase 5 (PRMT5)-mediated Nuclear Factor (NF)-κB p65 Methylation. *J. Biol. Chem.* **289,** 15328–15339 (2014).
234. Unterholzner, L. The interferon response to intracellular DNA: why so many receptors? *Immunobiology* **218,** 1312–1321 (2013).
235. Jønsson, K. L. *et al.* IFI16 is required for DNA sensing in human macrophages by promoting

production and function of cGAMP. *Nat. Commun.* **8,** 14391 (2017).

236. Gray, E. E. *et al.* The AIM2-like Receptors Are Dispensable for the Interferon Response to Intracellular DNA. *Immunity* **45,** 255–66 (2016).
237. Banerjee, I. *et al.* Gasdermin D Restrains Type I Interferon Response to Cytosolic DNA by Disrupting Ionic Homeostasis. *Immunity* 1–14 (2018). doi:10.1016/j.immuni.2018.07.006
238. Yan, S. *et al.* Deficiency of the AIM2–ASC Signal Uncovers the STING-Driven Overreactive Response of Type I IFN and Reciprocal Depression of Protective IFN-γ Immunity in Mycobacterial Infection. *J. Immunol.* **200,** 1016–1026 (2018).
239. Wang, Y. *et al.* Inflammasome Activation Triggers Caspase-1-Mediated Cleavage of cGAS to Regulate Responses to DNA Virus Infection. *Immunity* **46,** 393–404 (2017).
240. Swanson, K. V. *et al.* A noncanonical function of cGAMP in inflammasome priming and activation. *J. Exp. Med.* **214,** 3611–3626 (2017).
241. Brinkmann, V., Goosmann, C., Kuhn, L. I. & Zychlinsky, A. Automatic quantification of in vitro NET formation. *Front Immunol* **3,** 413 (2012).
242. Ritchie, M. E. *et al.* limma powers differential expression analyses for RNA-sequencing and microarray studies. *Nucleic Acids Res.* **43,** e47–e47 (2015).
243. Weiner, J. & Domaszewska, T. tmod: an R package for general and multivariate enrichment analysis. (2016). doi:10.7287/peerj.preprints.2420v1
244. Civril, F. *et al.* Structural mechanism of cytosolic DNA sensing by cGAS. *Nature* **498,** 332–7 (2013).

6 Appendix

Appendix A NET-associated proteins identified by mass spectrometry.

The table lists proteins that were identified on NETs by mass spectrometry. Proteins were included, if more than two unique significant peptides were identified, using a false discovery rate of 1 %.

#	Accession	Protein names	Num. of significant sequences	Num. of significant unique sequences
1	1433Z_HUMAN	14-3-3 protein zeta/delta	14	9
2	6PGD_HUMAN	6-phosphogluconate dehydrogenase	17	17
3	ACTB_HUMAN	Actin, cytoplasmic 1 (Beta-actin)	84	3
4	ACTBL_HUMAN	Beta-actin-like protein 2 (Kappa-actin)	28	3
5	ACTC_HUMAN	Actin, alpha cardiac muscle 1 (Alpha-cardiac actin)	38	3
6	ACTG_HUMAN	Actin, cytoplasmic 2 (Gamma-actin)	86	5
7	ACTN1_HUMAN	Alpha-actinin-1	6	4
8	ACTN4_HUMAN	Alpha-actinin-4	11	3
9	AL5AP_HUMAN	Arachidonate 5-lipoxygenase-activating protein	3	3
10	ALBU_HUMAN	Serum albumin	29	29
11	ALDOA_HUMAN	Fructose-bisphosphate aldolase A	4	4
12	AN32B_HUMAN	Acidic leucine-rich nuclear phosphoprotein 32 family member B	3	3
13	ANX11_HUMAN	Annexin A11	9	8
14	ANXA1_HUMAN	Annexin A1	32	32
15	ANXA3_HUMAN	Annexin A3	9	9
16	ANXA4_HUMAN	Annexin A4	8	7
17	ANXA5_HUMAN	Annexin A5	6	6
18	ANXA6_HUMAN	Annexin A6	26	25
19	APMAP_HUMAN	Adipocyte plasma membrane-associated protein	10	10
20	APOBR_HUMAN	Apolipoprotein B receptor	3	3
21	ARC1B_HUMAN	Actin-related protein 2/3 complex subunit 1B	4	4
22	ARGI1_HUMAN	Arginase-1	3	3
23	ARP2_HUMAN	Actin-related protein 2	3	3
24	ARP3_HUMAN	Actin-related protein 3	7	7
25	ARPC2_HUMAN	Actin-related protein 2/3 complex subunit 2	3	3
26	ARPC3_HUMAN	Actin-related protein 2/3 complex subunit 3	3	3
27	ARPC4_HUMAN	Actin-related protein 2/3 complex subunit 4	4	4
28	AT2A3_HUMAN	Sarcoplasmic/endoplasmic reticulum calcium ATPase 3	3	3
29	ATPA_HUMAN	ATP synthase subunit alpha, mitochondrial	6	6
30	ATPB_HUMAN	ATP synthase subunit beta, mitochondrial	7	7
31	B3AT_HUMAN	Band 3 anion transport protein	5	5
32	BAP31_HUMAN	B-cell receptor-associated protein 31	3	3
33	BASP1_HUMAN	Brain acid soluble protein 1	12	12
34	BLVRB_HUMAN	Flavin reductase	4	4

35	BPI_HUMAN	Bactericidal permeability-increasing protein	8	8
36	CAH1_HUMAN	Carbonic anhydrase 1	5	5
37	CAH2_HUMAN	Carbonic anhydrase 2	9	9
38	CALM1_HUMAN	Calmodulin-1	4	4
39	CALR_HUMAN	Calreticulin	12	12
40	CALX_HUMAN	Calnexin	13	13
41	CAMP_HUMAN	Cathelicidin antimicrobial peptide	3	3
42	CAP1_HUMAN	Adenylyl cyclase-associated protein 1	6	6
43	CAP7_HUMAN	Azurocidin	7	7
44	CAPG_HUMAN	Macrophage-capping protein	4	4
45	CAPZB_HUMAN	F-actin-capping protein subunit beta	7	7
46	CATA_HUMAN	Catalase	11	11
47	CATG_HUMAN	Cathepsin G	9	9
48	CAZA1_HUMAN	F-actin-capping protein subunit alpha-1	3	3
49	CD59_HUMAN	CD59 glycoprotein	3	3
50	CDC42_HUMAN	Cell division control protein 42 homolog	5	3
51	CDD_HUMAN	Cytidine deaminase	3	3
52	CEAM8_HUMAN	Carcinoembryonic antigen-related cell adhesion molecule 8	4	3
53	CH60_HUMAN	60 kDa heat shock protein, mitochondrial	4	4
54	CISY_HUMAN	Citrate synthase, mitochondrial	3	3
55	CLIC1_HUMAN	Chloride intracellular channel protein 1	3	3
56	COF1_HUMAN	Cofilin-1	3	3
57	COR1A_HUMAN	Coronin-1A	8	8
58	COX5A_HUMAN	Cytochrome c oxidase subunit 5A, mitochondrial	3	3
59	CP4F3_HUMAN	Docosahexaenoic acid omega-hydroxylase	7	7
60	CPNE3_HUMAN	Copine-3	4	4
61	CPZIP_HUMAN	CapZ-interacting protein	3	3
62	CY24A_HUMAN	Cytochrome b-245 light chain	4	4
63	CY24B_HUMAN	Cytochrome b-245 heavy chain	3	3
64	DEF3_HUMAN	Neutrophil defensin 3	4	4
65	DYSF_HUMAN	Dysferlin	7	7
66	ECP_HUMAN	Eosinophil cationic protein	6	6
67	EF1A1_HUMAN	Elongation factor 1-alpha 1	5	5
68	ELNE_HUMAN	Neutrophil elastase	34	34
69	ENOA_HUMAN	Alpha-enolase	10	10
70	ENPL_HUMAN	Endoplasmin	5	5
71	FA49B_HUMAN	FAM49B	3	3
72	FLNA_HUMAN	Filamin-A	4	4
73	FLOT1_HUMAN	Flotillin-1	3	3
74	G3P_HUMAN	Glyceraldehyde-3-phosphate dehydrogenase	15	15
75	G6PD_HUMAN	Glucose-6-phosphate 1-dehydrogenase	12	12
77	G6PI_HUMAN	Glucose-6-phosphate isomerase	24	24
78	GANAB_HUMAN	Neutral alpha-glucosidase AB	4	4
79	GBB2_HUMAN	Guanine nucleotide-binding protein G(I)/G(S)/G(T) subunit beta-2	9	3
80	GDIB_HUMAN	Rab GDP dissociation inhibitor beta	3	3
81	GDIR1_HUMAN	Rho GDP-dissociation inhibitor 1	5	5

82	GDIR2_HUMAN	Rho GDP-dissociation inhibitor 2	23	23
83	GELS_HUMAN	Gelsolin	33	33
84	GLU2B_HUMAN	Glucosidase 2 subunit beta	5	5
85	GLYG_HUMAN	Glycogenin-1	5	5
86	GNAI2_HUMAN	Guanine nucleotide-binding protein G(i) subunit alpha-2	13	9
87	GRAN_HUMAN	Grancalcin	6	6
88	GRN_HUMAN	Granulins	9	9
89	GRP78_HUMAN	Endoplasmic reticulum chaperone BiP	9	9
90	GSTO1_HUMAN	Glutathione S-transferase omega 1	4	4
91	GSTP1_HUMAN	Glutathione S-transferase P	5	5
92	GTR3_HUMAN	Solute carrier family 2	4	4
93	H12_HUMAN	Histone H1.2	13	5
94	H15_HUMAN	Histone H1.5	10	8
95	H2A1C_HUMAN	Histone H2A type 1-C	20	3
96	H2A1D_HUMAN	Histone H2A type 1-D	16	6
97	H2A1H_HUMAN	Histone H2A type 1-H	16	5
98	H2A2B_HUMAN	Histone H2A type 2-B	13	3
99	H2AV_HUMAN	Histone H2A.V	5	4
100	H2AX_HUMAN	Histone H2AX	18	3
101	H2AY_HUMAN	Core histone macro-H2A.1	11	5
102	H2B1B_HUMAN	Histone H2B type 1-B	21	4
103	H2B1D_HUMAN	Histone H2B type 1-D	19	19
104	H4_HUMAN	Histone H4	18	18
105	HBA_HUMAN	Hemoglobin subunit alpha (Alpha-globin)	46	46
106	HBB_HUMAN	Hemoglobin subunit beta (Beta-globin)	47	20
107	HBD_HUMAN	Hemoglobin subunit delta (Delta-globin)	31	4
108	HBG1_HUMAN	Hemoglobin subunit gamma-1 (Gamma-1-globin)	7	3
109	HCLS1_HUMAN	Hematopoietic lineage cell-specific protein	5	5
110	HMGB1_HUMAN	High mobility group protein B1	3	3
111	HMGB2_HUMAN	High mobility group protein B2	6	6
112	HMGN1_HUMAN	Non-histone chromosomal protein HMG-14	3	3
113	HMGN2_HUMAN	Non-histone chromosomal protein HMG-17	4	4
115	HNRPU_HUMAN	Heterogeneous nuclear ribonucleoprotein U	3	3
116	HORN_HUMAN	Hornerin	3	3
117	HS71A_HUMAN	Heat shock 70 kDa protein 1A	3	3
118	HS90A_HUMAN	Heat shock protein HSP 90-alpha	3	3
119	HSP7C_HUMAN	Heat shock cognate 71 kDa protein	11	5
120	HXK3_HUMAN	Hexokinase-3	5	5
121	ITAM_HUMAN	Integrin alpha-M	10	10
122	ITB2_HUMAN	Integrin beta-2	11	11
123	K1C10_HUMAN	Keratin, type I cytoskeletal 10	11	10
124	K1C9_HUMAN	Keratin, type I cytoskeletal 9	9	9
125	K22E_HUMAN	Keratin, type II cytoskeletal 2 epidermal	13	9
126	K2C1_HUMAN	Keratin, type II cytoskeletal 1	7	5
127	KPYM_HUMAN	Pyruvate kinase PKM	5	5
128	LASP1_HUMAN	LIM and SH3 domain protein 1	3	3

129	LDHA_HUMAN	L-lactate dehydrogenase A chain	8	8
130	LDHB_HUMAN	L-lactate dehydrogenase B chain	4	3
131	LEG10_HUMAN	Galectin-10	3	3
132	LKHA4_HUMAN	Leukotriene A-4 hydrolase	9	9
134	LOX5_HUMAN	Arachidonate 5-lipoxygenase	9	9
135	LSP1_HUMAN	Lymphocyte-specific protein 1	11	11
136	LYSC_HUMAN	Lysozyme C	4	4
137	MDHC_HUMAN	Malate dehydrogenase, cytoplasmic	4	4
138	MDHM_HUMAN	Malate dehydrogenase, mitochondrial	4	4
139	ML12A_HUMAN	Myosin regulatory light chain 12A	4	4
140	MMP9_HUMAN	Matrix metalloproteinase-9	4	4
141	MNDA_HUMAN	Myeloid cell nuclear differentiation antigen	6	6
142	MOES_HUMAN	Moesin	5	5
143	MYH9_HUMAN	Myosin-9	9	9
144	MYL6_HUMAN	Myosin light polypeptide 6	8	8
145	MYO1F_HUMAN	Unconventional myosin-If	3	3
146	NAMPT_HUMAN	Nicotinamide phosphoribosyltransferase	3	3
147	NGAL_HUMAN	Neutrophil gelatinase-associated lipocalin	4	4
148	PADI4_HUMAN	Protein-arginine deiminase type-4	8	8
149	PARK7_HUMAN	Protein/nucleic acid deglycase DJ-1	5	5
150	PDIA1_HUMAN	Protein disulfide-isomerase	5	5
151	PDIA3_HUMAN	Protein disulfide-isomerase A3	14	14
152	PDIA6_HUMAN	Protein disulfide-isomerase A6	3	3
153	PERE_HUMAN	Eosinophil peroxidase	27	22
154	PERM_HUMAN	Myeloperoxidase	45	45
155	PGAM1_HUMAN	Phosphoglycerate mutase 1	11	11
156	PGK1_HUMAN	Phosphoglycerate kinase 1	9	9
157	PHB2_HUMAN	Prohibitin-2	3	3
158	PLBL1_HUMAN	Phospholipase B-like 1	8	8
159	PLSL_HUMAN	Plastin-2	4	4
160	PNPH_HUMAN	Purine nucleoside phosphorylase	4	4
161	PPIA_HUMAN	Peptidyl-prolyl cis-trans isomerase A	4	4
162	PPIB_HUMAN	Peptidyl-prolyl cis-trans isomerase B	4	4
163	PRDX2_HUMAN	Peroxiredoxin-2	11	11
164	PRDX3_HUMAN	Thioredoxin-dependent peroxide reductase, mitochondrial	5	3
165	PRG2_HUMAN	Bone marrow proteoglycan	4	4
166	PROF1_HUMAN	Profilin-1	16	16
167	PRTN3_HUMAN	Myeloblastin	5	5
168	PTMA_HUMAN	Prothymosin alpha	4	4
169	PTPRC_HUMAN	Receptor-type tyrosine-protein phosphatase C	5	5
170	PYGL_HUMAN	Glycogen phosphorylase, liver form	5	5
171	RAB1B_HUMAN	Ras-related protein Rab-1B	5	3
172	RAC1_HUMAN	Ras-related C3 botulinum toxin substrate 1	6	3
173	RAN_HUMAN	GTP-binding nuclear protein Ran	3	3
174	RETN_HUMAN	Resistin	3	3
175	RHOA_HUMAN	Transforming protein RhoA	6	4

176	RHOG_HUMAN	Rho-related GTP-binding protein	4	3
177	RNAS2_HUMAN	Non-secretory ribonuclease	4	4
178	RS27A_HUMAN	Ubiquitin-40S ribosomal protein S27a	3	3
179	RTN4_HUMAN	Reticulon-4	4	4
180	S100P_HUMAN	Protein S100-P	3	3
181	S10A4_HUMAN	Protein S100-A4	3	3
182	S10A6_HUMAN	Protein S100-A6	3	3
183	S10A8_HUMAN	Protein S100-A8	9	9
184	S10A9_HUMAN	Protein S100-A9	16	16
185	S10AB_HUMAN	Protein S100-A11	3	3
186	S10AC_HUMAN	Protein S100-A12	6	6
187	SFPQ_HUMAN	Splicing factor, proline- and glutamine-rich	3	3
188	SH3L1_HUMAN	SH3 domain-binding glutamic acid-rich-like protein	3	3
189	SODC_HUMAN	Superoxide dismutase	4	4
190	SODM_HUMAN	Superoxide dismutase	7	7
191	SPB10_HUMAN	Serpin B10	3	3
192	SQOR_HUMAN	Sulfide:quinone oxidoreductase	3	3
193	STMN1_HUMAN	Stathmin	4	4
194	STOM_HUMAN	Erythrocyte band 7 integral membrane protein	10	10
195	SUN2_HUMAN	SUN domain-containing protein 2	3	3
196	TALDO_HUMAN	Transaldolase	6	6
197	TBA1A_HUMAN	Tubulin alpha-1A chain	5	5
198	TBB2A_HUMAN	Tubulin beta-2A chain	7	7
199	TBB4A_HUMAN	Tubulin beta-4A chain	13	13
200	TERA_HUMAN	Transitional endoplasmic reticulum ATPase	5	5
201	THIO_HUMAN	Thioredoxin	4	4
202	TKT_HUMAN	Transketolase	34	34
203	TLN1_HUMAN	Talin-1	3	3
204	TPIS_HUMAN	Triosephosphate isomerase	11	11
205	TPM3_HUMAN	Tropomyosin alpha-3 chain	7	7
206	TPM4_HUMAN	Tropomyosin alpha-4 chain	6	6
207	TRFL_HUMAN	Lactotransferrin	81	81
208	TYB4_HUMAN	Thymosin beta-4	5	5
209	UGPA_HUMAN	UTP--glucose-1-phosphate uridylyltransferase	3	3
210	VASP_HUMAN	Vasodilator-stimulated phosphoprotein	5	5
211	VAT1_HUMAN	Synaptic vesicle membrane protein VAT-1 homolog	7	7
212	VIME_HUMAN	Vimentin	3	3
213	VINC_HUMAN	Vinculin	3	3
214	WDR1_HUMAN	WD repeat-containing protein 1	8	8
215	ZYX_HUMAN	Zyxin	3	3

7 Selbstständigkeitserklärung

Hiermit erkläre ich, dass ich die vorliegende Arbeit selbstständig verfasst und keine anderen als die angegebenen Quellen und Hilfsmittel verwendet habe. Ich versichere, dass diese Arbeit in dieser oder anderer Form noch keiner anderen Prüfungsbehörde vorgelegt wurde. Der Inhalt der Promotionsordnung der Mathematisch-Naturwissenschaftlichen Fakultät I der Humboldt Universität zu Berlin vom 27. Juni 2012 ist mir bekannt.

Berlin, 1. Oktober 2018

Falko Apel

8 Acknowledgements

Science, and a PhD in particular, is a journey that cannot be finished alone. I want to use these last lines of my thesis to thank all the people that helped me on this long way to reach this moment.

Arturo, thank you for being a great mentor. Your scientific spirit has always inspired and motivated me and without your constructive guidance, the project wouldn't have ended so well. Also I would like express my deep gratitude for your support with all the little stumbling rocks that I had to deal with outside of the lab.

It was a pleasure and privilege to work with a group of people that is so enthusiastic about science. Thank you to all the members of the Zychlinsky lab for creating such a great working environment; you are a fantastic and colorful pile of extraordinary people.

Gabriel, although never officially my supervisor, you always were a great support. Thank you for all your time and help, may it be with the little details or the big picture.

Lorenz, thank you everything, not only for being my butcher when I was not skilled enough, but also for your motivating, enthusiastic nature and being a friend. Long live the DOSENBIER!

Garth, Gerben and Borko, thank you for proof reading my thesis and for all the discussion and comments in countless lab meetings, from which my work benefited so much.

Bärbel, thank you for writing the Mausantrag "with" me, without you I would have never done an *in vivo* experiment.

Yvonne, thank you for being my third and fourth hand and my second brain. Without you, my PhD would have taken another five years.

Thank you to my Gang, not only for cooking amazing food, but especially for being this kind of great friends everyone needs to live a happy and fulfilled life.

Eike, thank you for all the years of patience and support, for always covering my back, being a partner in crime and especially being a great mother for our Möpschen. You two are my true motivation and love.

Lastly, I would also thank my parents for being a save harbor whenever one is needed and for never asking when my PhD is finally over.

It is now.